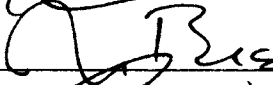CHARACTERIZATION OF PERMAFROST DEVELOPMENT

BY ISOTOPIC AND CHEMICAL ANALYSIS OF SOIL CORES

TAKEN FROM THE COPPER RIVER BASIN

AND AN UPLAND LOESS DEPOSIT IN INTERIOR ALASKA

By

Lola Kay Oliver

RECOMMENDED:

_____

_____
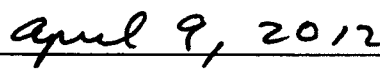
_____
Advisory Committee Chair

_____
Chair, Department of Geology and Geophysics

APPROVED:

_____
Dean, College of Natural Science and Mathematics

_____
Dean of the Graduate School
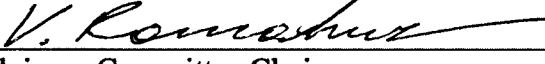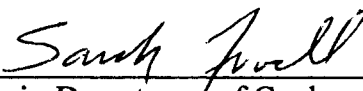
_____
Date _____ April 9, 2012

CHARACTERIZATION OF PERMAFROST DEVELOPMENT

BY ISOTOPIC AND CHEMICAL ANALYSIS OF SOIL CORES

TAKEN FROM THE COPPER RIVER BASIN

AND AN UPLAND LOESS DEPOSIT IN INTERIOR ALASKA

A

DISSERTATION

Presented to the Faculty

of the University of Alaska Fairbanks

in Partial Fulfillment of the Requirements

for the Degree of

DOCTOR OF PHILOSOPHY

By

Lola Kay Oliver, B.A., M.S.

Fairbanks, Alaska

May 2012

UMI Number: 3528853

UMI®

Dissertation Publishing

ProQuest®

Abstract

Chemical and isotopic analyses of pore water from permafrost cores taken from the dry lake bed of ancient Lake Atna in the Copper River Basin and from an upland loess deposit northeast of Fairbanks, Alaska reveal information about the local past environments not available by other means. Thawed core samples from both sites were analyzed for $\delta^{18}O$ and δD values using an isotope ratio mass spectrometer. Water content was determined as well, and subsamples of the cores were analyzed for nitrogen and carbon content. Water extracts of the core samples were analyzed for cations (Ca, Mg, K and Fe), as well as pH, electrical conductivity, and bicarbonate. Magnetic susceptibility was determined on samples from the Fairbanks site.

Data from samples taken from the Lake Atna site revealed a sequence of events that occurred in the basin after the lake drained about 10,000 years ago. At one location, oxygen isotopes show that permafrost formed continuously down through the lakebed. At the other location, 400 m distant, oxygen isotopes show that after permafrost formed, a thaw lake was produced on top of the permafrost. After the thaw lake had drained at least one wildfire passed through the area, large enough to thaw the surface permafrost to a depth of over 2 m at both core sites. The surface permafrost refroze, and currently the permafrost at the research site extends from 1 m depth to between 45 and 55 m depth.

At the Fairbanks site chemical analyses showed indications of pedogenesis at several depths in the loess profile of the permafrost core. Water isotope data from a site where the permafrost table is at less than 1 m depth show repeated episodes of thawing and refreezing. Charcoal and ash in several layers of soil in the area and from the sample

core suggest that fire may be the cause for the thawing events. The primary core water

isotope analyses also show several thawing and refreezing events, but the depths of the

signatures in the core indicate that these episodes happened thousands of years ago when

the ground surface was much lower than it is today.

Table of Contents

List of Figures   Page

List of Tables   Page

Chapter 1

Introduction

Permafrost, defined as subsoil that remains at temperatures below 0°C for 2 or more years, occurs generally where the average annual air temperature is less than 0°C, although it has been shown to become discontinuous at mean annual air temperatures as low as -5°C (Osterkamp and Romanovsky, 1999). In the northern hemisphere, permafrost occurs on about 23% of the land area, and 17% of the land area has discontinuous permafrost (Jorgenson et al., 2010, Brown et al., 1997, Brown and Haggerty, 1998). Approximately 80% of Alaska is underlain by permafrost (Osterkamp et al., 1998).

A great deal of attention has been paid to permafrost in soils, particularly those soils containing pore ice in the discontinuous zone where there is intermittent warm permafrost which is susceptible to thaw. Although permafrost may be dry (without pore ice), it is the melting of ice in thawing ground that can cause soil subsidence. This is an important topic of concern primarily because of the potential for creating engineering problems as permafrost thaws and ground surfaces become unstable (Osterkamp et al., 2009; Romanovsky, 2009).

Interest in global change, especially warming trends in the arctic and subarctic, has also contributed to the interest in permafrost (Walter et al., 2006, Hinzman et al., 2005). Current research warns of increased CO_2 release from thawing permafrost which

could exacerbate the warming trends (Jorgenson et al., 2010; Lee et al., 2010; Schaefer et al., 2011; Schuur et al., 2009; Vogel et al., 2009).

The present research looks at permafrost as an archive of environmental changes recorded in water isotopes of pore ice in frozen soils.

HYPOTHESIS AND PURPOSE OF THIS RESEARCH

The hypothesis for this research is that permafrost pore ice isotope fractionation, as shown by the isotope signatures in frozen groundwater, can provide information on environmental events that is not available from other sources. Pore ice in permafrost soil contains a record of changes in the water isotope signatures caused by the freezing front passing through soil during permafrost formation. This record is unique and timely as the loss of permafrost can result in the loss of information about the environment in existence at the time the permafrost formed.

This study follows those of early researchers (Fritz and Michel, 1977; Mackay and Lavkulich, 1974; Mackay, 1972) who discovered large fractionation shifts in oxygen isotopes of some permafrost pore ice which they interpreted to mean either

1) fractionation of the isotopes during freezing or 2) emplacement of isotopically different waters, either as a result of climate change or as a result of two separate groundwater masses being encountered during permafrost aggradation. Stuiver et al., (1976) suspected that permafrost waters could provide information on paleoclimate. The work done by Michel (1982) and Michel and Fritz (1982) in northern Canada used permafrost pore ice isotopes to identify climate shifts and groundwater movement in lake

beds. The present research examines permafrost pore ice isotopes in lake bed cores from

the Copper River Basin as well as cores taken from upland loess deposits near Fairbanks,

Alaska (Figure 1.1, Pearson and Hermans, 2008).

WATER ISOTOPE FRACTIONATION IN SOILS

When water freezes, heavier, kinetically less energetic water molecules are frozen

preferentially over lighter water molecules (O'Neil, 1968). In a closed system this effect

would proceed through the limited water supply so that eventually the last unfrozen water

would be made up of lighter molecules. In an open system heavier molecules are still

preferentially frozen, but since the residual water has free access to water that has not

been depleted of heavier molecules, fractionation is limited and variations occur in the

isotope signature indicating changes in the preferential freezing rate of heavier isotopes

over lighter isotopes.

Isotope fractionation during freezing of groundwater is a process sensitive to

changes in the soil-water environment. The degree of fractionation in permafrost is

determined by the speed at which the freezing front passes through the soil column and

the amount of mixing (agitation) during freezing (Suzuoki and Kimura, 1973). Agitation

is unlikely in groundwater except in laboratory situations, but freezing front speeds may

vary for a number of reasons, including changes in soil texture, a change in the

temperature of the soil matrix, and meeting a frozen layer in the soil column.

For freezing front speeds in excess of 2 mm per hour, fractionation is noticeably

decreased (Suzuoki and Kimura, 1973) and may even appear to stop (Michel, 1982).
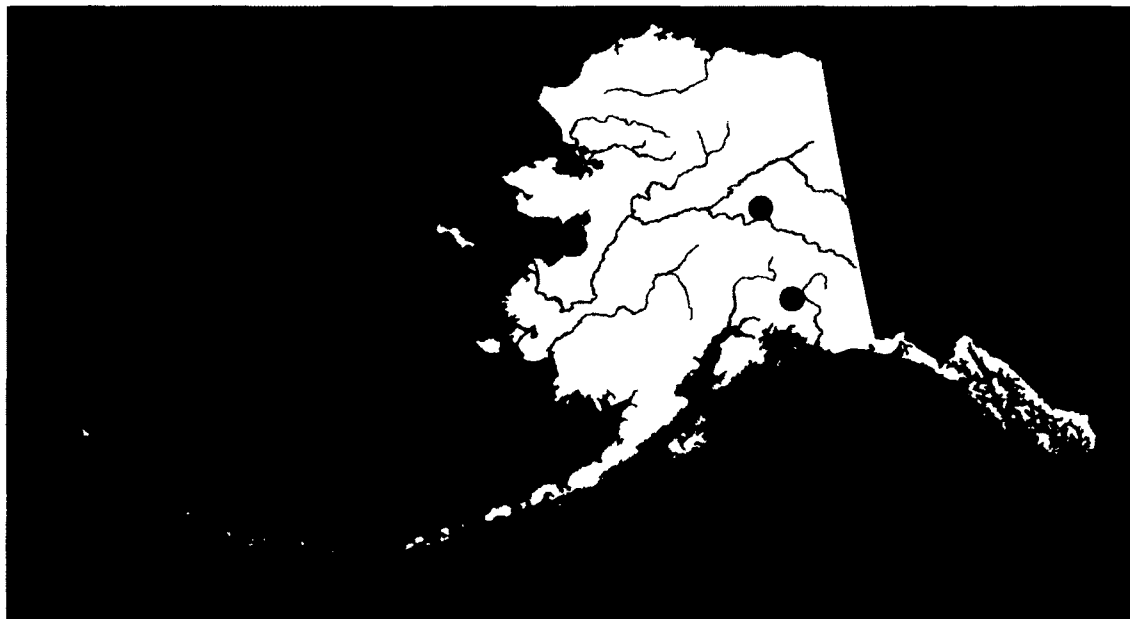
Figure 1.1 Study site locations

● = Copper River Basin Lake Atna site.
● = Fairbanks Hagelbarger site.

When the freezing front proceeds down the soil column at speeds slower than 2 mm per

hour, the extent of fractionation depends on how slowly the freezing front is moving;

slower movement produces greater fractionation.

There is a noticeable zigzag pattern of isotope signatures on data graphs in the

current research. These minor variations are less than 1‰ in size for oxygen isotopes

and 10‰ in size for deuterium isotopes. The zigzag patterns have occurred in other

water isotope research on soil cores (Michel, 1982) and appear to be created by a natural

process in the formation of permafrost in soil. There may be several factors contributing

to this phenomenon. For one, when a freezing front passes through soil, the fractionation

of the pore water is effected by the complex relationship among the soil particles, water

and ice in addition to the preference for heavier molecules. It has been shown in

laboratory experiments that fractionation produced by the freezing front cannot be

maintained down the soil column (Michel, 1982), so the zigzag pattern may reflect, in

sum, the average signature bracketed by the relative extremes produced in the freezing

process. Also, the freezing front in soil proceeds in an irregular manner down the soil

column since the soil has voids, pore size differences, and particle differences as well as a

film of unfrozen water on fine-grained soil particles down to quite low temperatures that

can transport water behind the freezing front (Davis, 2000; Williams and Smith, 1989).

One other contributor may be that small variations in data may be magnified by the range

of instrument precision (especially for deuterium in the current research, since instrument

precision for deuterium on the mass spectrometer used is less than that for oxygen).

PATTERNS IN FRACTIONATION DATA

Changes in a groundwater isotope data profile can provide information that may indicate the source of the groundwater, whether disturbances to the groundwater environment occurred, what those disturbances may have been, and what alterations such disturbances may have made to the permafrost. Changes in the speed of the freezing front as it moves down the soil column causes fractionation that is shown graphically by peaks or individual data point outliers outside the main data profile. Such variations in a column of data indicate alterations in the environmental conditions affecting the freezing front speed. Some of these conditions may be distant from the freezing front, such as a change in the ground surface temperature which changes the heat flux down the soil column; some may be immediate to the freezing front, such as a change in substrate when the freezing front passes from soil to bedrock. Even when sampling is done at 15 cm spacing fractionation peaks may be identified.

Context within the soil profile helps identify a probable cause where there are changes as indicated by fractionation peaks in the data or slanted data profiles. The isotope signatures above and below a fractionation peak, the shape of the isotope signature profile, and environmental changes at the permafrost site being examined are some of the indicators used to define the processes that produce particular fractionation peaks.

Data graph profiles from the current study show that there are indicators that occur fairly commonly in permafrost isotope data. The depth of the active layer/permafrost table intersection can be identified by the double peak produced when

the active layer freezing front descending from the soil surface meets the permafrost table

(Michel, 1982). This same profile occurs when the freezing front passes from one soil

texture to another, and where there have been partial thawing events followed by

refreezing of permafrost and the new and old permafrost meet. Double peaks are

produced by fractionation and do not reflect an actual change in the isotopic signature of

the ground water. Figure 1.2A is a stylized illustration of this profile as it would be seen

on a vertical data graph.

Another common indicator is a slanted column of permafrost data which looks as

if the isotope signature is changing slowly with depth. This profile represents a mixing

zone of waters with different signatures (Michel, 1982). Since ice cannot mix, the

mixing zone would have formed in the groundwater before freezing. Fractionation in an

open ground water system cannot be maintained with depth (Michel, 1982), so this is a

change in the ground water signature, and is not produced by fractionation. Figure 1.2B

is a stylized illustration of this profile as seen on a vertical data graph.

A third indicator that occurs in the current study is related to the slanted profile; a

column of data with a profile of data points above or below it (or both) that goes in a

different direction. Since the slanted profile illustrates water from two isotopically

different sources, one at the top and one at the bottom of the mixing zone, the column of

data linked to a differently sloped data profile represents an event that has isolated the

sets of data from each other. An example could be two separate permafrost events that

occur sequentially at different times allowing the unfrozen water of the second event to
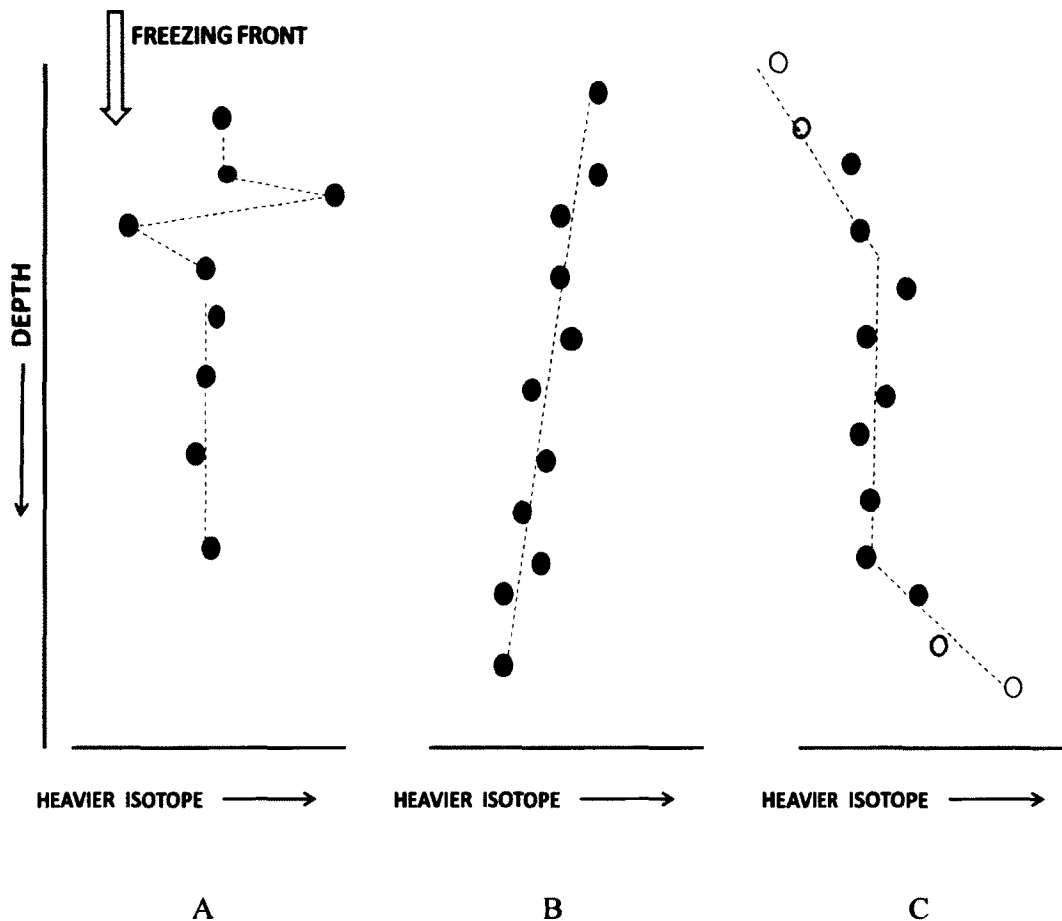
Figure 1.2 Fractionation data profile patterns.

A. Double peak (fractionation caused by change in freezing front speed,
   Suzuoki and Kemura, 1973)
B. Slanted (mixing zone, Michel, 1982)
C. Slanted-vertical, vertical-slanted or slanted-vertical-slanted
   (different waters, different freezing events)

develop a different data profile prior to freezing. Figure 1.2C is an illustration of a

hypothetical profile where there could have been 3 events; mixing zone, homogenous

water, different mixing zone. This pattern is also not caused by fractionation, but

represents isotopically different waters.

Context is important to interpreting the environmental effects that produce a

particular profile in an isotope data chart. For instance, if fire effects are suspected, the

site has to be capable of supporting fire, or if the data seem to indicate the presence of a

lake, there should be appropriate terrain for a lake. With environmental factors in mind,

and by identifying the various processes that produce the fractionation peaks and data

profiles of water isotope data in a soil sample, the relative sequence of events that

produced the data can sometimes be determined.

CHEMISTRY OF PERMAFROST WATERS

Water extractable chemistry, nitrogen and carbon contents of the soils and

magnetic susceptibility of core sections provide a chemical picture of the permafrost

matrix at the sample sites. The relationships among the chemical analyses done on the

cores help to define the environmental history of the sites, supplementing the water

isotope data. Statistical comparisons of the chemical analyses done on water from two

cores taken in the Copper River Basin help to confirm that some of the permafrost water

in the one of the cores had a different source from the water in the other core. Some of

the analyses at the Fairbanks site record trends relating to changes that may have

occurred in geologic time. In particular, increases in those parameters related to soil

formation indicate depths where pedogenesis occurred in the core. Comparing those depths with analytical results from similar depths from prior studies in the area makes it possible to define possible ages for certain depths in the core. Certain water isotope signatures indicate processes that would be most likely to occur close to the ground surface, and so suggest that the permafrost was formed at a time when the ground surface was nearer to the 6.1 m depth of the current permafrost table.

Permafrost signature information is unique and specific to the particular situation under which the permafrost formed. The addition of water chemistry information to the isotopic data helps confirm what those particular circumstances were. Comparison of data from more than one source at a site also helps confirm the conditions under which the permafrost formed. Two cores were taken from each of the two study sites in this investigation. Data from the Fairbanks site are from two cores from different depths with different local conditions, and also include additional samples from augered material. The two cores from the Copper River Basin site go to more similar depths, and provide comparisons for isotope and chemical data.

LITERATURE CITED

Brown, J., O. J. Ferrians, Jr., J. A. Heginbottom and E. S. Melnikov. 1997. *Circum-Arctic Map of Permafrost and Ground Ice Conditions.* U.S. Geological Survey for the International Permafrost Association, USGS Circum-Pacific Map Series, scale 1:10,000,000, Map CP-45.

Brown, J. and C. Haggerty. 1998. Permafrost Digital Databases Now Available, Eos Trans. AGU, 79(52), 634, doi:10.1029/98EO00451.

Davis, T.N. 2000. *Permafrost, A Guide to Frozen Ground in Transition.* University of Alaska Press. Fairbanks. 351 pages.

Fritz, P. and F.A. Michel. 1977. Environmental isotopes in permafrost related waters along two proposed pipeline routes. Report on Project No. 606-12 for Canada Department of Energy, Mines and Resources, File No. 05SU.23235-6-0681, Waterloo Research Institute, University of Waterloo. 51 pages.

Hinzman, L.D., N.D. Bettez, W.R. Bolton, F.S. Chapin, M.B. Dyurgerov, C.L. Fastie, B. Griffith, R.D. Hollister, A. Hope, H.P. Huntington, A.M. Jensen, G.J. Jia, T. Jorgenson, D.L. Kane, D.R. Klein, G. Kofinas, A.H. Lynch, A.H. Lloyd, A.D. McGuire, F.E. Nelson, W.C. Oechel, T.E. Osterkamp, C.H. Racine, V.E. Romanovsky, R.S. Stone, D.A. Stow, M. Sturm, C.E. Tweedie, G.L. Vourlitis, M.D. Walker, D.A. Walker, P.J. Webber, J.M. Welker, K. Winker and K. Yoshikawa. 2005. Evidence and implications of recent climate change in northern Alaska and other arctic regions. Clim. Change, 72, 251-298.

Jorgenson, M.T., V. Romanovsky, J. Harden, Y. Shur, J. O'Donnell, E.A.G. Schuur, M. Kanevskiy and S. Marchenko. 2010. Resilience and vulnerability of permafrost to climate change. Can. J. For. Res. 40:7, 1219-1236.

Lee, H., E.A.G. Schuur and J.G. Vogel. 2010. Soil CO_2 production in upland tundra where permafrost is thawing. J. Geophys. Res. 115, G01009, doi:10.1029/2008JG000906. 11 pages.

Mackay, J.R. 1972. Offshore permafrost and ground ice, southern Beaufort Sea, Canada. Can. J. Earth Sci., 9, 1550-1561.

Mackay, J.R. and L.W. Lavkulich. 1974. Ionic and oxygen isotopic fractionation in permafrost growth. Geol. Surv. Can., Paper 74-1B, 255-256.

Michel, F.A. 1982. Isotope investigations of permafrost waters in northern Canada. Ph.D. dissertation, University of Waterloo, Waterloo, Ontario. 424 pages.

Michel, F.A. and P. Fritz. 1982. Significance of isotope variations in permafrost waters at Illisarvik, N.W.T. *In*: Proceedings of the Fourth Canadian Permafrost Conference, Calgary, Alberta. 173-181.

O'Neil, J.R. 1968. Hydrogen and oxygen isotope fractionation between ice and water. J. Phys. Chem., 72:10, 3683–3684.

Osterkamp, T.E. and V.E. Romanovsky. 1999. Evidence for warming and thawing of discontinuous permafrost in Alaska. Permafrost and Periglacial Processes, 10, 17-37.

Osterkamp, T E., V.E. Romanovsky, T. Zhang, V. Gruol, J.K. Peterson, T. Matava and G.C. Baker. 1998. A history of continuous permafrost conditions in Northern Alaska. Invited paper. EOS, Transactions of the American Geophysical Union, 79: F833.

Osterkamp, T.E., M.T. Jorgenson, E.A.G. Schuur, Y.L. Shur, M.Z. Kanevskiy, J.G. Vogel and V.E. Tumskoy. 2009. Physical and ecological changes associated with warming permafrost and thermokarst in Interior Alaska. Permafrost and Periglacial Processes, 20, 235–256.

Pearson, R.W. and M. Hermans, eds. 2008. *Alaska in Maps: A Thematic Atlas*. CD-ROM. Fairbanks: University of Alaska Fairbanks.

Romanovsky, V. 2009. Establishing permafrost observatory at the HAARP site. Final report to the ONR. 22 pages.

Schaefer, K., T. Zhang, L. Bruhwiler and A. P. Barrett. 2011. Amount and timing of permafrost carbon release in response to climate warming. Tellus B 63, 165-180.

Schuur, E.A.G., J.G. Vogel, K.G. Crummer, H. Lee, J.O. Sickman and T.E. Osterkamp. 2009. The effect of permafrost thaw on old carbon release and net carbon exchange from tundra. Nature 459, 556-559.

Stuiver, M., I.C. Yang and G.H. Denton. 1976. Permafrost oxygen isotope ratios and chronology of three cores from Antarctica. Nature 261, 547-550.

Suzuoki, T. and T. Kemura. 1973. D/H and $^{18}O/^{16}O$ fractionation in ice-water system. Mass Spectroscopy 21:3, 229-233.

Vogel, J., E.A.G. Schuur, C. Trucco and H. Lee. 2009. Response of CO_2 exchange in a tussock tundra ecosystem to permafrost thaw and thermokarst development. J. Geophys. Res. 114, G04018, doi: 10.1029/2008JG000901. 14 pages.

Walter, K.M., S.A. Zimov, J.P. Chanton, D.Verbyla and F.S. Chapin III. 2006. Methane bubbling from Siberian thaw lakes as a positive feedback to climate warming. Nature 443, doi:10.1038/nature05040, 71-75.

Willliams, P.J. and M.W. Smith. 1989. *The Frozen Earth, Fundamentals of Geocryology*. Cambridge University Press. Cambridge. 306 pages.

Chapter 2

Chemical and Isotopic Investigation of Cores from
Lake Atna Lake Bed, Copper River Basin, Alaska

INTRODUCTION

The Copper River Basin in south-central Alaska is an intermountain basin of over

13,000 km^2 in area (Ferrians, 1989) surrounded by mountains; the Alaska Range lies to

the north, the Talkeetna Mountains to the west, the Wrangell Mountains to the east and

the Chugach Mountains to the south. The Copper River bisects the Chugach Mountains

on its way to the Gulf of Alaska. The Copper River drainage is the largest into the Gulf

of Alaska.

The basin is located near the southern limit of the Alaskan permafrost zone but

most of it lies north of the Chugach Mountains, which gives it a continental climate

similar to interior Alaska due to being in a rain shadow of the surrounding mountains

(Riordan et al., 2006). The mean annual air temperature is cold enough so that

permafrost is widespread (Romanovsky, 2009). From the first reconnaissance study done

in 1898 (Schrader, 1900), it was recognized that the basin deposits were glaciolacustrine

in nature. Several times during the Pleistocene, glaciers advanced down the surrounding

mountains and dammed the outflow rivers, thereby forming large paleolakes in the basin.

The latest (known as Lake Atna) formed more than 58,600 ± 1100 ^{14}C yr BP (Ferrians,

1984).

Studies of the Copper River Basin have tended to concentrate on the nature of the basin sediments (Bennett et al., 2002; Williams and Galloway, 1986), or the glaciers that blocked the river drainage from the basin to form huge lakes (Ferrians, 1989; Kaufman and Manley, 2004; Nichols, 1989; Wiedmer et al., 2010; Williams, 1989). This study focuses on the permafrost ice of the basin glaciolacustrine deposits, which are among the most ice rich developed in the last glaciation (Romanovsky, 2009), making them ideal for water isotope research on ancient pore ice related to Lake Atna.

Isotopic analyses for $\delta^{18}O$ and δD of two cores drilled near the HAARP (High Frequency Active Auroral Research Program) Permafrost Observatory in the Copper River Basin provide evidence for not only glacial source water for Lake Atna, but also suggest formation of a pond or smaller lake after Lake Atna drained, and indicate that a forest fire occurred after both bodies of water were overgrown with vegetation.

SITE HISTORY AND DESCRIPTION

The highest Lake Atna sediments, suggesting the highest lake level, are at about 975 m amsl (above mean sea level) at the northwestern part of the basin, but the highest *prolonged* lake elevation indicated by sediments is at about 914 m amsl. Between 32,000 and 25,000 years ago the lake level lowered with some fluctuations to approximately 747 m, as indicated by shorelines, and persisted at that elevation until the glaciers receded. At the 747 m lake level the area of Lake Atna would have been over 9,000 km^2 (Williams and Galloway, 1986). The ultimate drainage date of the lake due to the failure of ice dams is difficult to determine with accuracy, but various times have been

published, including 11,090-10,270 yr BP (Rubin and Alexander, 1960), around

14,000 yr BP (Williams, 1989), and 9,400±300 yr BP (Ferrians, 1989).

The sedimentary record in the lake bed (the unconsolidated material above an

impermeable base) is complicated, being dominated by a series of subaqueous fans

produced by gravity-driven processes including slumping, debris flow, density flows and

turbidity currents, and further complicated by erosion and flushing of sediment from the

basin by catastrophic lake drainages (Bennett et al., 2002). Aside from the variable facies

architecture (which appear as non-homogenous mixed clasts in cores), the lake bed

deposits are rich in perennial ice (Bennett et al., 2002, Romanovsky, 2009).

Permafrost was completely thawed under the deep and large ice-dammed lake

formed during the last glaciation (Romanovsky, 2009). After the lake drained,

permafrost of high ice content formed in the lake deposits and has persisted to this day,

becoming a serious engineering problem for construction in the basin (Romanovsky,

2009). Building sites, parking areas and roads require removal of the vegetation that

insulates the ice-rich soil from solar radiation and replacing it with structures that

increase heat flow into the ground. Permafrost in such areas thaws and with the loss of

ice, the soil deflates and the ground settles unevenly, often producing thermokarst pits in

the most ice-rich areas (Shur and Zhestkova, 2003; Osterkamp et al., 2000).

The HAARP Permafrost Observatory is located about 2 km west of the Copper

River in the upper part of the Copper River Basin, approximately 300 km south of

Fairbanks, Alaska and north of the junction of the Gakona and Copper Rivers, (Figure

2.1; Pearson and Hermans, 2008). The Observatory was established by Dr. Vladimir

**Figure 2.1 Copper River Basin. Study site is indicated by star.
Dashed line outlines approximate extent of Lake Atna.**

Romanovsky in 2003 to provide information on permafrost and other environmental dynamics within the HAARP site, to insure the safe running of the HAARP project, and to assess permafrost response to changing climate (Romanovsky, 2009). Researchers from the University of Alaska Fairbanks Geophysical Institute associated with the Permafrost Laboratory have made observations on permafrost degradation near the HAARP project antenna array. Ground temperature measurements near the array were made to determine original permafrost degradation at the time it was installed. A number of boreholes were drilled in 2003 for various measurements including water content and air temperature in addition to ground temperature. DC resistivity and ground penetrating radar were also used to investigate permafrost distribution within the array and the adjacent area. The DC resistivity survey shows that permafrost beneath forest cover is stable, but under some man-made structures the ground appears to be unfrozen or else contains a significant amount of unfrozen water. Ground penetrating radar confirms this result (Romanovsky, 2009).

The ground surface in the area of the Observatory is generally flat although it slopes gently to the south and southeast towards the Copper River. Dominant vegetation at the site is black spruce and sedge (Connor, 1984). The sedge grows in 10 m to 800 m wide open bands, running generally NE to SW (Romanovsky, 2009), and visually forms a light green channel through the forest. Due to the near-surface permafrost in the area, these channels may define actual drainage of surface run-off, where water content is too high for trees to grow.

SAMPLE COLLECTION AND PREPARATION

In the fall of 2007 after freeze-up, a core was drilled in the same general area as the HAARP monitoring equipment (62.3947° north latitude, 145.15687° west longitude, ~573.7 m asl, Figure 2.2). The core was meant to go to the full depth of the permafrost as long as there was either water or ice in the sediment. At a depth of 15 m the drilling equipment failed. The core already collected was saved, and after equipment repairs another core was taken at a location about 400 m north of the original core (62.4115° north latitude, 145.1474° west longitude, ~576.9 m asl). The depth of ice-rich permafrost in the second core was 19 m. Drilling was continued to a depth of over 40 m, but below 19 m the sediment had become consolidated, being coarse, dense and without ice or water content.

Temperature measurements monitored in the second borehole showed deep permafrost, to more than 45 m depth, but coring did not go to the bottom of the permafrost. The total depth of the permafrost has been estimated to be from 45 to 55 m using the temperature gradient (Figure 2.3). The 2007 temperature data were collected right after drilling so the upper part of the permafrost was still thermally disturbed. Later data show that the borehole reached equilibrium with the surrounding material (V.E. Romanovsky, personal communication, January 16, 2012).

The two cores were transported to the University of Alaska Fairbanks in insulated containers and were kept frozen for analyses to complement the data gathered on site. The total core lengths that were actually sent to the University were from 1.57 m (starting depth) to 14.78 m (total core depth) for core H1 (the original core) and 5 cm (starting
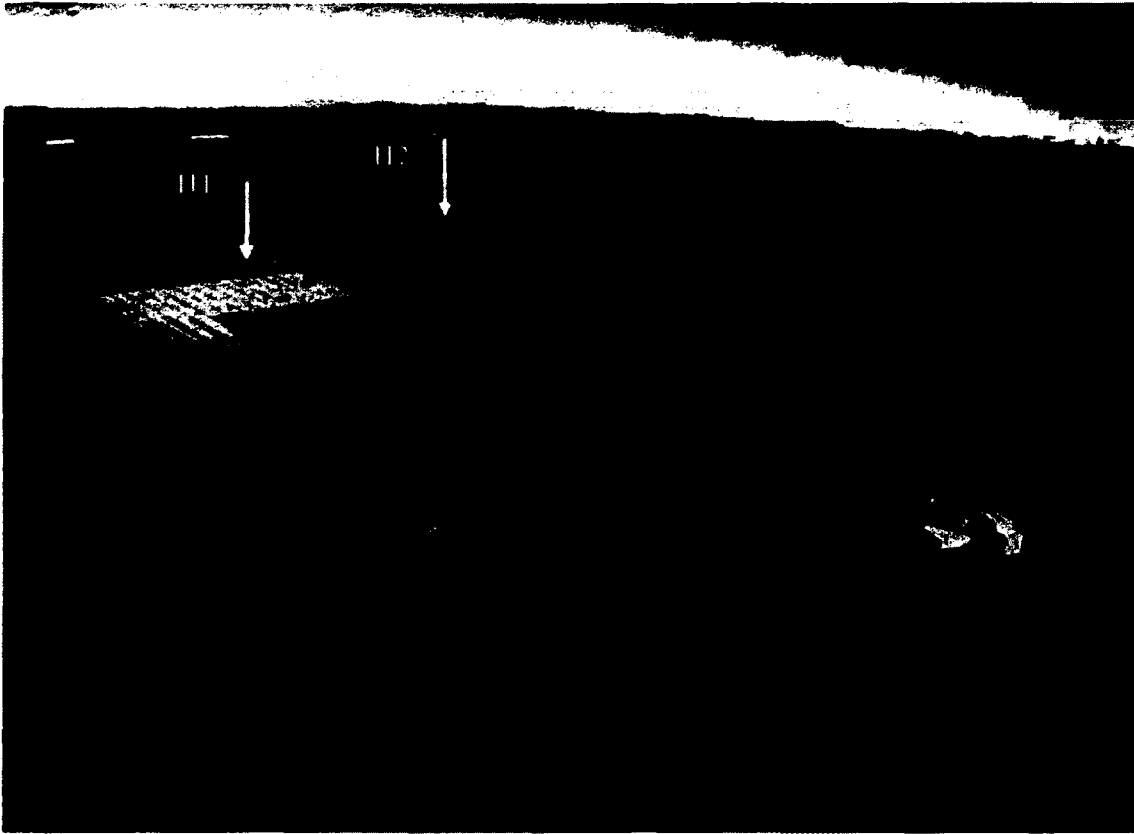
Figure 2.2 Locations of core H1 and core H2 at HAARP research site. (*Photo by Marty Karjala.*)
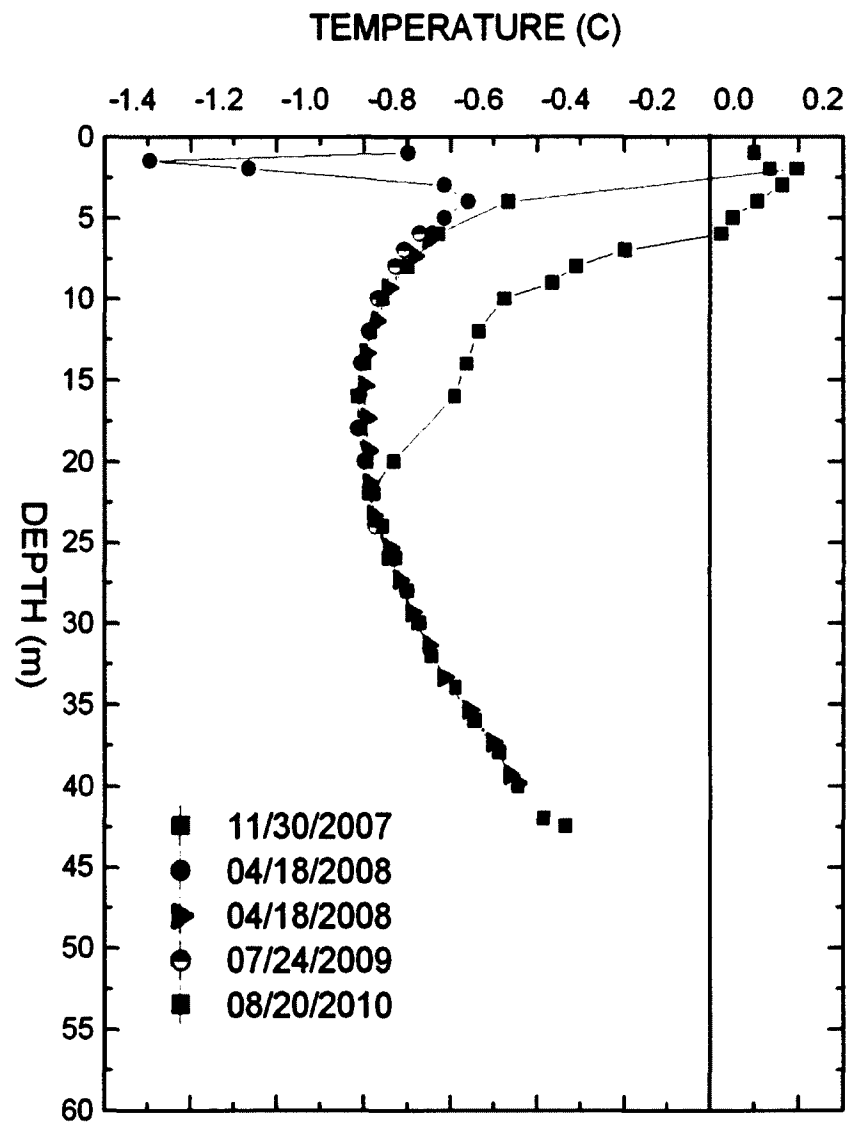
**Figure 2.3 Borehole temperatures for core H2. Temperature
variations for 2007 reflect disturbance due to drilling.
(*Figure courtesy of V.E. Romanovsky*).**

depth) to 19.11 m (total core depth) for core H2 (the second core). The core diameters

were approximately 8 cm.

The cores had been separated at the drilling site into approximately half-meter

core sections which were stored in plastic sleeves and labeled for core number (1 or 2),

depth from top of core, and length of core section. Five centimeter samples were taken at

approximately 30 cm intervals from the two cores by researchers from the Institute of

Northern Engineering (INE) for water content analysis. The remaining material was

returned to the plastic sleeves and stored in freezers.

After being transferred to the Forest Soils Laboratory, core samples for chemical

and water isotope analysis were taken every 10 cm down each section, starting 5 cm from

the top of the section. Wafers of about 1 cm thickness were broken off from the lower

part of each subsample with a chisel. Small rocks and gravel were removed from the

wafers before they were transferred into numbered Whirl-pak™ plastic bags. The bagged

samples were labeled with sequential numbers as samples were taken from each section

subsample, and the numbers were recorded along with the section information. The bag

numbers were sequential for each individual section, but core sections were drawn from

the freezer randomly so that sample numbering was neither entirely sequential nor

entirely random. The sample bags were placed into a freezer as soon as each core section

was sampled.

Other than samples collected by INE researchers from both cores, missing core

sections include the first 157 cm of core H1 and 76 cm from core H2 that appears to be

the second section from the top of the core. Neither of these sections appears to have been collected.

LABORATORY ANALYSIS

Oxygen and Hydrogen Isotopes

Samples were prepared to be analyzed by an *in situ* method (Koehler et al., 2000), which allows water isotopes to be analyzed without extracting the water from the soil sample. Subsamples were taken from several sample bags and were weighed, dried at 65° C for 48 hours and reweighed to determine water content. The gravimetric water content from these subsamples ranged from 20% to 25% so the calculated amount of frozen soil to be weighed for analysis was about 2.5 g in order to analyze approximately 0.5 ml water. Three replicates were prepared from each sample by taking the frozen wafers from the freezer, cutting small pieces off the wafer with garden clippers and weighing the pieces into an exetainer vial (Labco Intl. Inc.) until there was about 2.5 g of material. The weight was recorded and the vial was firmly sealed with a cap lined with a pierceable rubber wad. The exetainer samples were kept frozen until analysis.

The samples were analyzed at the University of Alaska Fairbanks Forest Soils Laboratory on a PDZ Europa GEOS 20-20 isotope ratio mass spectrometer with a Gilson autosampler using the equilibration method for water analysis (Scrimgeour, 1995). A small vial insert with about 2 g of 5% platinum on alumina was added to both sample and reference exetainers to catalyze hydrogen equilibration for deuterium analysis. The exetainers were purged with hydrogen and allowed to equilibrate for three days before

being analyzed for δD using the mass spectrometer. After deuterium analysis the same

samples were purged with bone-dry carbon dioxide and equilibrated overnight before

being analyzed for $\delta^{18}O$. Analytical results were normalized for oxygen and hydrogen

isotope data as described by Coplen (1988).

Water Content

After isotope analysis, sample exetainers were uncapped and the vial inserts were

removed before the samples were placed in an oven at 65° C for a minimum of 48 hours

and then weighed. Dry weights were compared to the original wet weights in the

exetainers to determine the individual sample water content. The three replicate water

contents were averaged to give percent water on a wet weight basis for each subsection.

The dried material in the three replicate exetainers for each sample was combined and

roughly broken up before being placed into a new Whirl-pak™ bag that was once again

labeled with the original sample number.

Chemical Analyses

(N, C, pH, Conductivity, K, Ca, Mg, Fe, and Bicarbonate)

Nitrogen and carbon were analyzed from the dried recombined samples on a

LECO Truspec CN analyzer that measures percent carbon from combustion products of a

950° C burn cycle using a CO_2 infrared detector and percent nitrogen from gases of the

same burn that are passed through a thermal conductivity cell.

The other chemical analyses were done on solutions of the recombined samples. Five grams of material were weighed into a 15 ml test tube and 5 mls of distilled water added (1:1 dilution). The samples were capped and thoroughly mixed by shaking for one hour on a reciprocating shaker. The shaken samples were analyzed for pH using an Oakton pH/CON 510 series combination pH/Conductivity/TDS/°C/°F meter. For conductivity analysis 5 more milliliters of distilled water were added to each sample test tube (2:1 dilution) in order to accommodate the short length of the conductivity probe. The tubes were hand shaken about 10 times to mix the added water, and the samples were analyzed for conductivity using the same Oakton pH/CON 510 meter. The contents of each test tube were then rinsed into a 125 ml polyethylene bottle and about 30 ml of distilled water added. The bottles were shaken on a reciprocating shaker for a minimum of 30 minutes before the samples were filtered through Whatman GF/A filter paper. The solids were discarded and the filtrate brought to 100 ml with distilled water (20:1 dilution). Each liquid sample was divided into a 15 ml subsample for spectroscopic analysis, and a 50 ml subsample for titration for bicarbonate (Jackson, 1958, Rhoades, 1982).

The 50 ml subsample was analyzed by titration for meq/l bicarbonate. The 15 ml subsample was analyzed on a ThermoElemental Iris DCP Direct Current Plasma spectrometer for mg/l of K, Ca, Mg and Fe.

RESULTS

Percent Water Content

Core H1 %H_2O (Figure 2.4A) has an initial spike in water content (77.01%) at

1.78 m depth, but the remainder of the core shows relatively small fluctuations, varying

from 31.98% (at 2.34 m) to about 9% (at several depths below 8.13 m). The overall

average is 16.3%. Below a depth of 3.80 m moisture content is typically less than 20%,

with an average of about 14.4%, including a change of %H_2O at depths 10.31 m through

11.73 m where the moisture content rises to almost 30% before dropping back to less

than 20%. Standard deviation is 7.9% for the moisture contents of the full length of the

core (Table 2A-1).

Core H2 is has seven spikes where the moisture content is over 40% (Figure

2.4B) which occur between 4.93 m and 14.22 m depth, with the largest spike being

98.51% at 5.38 m. Average moisture content for the whole core is 19.9%. Excluding the

seven spikes, moisture contents average 17.6%. The general trend is for moisture

contents to gradually decrease from around 20% to less than 15% at the bottom of the

core. Standard deviation is 12.3% for the full length of the core. Excluding the seven

spikes, standard deviation is 4.9% (Table 2A-2).

Oxygen Isotopes

The isotope analytical method used for this study has shown that samples with

water contents of 10% or less may give ambiguous results (Koehler et al., 2000);

2.4A Core H1

2.4B Core H2
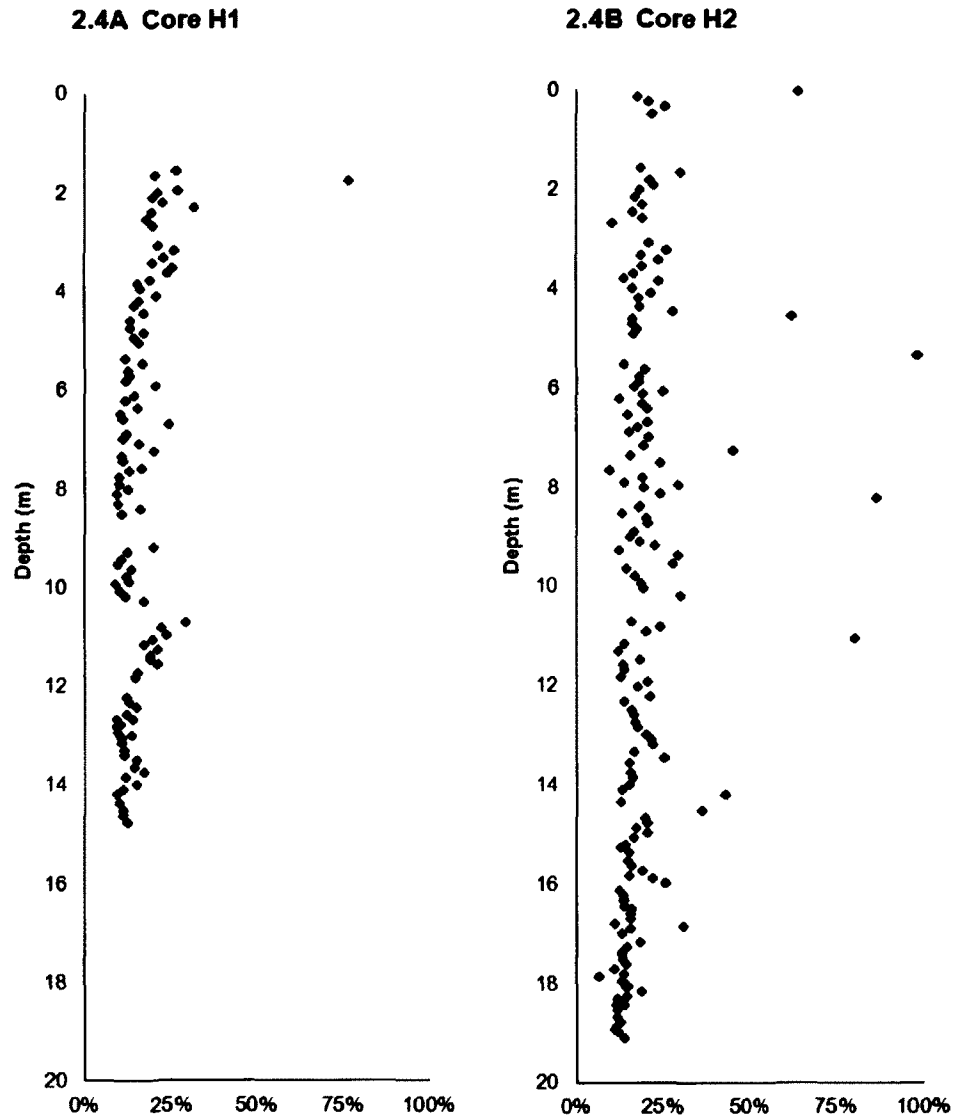
Figure 2.4 Gravimetric % water content, Lake Atna core H1 and H2.

therefore, for the isotopic data, those samples with less than 11% water content were eliminated from data analysis.

Inspection of the data for $\delta^{18}O$ water stable isotopes of core H1 (Figure 2.5A) shows the isotope values start at an isotopically light $\delta^{18}O$ value (less than -19‰), but at 2.69 m depth increase to -17.46‰. Immediately after this relatively enriched sample, the values drop and vary between -19‰ and -18‰ to a depth of 7.67 m. Below 7.67 m $\delta^{18}O$ values generally decrease again to values lower than -19‰ and continue at near that value for the length of the core (14.78 m) except for a few spikes of enriched $\delta^{18}O$ values (-17.85‰ at 8.43 m, -17.99‰ at 9.20 m, -17.89‰ at 11.73 m, -16.48‰ at 11.84 m and -17.95‰ at 14.53 m). The spikes between 8 m and 10 m are from samples surrounded by soil too dry to provide reliable isotope data, which makes the included values less reliable as well. When the spikes and the values above 3.10 m depth are excluded, the data plots on a generally linear trend from - 18.19‰ at 3.10 m to -19.62‰ at 14.63 m.

The average $\delta^{18}O$ value for the entire length of core H1 is -18.8‰, with a standard deviation of 0.7‰. If the excluded low water content samples are included, the average $\delta^{18}O$ value for the entire length of core H1 is -18.7‰, with a standard deviation of 0.8‰. The average for the lighter section at the top of the core (from 1.57 m to 2.59 m) is -19.1‰ with a standard deviation of 0.8‰ (Table 2A-3).

Inspection of the core H2 data for $\delta^{18}O$ water isotopes shows the isotope values vary significantly in several parts of the core (Figure 2.5B). There is a cluster of $\delta^{18}O$ values between -19‰ and -18‰ at the very top of the core (down to 0.51 m). Below the

2.5A. Core H1

2.5B. Core H2
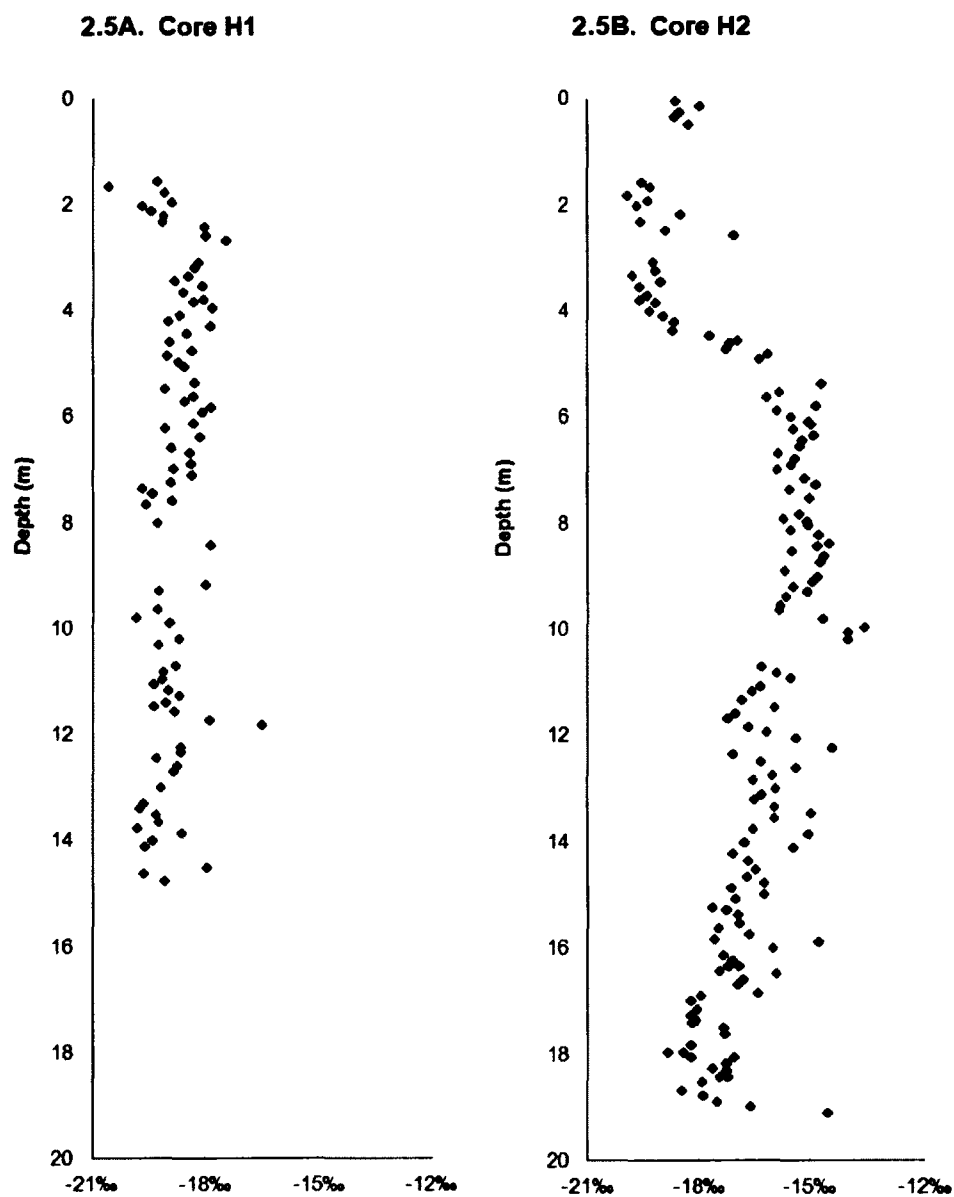
Figure 2.5 Lake Atna core H1 and core H2 $\delta^{18}O$ values in ‰
relative to VSMOW.

data gap that exists from 0.51 m to 1.58 m there are several values less than -19‰ and then there is an abrupt spike of enriched samples (-18.48‰ at 2.18 m, -17.09‰ at 2.59 m), followed by an equally abrupt drop in value to -19.21‰ at 3.10 m. From 3.10 m to 5.90 m the $\delta^{18}O$ values increase steadily from -19.21‰ to -15.89‰. Below 5.90 m to 9.65 m the data is fairly steady around a value of about -15‰. At 9.96 m the data spikes to -13.55 ‰ and then abruptly decreases to about -16.33‰ at 10.72 m depth. From that point to the bottom of the core $\delta^{18}O$ values decrease gradually and steadily to -17.87‰ at 18.80 m. The data are more variable in the lower portion of the core (from 10.21 m to 19.11 m) so spikes are less obvious, but at the very bottom of the core (19.11m) there is a $\delta^{18}O$ spike of -14.50‰.

The average of $\delta^{18}O$ values for the full length of core H2 is -16.7‰ with a standard deviation of 1.5‰. If excluded low water content samples are included the average of $\delta^{18}O$ values for the full length of core H2 is -16.8‰ with a standard deviation of 1.5‰. The average for the lighter section at the top of the core (from 1.57 m to 2.59 m) is -19.1‰ with a standard deviation of 0.9‰ (Table 2A-4).

Deuterium

Deuterium values are variable throughout core H1 (Figure 2.6A). In a very general way deuterium trends from light (-173.37‰ at 1.78 m) to heavy (-125.83‰ at 5.84 m) then shifts back to lighter values (between -160‰ and -140‰ from 6.40 m to 13.00 m) with only 3 values that stand outside the general range (-123.84‰ at 9.80 m,

2.6A. Core H1

2.6B. Core H2
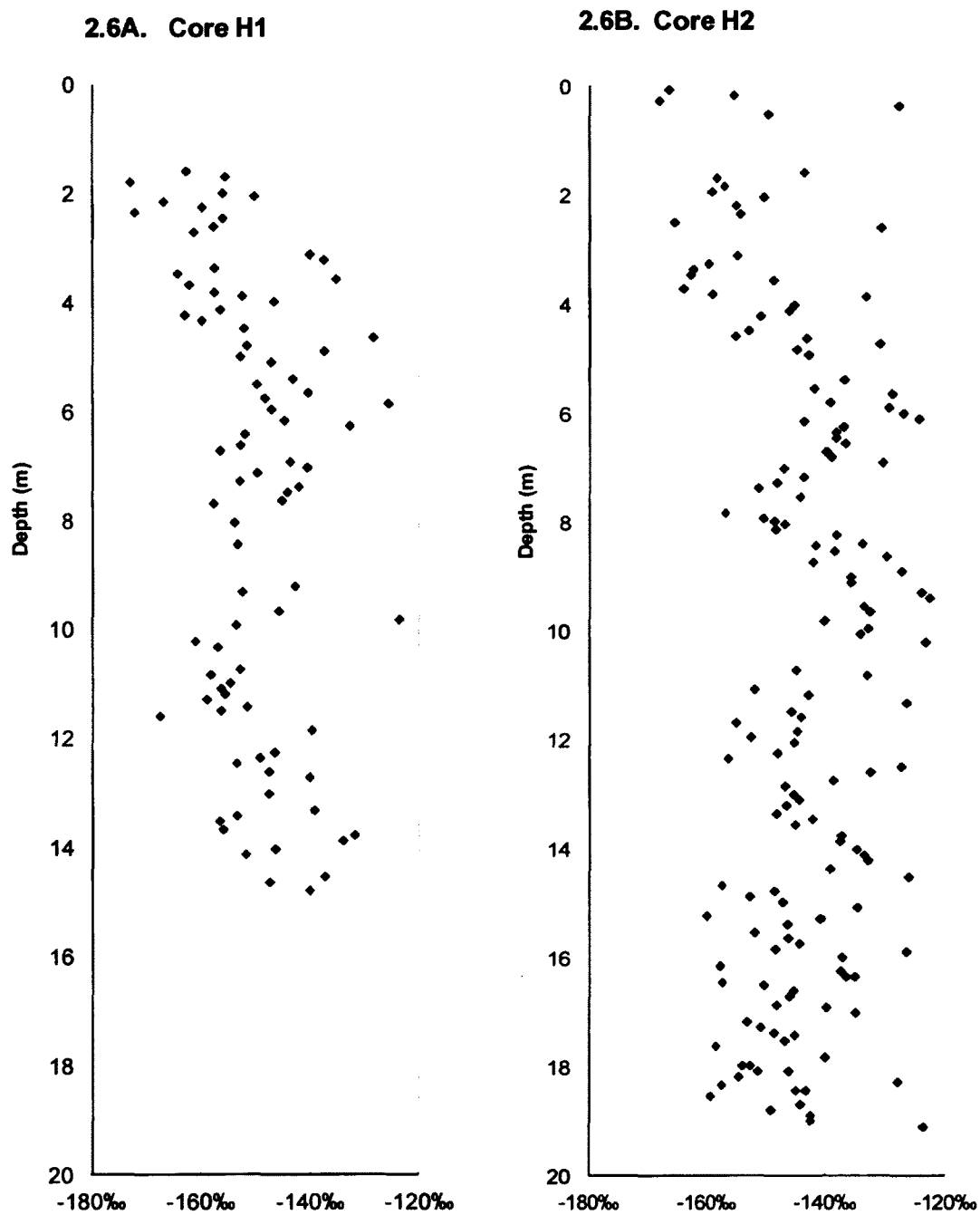
Figure 2.6 Lake Atna core H1 and core H2 δD values in ‰ relative to VSMOW.

-119.87‰ at 11.73 m and -167.83‰ at 11.58 m). Below 14 m the trend appears to be toward heavier values again, but the data ends before that is clear.

The average δD value for the entire length of core H1 is -149.8‰, with a standard deviation of 10.5‰. If the excluded low water content samples are included, the average δD value for the entire length of core H1 is -147.9‰, with a standard deviation of 11.7‰.

The average for the lighter section at the top of the core (from 1.57 m to 2.59 m) is -161.4‰ with a standard deviation of 7.6‰ (Table 2A-3). Inspection of the data for deuterium water isotopes of core H2 shows the isotope values vary throughout the core with only one distinct section (Figure 2.6B). In general, the values are slightly lighter in the first section of the core, (from 0.05 m to 6.81 m), ranging from -168.00‰ at the top of the core (0.25 m) to -124.21‰ at 6.10 m. There are a few samples that appear to be enriched in this section, (-127.55‰ at 0.36 m, -130.55‰ at 2.59 m, -133.02‰ at 3.86 m and -117.76‰ at 4.38 m). The distinct section occurs between 6.15 m and 9.20 m where the data values decrease sharply to -156.57‰ at 7.83 m, and then rise just as sharply to as high as -119.21‰ at 9.20 m. Below 9.20 m the values drop back to varying between -160‰ and -120‰ without apparent pattern. The very last sample, however, is noticeably enriched (-123.66‰ at 19.11 m) compared to the samples above it in the core. The average of δD values for the full length of core H2 is -143.2‰ with a standard deviation of 10.9‰. If the excluded low water content samples are included, the average of δD values for the full length of core H2 is -143.2‰ with a standard deviation of 10.8‰. The average of δD values for samples between 1.57 m and 2.59 m, is -152.4‰ with a standard deviation of 10.3‰ (Table 2A-4).

Cations (Ca, Fe, K, Mg)

Core H1 concentrations of cations (Ca, Fe, K, and Mg) were less than 1 mg/l

except for a single data point for iron at 4.11 m depth, which had a value of 1.460 mg/l,

which was the highest cation concentration for any of the core samples (Figure 2.7A).

Generally, iron and calcium had higher concentrations than magnesium or potassium, but

concentrations of all cations from core H1 tended to vary between 0.1 and 0.5 mg/l.

Average of all concentration values from core H1 for calcium was 0.46 mg/l, with

a standard deviation of 0.14 mg/l. Average for magnesium was 0.19 mg/l, with a

standard deviation of 0.09 mg/l. Average for potassium was 0.23 mg/l, with a standard

deviation of 0.07 mg/l. Average for iron was 0.34 mg/l with a standard deviation of

0.22 mg/l (Table 2A-5).

In core H2 the first potassium data point at the very top of the core (0.05m) has a

concentration of 1.240, the only measured cation in core H2 with a concentration over

1 mg/l (Figure 2.7B). However, the concentration of calcium at the next lower depth

(0.15 m) is also elevated (0.987 mg/l). For the rest of the depth of the core there are no

other measured cation concentrations over or near to 1 mg/l. The concentrations for Mg,

Fe and K below 16 cm are well below 0.5 mg/l and are fairly consistent with each other.

Calcium concentrations are higher at the top of the core than the concentrations of the

other three cations, but drop steadily down the core. At a depth of about 12 m the

calcium data no longer has a generally higher concentration compared to the other cations

(Table 2A-6).

2.7A. Core H1 **2.7B. Core H2**
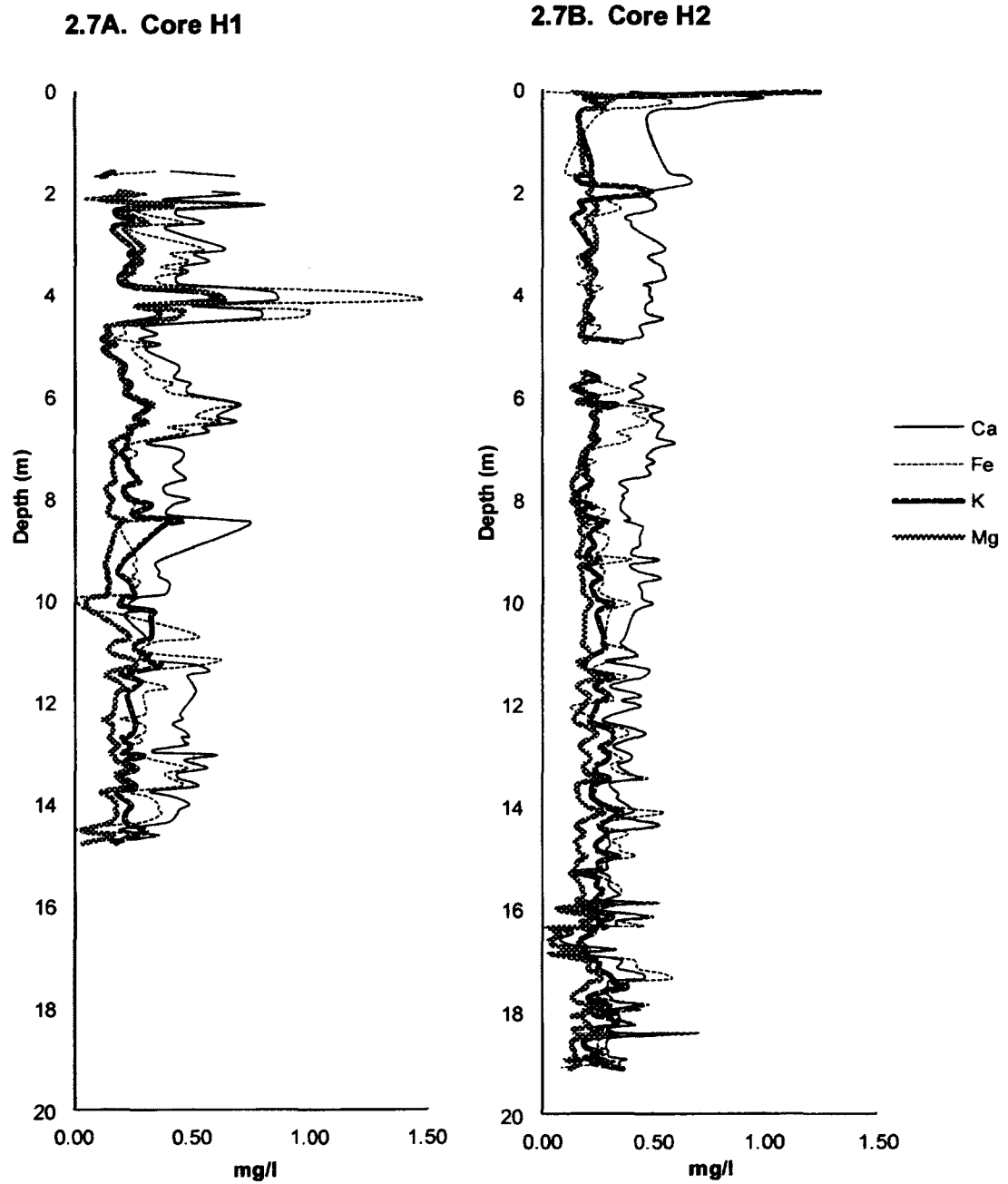
Figure 2.7 Lake Atna core H1 and core H2 cation values in mg/l.

There is one anomaly in the data; from 16.36 m to 16.92 m depth all cation values except potassium are noticeably lower than at any other depth in the core. Aside from these samples, the other data for H2 cations generally plot between 0.1 and 0.5 mg/l.

The average calcium concentration for core H2 is 0.41 mg/l with a standard of 0.12 mg/l. The magnesium value is 0.18 mg/l with a standard deviation of 0.05 mg/l. The average potassium value is 0.24 mg/l with a standard deviation of 0.10 mg/l. The average iron value is 0.29 mg/l with a standard deviation of 0.12 mg/l.

pH

There were no measured pH values less than 7.36 in core H1 samples (Figure 2.8A). Near the top of the core the values are more acidic, but they shift from 7.36 to 8.07 within less than a meter increase in depth. Most of the pH values below 3.10 m depth are slightly over 8.0, but below about 11.5 m there is a gradual increase in pH to about 8.6. These values drop below 8 again at the very bottom of the core. For core H1, pH values average 8.2 with a standard deviation of 0.2 (Table 2A-7).

Almost all of the pH values of core H2 are all slightly over or just under 8, the average being 8.2, with a standard deviation of 0.3 (Figure 2.8B). There are a few more acidic values at the surface of the core, even one below 7.0, which would not be unusual for an organic horizon source of mosses or a coniferous forest floor. The pH values tend to increase slightly with depth, going from below 8 at 1.93 m depth to over 8.5 for much of the bottom 1.5 m of the core (Table 2A-8).

2.8A. Core H1

2.8B. Core H2
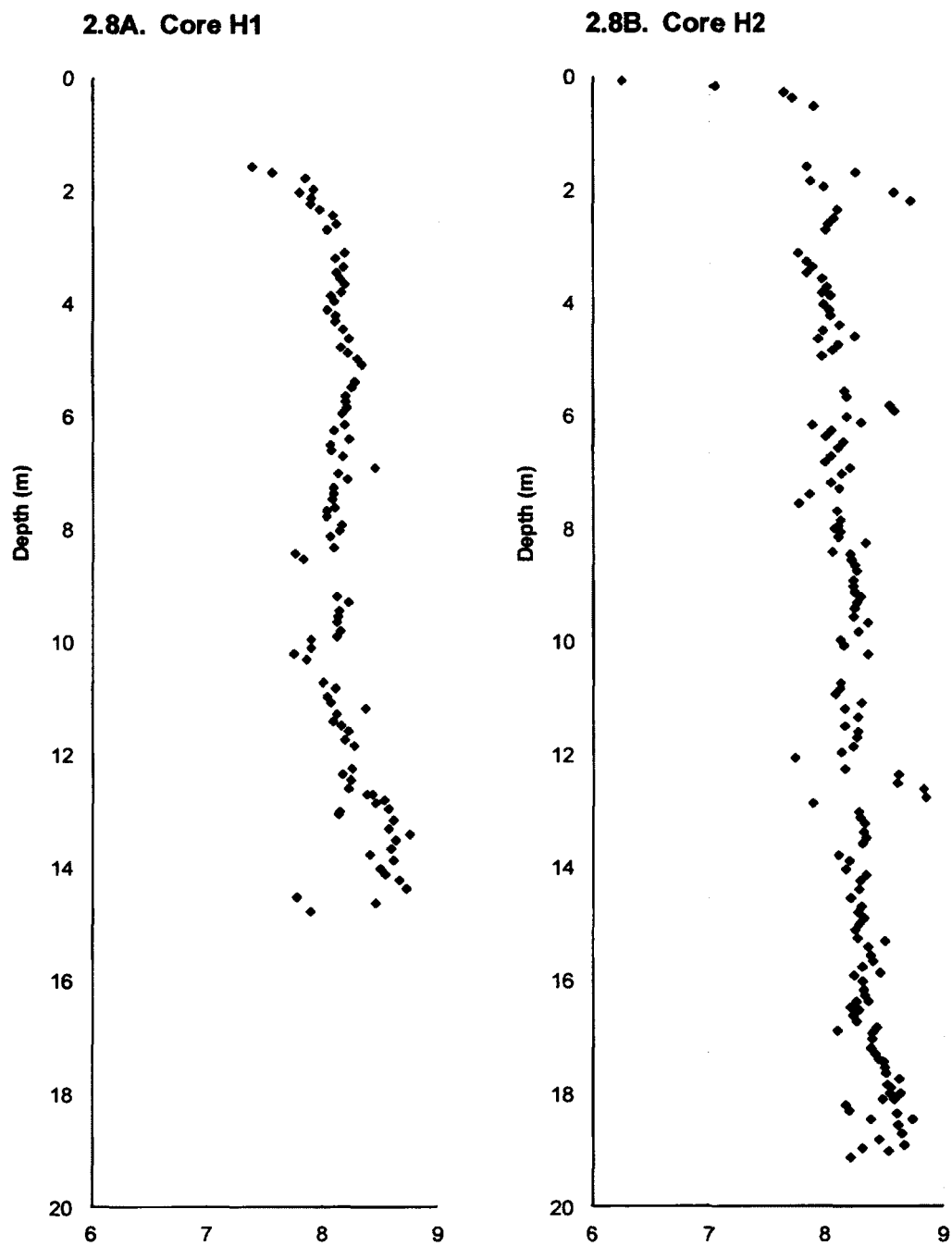
Figure 2.8 Lake Atna core H1 and core H2 pH values.

Conductivity

For core H1, conductivity averages 189 μS/cm with a standard deviation of

47 μS/cm (Figure 2.9A). Even though the variability of the data is high, most

conductivity values are near the average, with the greatest conductivity value of

348 μS/cm at 12.34 m, and the lowest value of 71 μS/cm at 10.82 m (Table 2A-9).

For core H2, conductivity averages 209 μS/cm, with a standard deviation of

56 μS/cm (Figure 2.9B). This reflects a similar situation to core H1, because most

conductivity values are near the average, with the high for conductivity being 538 μS/cm

(near the surface of the core). and the low being 67 μS/cm at 15.24 m (Table 2A-10).

Bicarbonate

For core H1, the average bicarbonate value was 0.4 meq/l with a standard

deviation of 0.1 meq/l (Figure 2.10A). The high value was 0.70 meq/l at 2.23 m depth,

and the low value was 0.01 meq/l at 6.70 m depth. Generally, bicarbonate values varied

throughout the length of the core from 0.2 meq/l to 0.7 meq/l (Table 2A-11).

Core H2 values for bicarbonate averaged 0.5 meq/1 with a standard deviation of

0.1 meq/l (Figure 2.10B). The high value was 0.72 meq/l at 14.98 m depth, and the low

value was 0.10 meq/l at 5 cm depth. Just as in core H1 the values for bicarbonate varied

throughout the length of the core, generally from 0.2 meq/l to 0.7 meq/l (Table 2A-12).

2.9A. Core H1

2.9B. Core H2
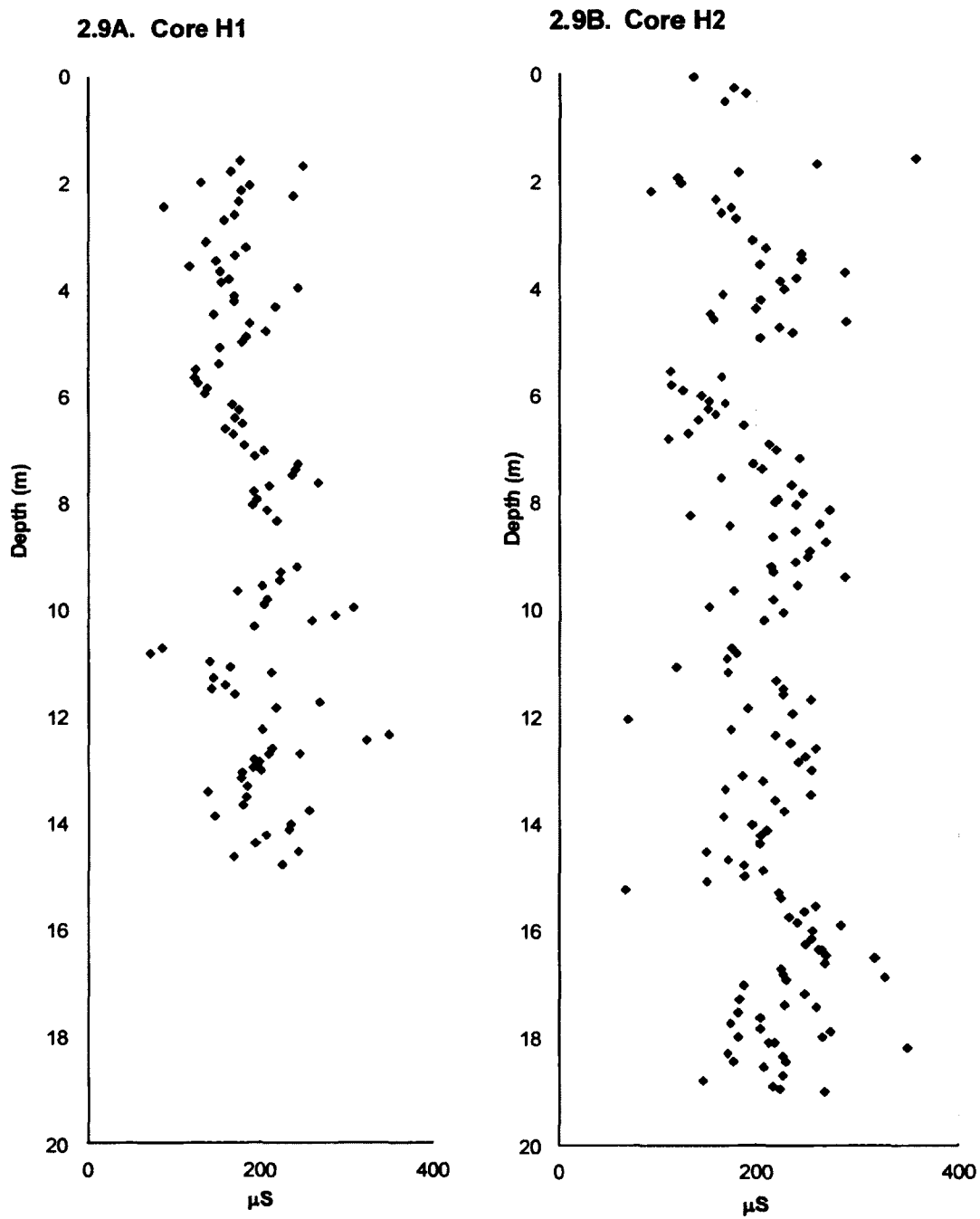
Figure 2.9 Lake Atna core H1 and core H2 conductivity values in μS/cm.
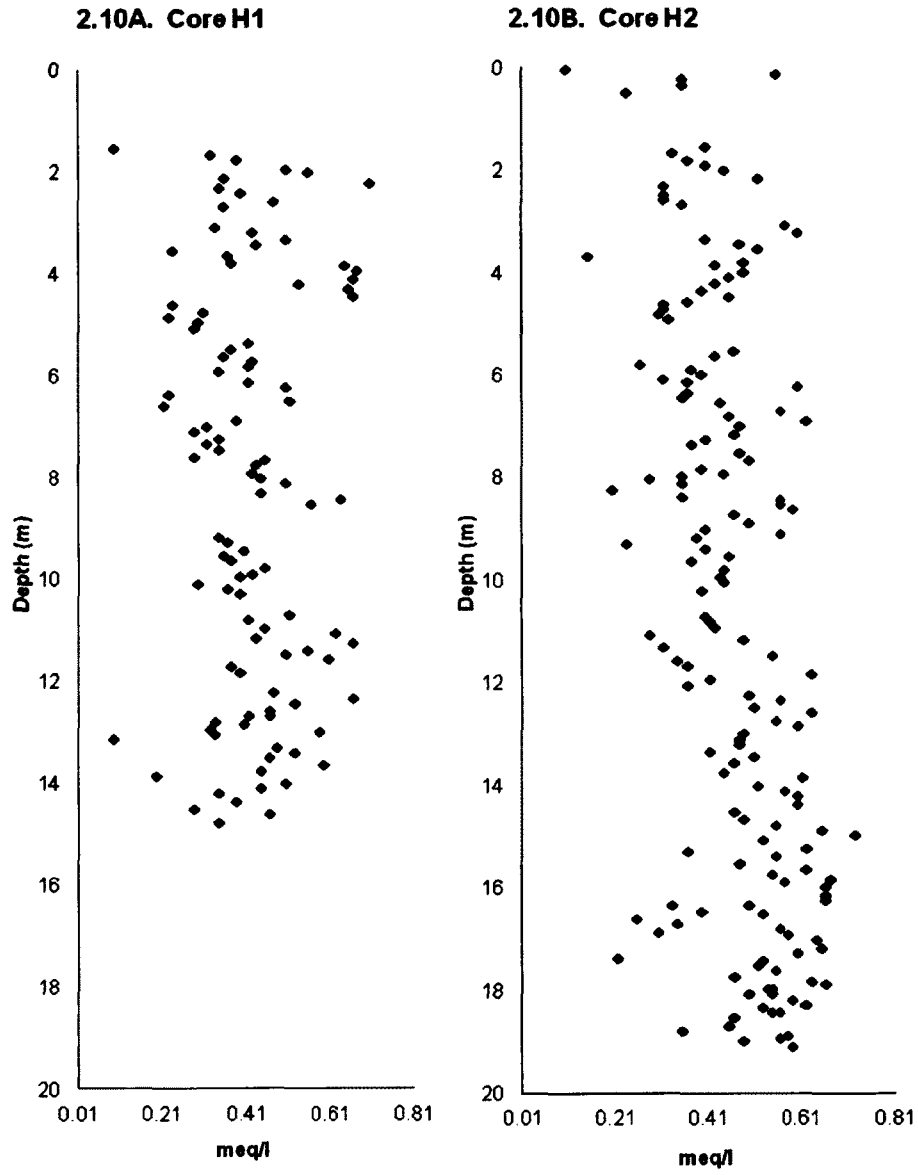
Figure 2.10 Lake Atna core H1 and core H2 bicarbonate values in meq/l.

%N and %C

There are very high values for percent nitrogen and percent carbon from the top of core H2 (0.05 m depth) that strongly suggest organic matter content at the surface of the core (%N of 0.623 and %C of 14.257%). These samples have been eliminated from the statistical analysis of core H2 %C and %N for two reasons: they are not representative of the carbon and nitrogen contents for the lakebed material; and these data strongly skew the statistics for %N and %C so that data differences from samples taken at deeper levels in the core are more difficult to interpret.

Almost all the percent nitrogen samples for core H1 have values below 0.1%. The values start slightly higher (0.170% at 0.16 m, 0.111% at 0.17 m) but within 20 cm the values drop below 0.1% and only rise slightly above that level 6 times (0.117% at 2.34 m depth, 0.118% at 3.66 m depth, 0.109% at 10.72 m depth, 0.114% at 10.82 m depth, 0.107% at 10.97 m depth, and 0.103% at 11.28 m depth) for the rest of the core (Figure 2.11A). The nitrogen values for core H1 average 0.06% with a standard deviation of less than 0.03%. The high value is 0.170% at 1.58 m depth. The low value is 0.017% at 6.15 m depth (Table 2A-13).

All nitrogen percents below 0.25 m depth for core H2 are lower than 0.1% (Figure 2.11B). The percent nitrogen values for core H2 below the 0.51 m depth average 0.06% with a standard deviation of 0.02%. The high value is 0.123% at 0.15 m and the low value is 0.016% at 5.80 m depth (Table 2A-14).

The percent carbon values for core H1 start high, drop below 1% after about 1 m and with two exceptions stay between 0.5% and 1% until a depth of 10.31 m

2.11A. Core H1

2.11B. Core H2
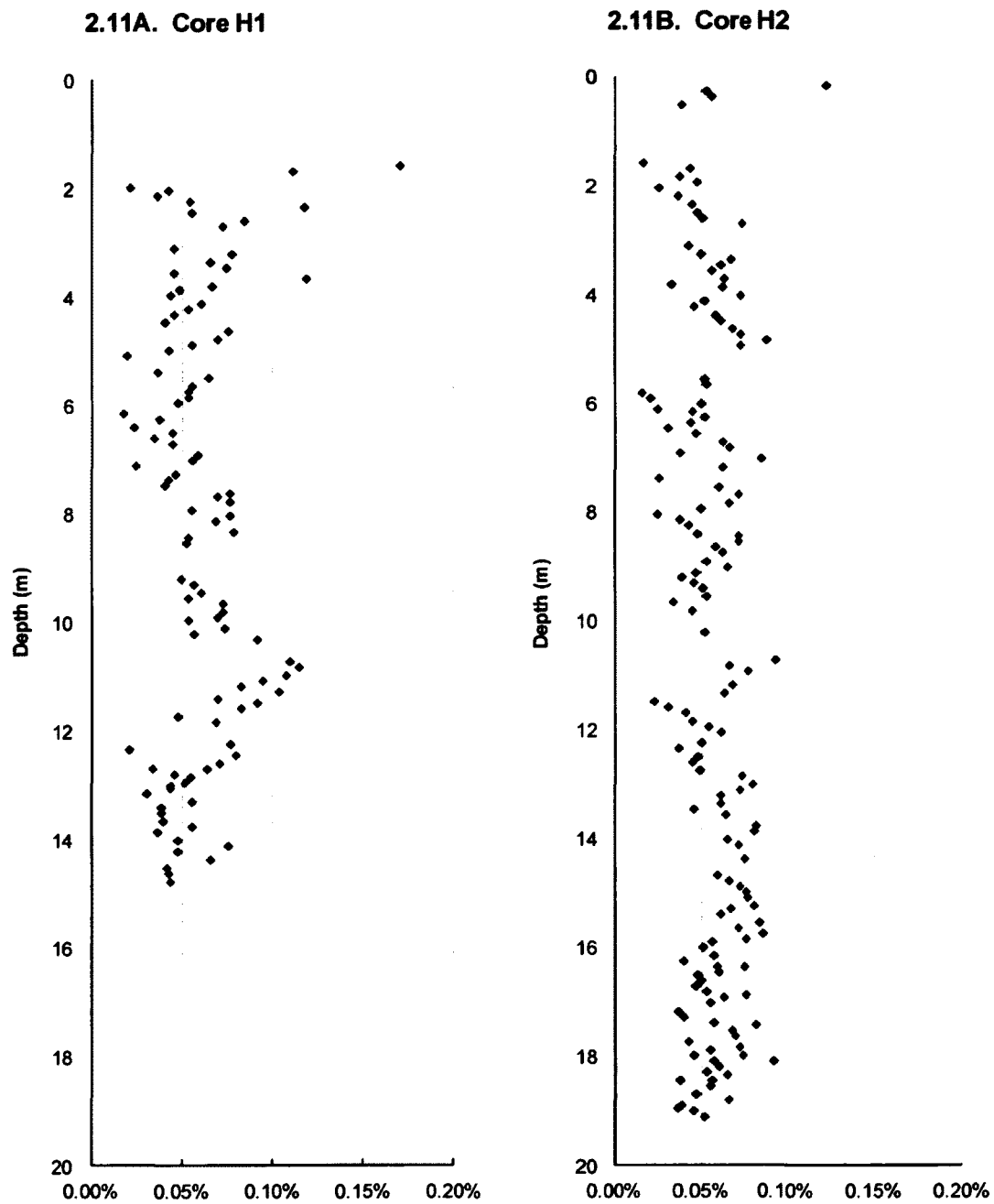
Figure 2.11 Lake Atna core H1 and core H2 nitrogen values in %.

(Figure 2.12A). At that point the values drop below 0.5% until a depth of 11.28 m. The values then climb to 1.427% by 12.24 m depth, and then drop back to below 1% by 12.70 m depth. Carbon values for core H1 average 0.86% with a standard deviation of 0.28%. The high value is 2.216% at 1.58 m depth and the low value is 0.131% at 12.34 m depth (Table 2A-13). Two anomalous values (the low value of 0.131% at 12.34 m depth and a value of 1.814% at 13.16 m depth) are the only outliers in this (lower) section of the core.

Percent carbon values for core H2 vary down the length of the core from 0.5% to 1.2% with the single exception of the low value (0.476% at 4.22 m depth, Figure 2.12B). Values below 0.05 m depth average 0.82% with a standard deviation of 0.17% (Table 2A-14). The high value is 2.136% at 0.152 m depth and the low value is 0.476% at 4.2 m depth.

DISCUSSION

Correlations of the various chemical and isotopic analyses of the two cores are not significant within each core for any two parameters at more than the 0.7 level (at least 0.5 r^2) except for the correlation of (water soluble) calcium to magnesium, and iron to magnesium (Table 2A-15 for core H1, Table 2A-16 for core H2). These statistical correlations probably reflect the chemical linking of calcium and magnesium in carbonate minerals and magnesium and iron in mafic minerals. The amount of organic material in these samples (as reflected by low total carbon and nitrogen percents) precludes the calcium-magnesium linkage found in plant and animal tissues.

2.12A. Core H1

2.12B. Core H2
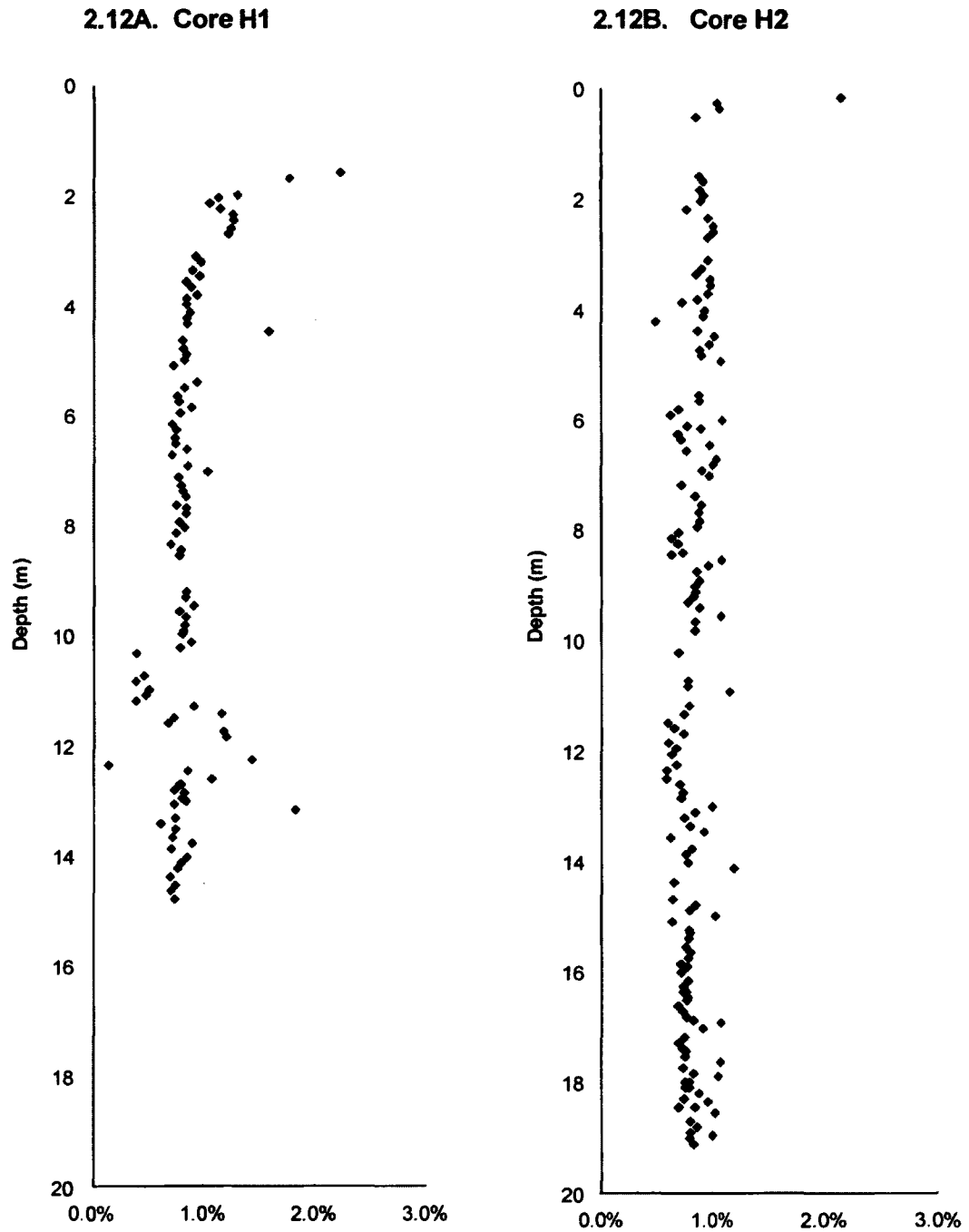
Figure 2.12 Lake Atna core H1 and core H2 carbon values in %.

The lack of within-core correlations among most analyses indicates that statistical relationships between the analytical data sets are due to influences other than the chemical relationships among the parameters.

The relationships of the various parameters *between* the two cores are more complicated. Two cores that are field replicates of this area of the Lake Atna lake bed would have provided an opportunity for better representation of chemical and isotopic properties of the lake bed permafrost. However, the differences in the analytical results for several of the parameters indicate that these two cores are not field replicates of permafrost. There are a number of differences between them, and the differences in some cases are striking.

In order to sort out the significant differences between the cores, a t-test was used to compare each parameter of core H1 with that same parameter of core H2 for similarity at the 1% level of probability. A t-test that shows a high probability of similarity of mean distributions for a parameter indicates the parameter is similar in both cores which would suggest that the cores have similar sources and environments for the parameter tested. This would be the result expected for field replicate cores, and such a result is shown by the relatively high probabilities of similarity between cores H1 and H2 for %N (37% probability), %C (42% probability), mg/l Fe (1.05% probability), mg/l K (26% probability), mg/l Mg (15% probability) and pH (4.9% probability).

The lower the t-test result, the less similar the core H1 parameter is to the core H2 parameter. A low probability of similarity, indicating the mean distributions of data are not similar, suggests a parameter from cores with different sources or environments for

the parameter tested. Those parameters that show less than 1% probability of being

similar are %H$_2$O (0.23% probability), δ^{18}O (1.2E-30% probability), δD (0.05%

probability), mg/l Ca (0.09% probability, μS/cm conductivity (0.12% probability) and

meq/l HCO$_3$ (0.16% probability). Table 2A-17 shows the t-test results in evaluating

similarities between core H1 and core H2 parameters.

The six parameters with low probability of similarity can be divided into two

types: bicarbonate, conductivity and mg/l Ca are measures relating to ion content in the

permafrost water; water content and isotopes of oxygen and hydrogen are direct measures

of the permafrost water itself. The data show that several analytical parameters of core

H2 are dissimilar to those of core H1, which indicates that at least some of H2 core water

is fundamentally different from H1 core water.

Bicarbonate, Conductivity and Calcium

The analysis of bicarbonate (Figure 2.10; Table 2A-11 and Table 2A-12) shows

that the amount of soluble bicarbonate is low, but bicarbonate is present down the entire

depth of both cores. This is chemically consistent with the pH of the pore water which is

more than 7 and less than 9 (Figure 2.8; Table 2A-7 and Table 2A-8) with one single

exception (pH of 6.23 at the very top of core H2). This pH zone (more than 7 and less

than 9) is where bicarbonates are at equilibrium (Lindsay, 1979).

Calcium combines readily with carbonate species (Lindsay, 1979), so there is a

tendency for a statistical relationship between calcium and carbonates. If quantitative

changes occur in a carbonate, calcium may experience a similar effect.

Conductivity (Figure 2.9; Table 2A-9 and Table 2A-10), a general measure of the amount of salts (anions and cations) in a solution (Jackson, 1958), is also related to pH, which has an effect on the solubility of salts. Since calcium is one of the most abundant cations in the soil (Lindsay, 1979), soluble Ca would also be reflected in conductivity (as well as carbonate content).

The averages, standard deviations and high and low values for these three parameters (mg/l Ca, uS/cm conductivity, and meq/l bicarbonate) are very similar for core H1 and H2 (Tables 2A-5 and 2A-6, Tables 2A-9 and 2A-10, and Tables 2A-11 and 2A-12, respectively). These statistics (average, standard deviation, high and low values) do not reflect differences in the statistical mean distribution between the two cores, but the t-test does, showing that the changes in these parameters throughout the cores are different between core H2 and core H1.

The differences in the bicarbonate readings, conductivity readings and calcium readings for cores H1 and H2 could have been caused by water source differences in the cores. Surface runoff water collected in a thaw lake could have produced enough of a difference in the values for these parameters in core H2 from the glacially sourced Lake Atna water of core H1 that statistically they could be different, particularly in the way the values vary within the data set rather than in the more common statistics (average, standard deviation, high and low values). The values are low, so minor variations in interactions with soils could possibly produce these differences as well, but there is no evidence that the soils at one site were especially different from the other, while there is evidence that the source for the permafrost water was different.

Percent Water Content, Oxygen and Deuterium Isotopes

There is a gap in the data at about 9 m depth where data from several samples is not used because the water content is less than 11%, which is less than what is required for the analytical method used.

Although the newly drained lake bed was originally saturated, the water table would have reached a new equilibrium in the non-homogenous material of the lake bed. That stability is reflected in the water content of core H1, which is fairly consistent and generally around 25% except for one spike near the top of the core, probably due to segregation ice formation when permafrost was aggrading.

Core H1 has a water content profile (Figure 2.4A) that is consistent down the core (variance of 0.62%) except for an initial peak of 77% water content at 1.8 m depth. Core H2 (Figure 2.4B) shows a regular pattern of high moisture content throughout the depth of the core (variance of 1.49%), although there are fewer and less dramatic spikes in water content below 12 m. Current depth to permafrost is about 1 m (Romanovsky, 2009) and within the first meter is a spike that would be consistent with base-of-active-layer lens formation (Davis, 2000; Williams and Smith, 1989). There is variable moisture content down to 6 m in core H2, and major peaks in water content at about 4.48 m, 5.38 m, 7.27 m, 8.24 m, 11.07 m, and 14.22 m. There may be several reasons for this, including differences in pore space size because of changing matrix materials, but the pattern suggests rhythmic ice banding, a frequent phenomenon in segregation ice formation (Taber, 1929, 1930; Williams and Smith, 1989) resulting from water migration during freezing. Below 14 m there is less variability in moisture content.

There are substantially larger and more numerous spikes in water content for core

H2 compared with core H1. The amount of lens formation depends on both the texture of

the soil and the size of hydraulic pressure differences in the water column created by an

advancing freezing front (Davis, 2000; Williams and Smith, 1989). In two cores under

similar conditions, such as H1 and H2 appear to be, the differences in ice lens production

as indicated by differences in water content are evidence of some significant difference in

the conditions present during permafrost formation in the two soil columns. In the case

of core H2, ice banding indicates that water migrated to form the lenses (Davis, 2000;

Williams and Smith, 1989), and it can be inferred that more water was available in core

H2 than in core H1 for this to happen. The greater number of lenses may have resulted in

greater total frost heave within the soil column for core H2 (Williams and Smith, 1989).

Oxygen isotope data show even greater differences between the two cores. The

core H1 $\delta^{18}O$ profile shows a very gradual and regular decrease in value from about

-18.2‰ $\delta^{18}O$ at 3 m depth to about -19.0‰ $\delta^{18}O$ at 14.8 m depth, with minor variations.

The core H2 $\delta^{18}O$ profile shows much larger variations in $\delta^{18}O$ signature at various

depths (Figure 2.5). Since the changes in core H2 and the differences with core H1 are

complicated, an annotated version of Figure 2.5 (Figure 2.13) will be referred to in the

following discussion.

The range of $\delta^{18}O$ values in core H2 at the very top of the core (between -18‰

and -19‰, Figure 2.13 arrow #1) does not have a counterpart in core H1 because the top

meter of core H1 was not collected. However, at a depth between 1.5 m and 3 m on both

cores, the $\delta^{18}O$ values drop to between -20‰ and -19‰ for several centimeters, and then

2.13A. Core H1

2.13B. Core H2
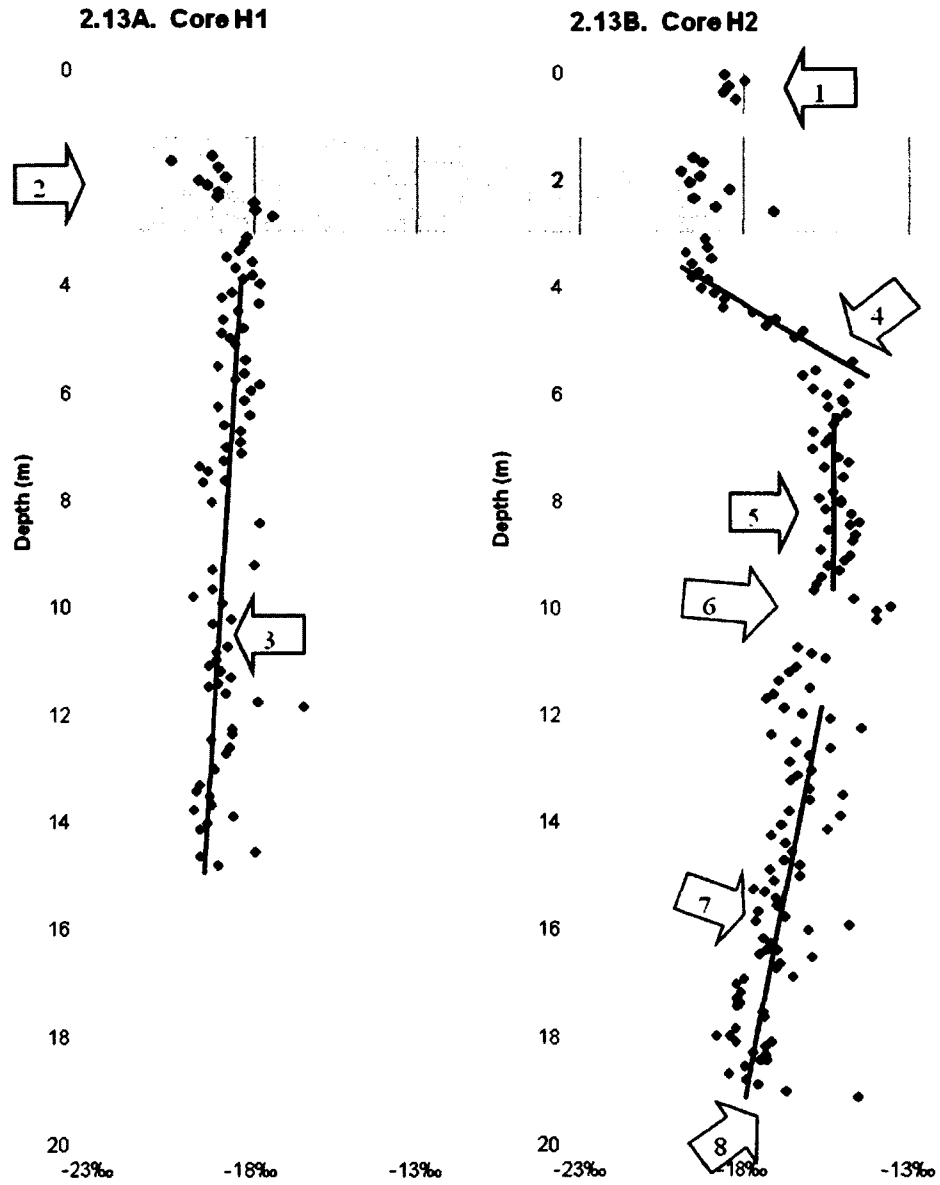
Figure 2.13   Lake Atna core H1 and core H2 $\delta^{18}O$ values in ‰ relative to VSMOW. Refer to text for discussion of areas indicated by arrows.

abruptly rise to values between -17‰ and -18‰ (Figure 2.13 arrow #2). This brief

positive spike in $\delta^{18}O$ is at almost an identical depth in both cores and with almost

identical values. Negative-positive $\delta^{18}O$ spike couplets that take place over a small depth

interval in a core are typically fractionation variations and can be caused by an advancing

freezing front from the active layer meeting an aggrading freezing front from the

permafrost layer (Michel, 1982). Since this spike couplet is below the current permafrost

table, it shows an isotopic history of thawing and refreezing that occurred in both cores.

The meteoric groundwater $\delta^{18}O$ signature is indicated by the data at the top of

core H2, less than 1 m from the top of the core (Figure 2.13, arrow #1). The original pore

water signature at the top of the mixing zone for core H1 (from 3 m downward) is similar

to that of the meteoric groundwater. From 3 m depth, core H1 $\delta^{18}O$ values decrease

gradually to a value of about -19‰ at the bottom (14.78 m) of the core. This sloped data

profile (Figure 2.13, arrow #3) could be expected for a closed water reservoir that froze

from the top down (Lorrain et al., 2002; Jouzel and Souchez, 1982), but this is not a

closed system. One explanation for the slope is the probability of slower freezing rates as

the original permafrost aggrades downward, which produces fractionation (Mackay,

1983), but fractionation in soil does not persist with depth (Michel, 1982). It is more

probable that the slight slope in the data profile is due to mixing of meteoric water with

the residual lake water prior to permafrost formation.

There are irregularities in the profile of the H1 data between 7 m and 10 m depth.

Some data is missing because of low water content, and the low water content may also

have contributed to the variable data. Further down there is a strong positive spike at about 12 m, a fractionation peak possibly indicating temporary slowing of the freezing front because of a change in soil texture or composition. Core H1 is incomplete and stops at less than 15 m depth, so there is no data for the bottom of the lakebed.

The mixing zone in core H2 (from 3 m to 5 m depth, Figure 2.13, arrow #4) is more pronounced than that for core H1 because the $\delta^{18}O$ signature of the H2 pore water at 5 m is much more enriched than the signature at 3 m. Core H2 $\delta^{18}O$ values climb from near -20‰ at 3.10 m to over -15‰ at 5.38 m depth.

Below 5.38 m values varying between -14‰ and -16‰ form a columnar profile down to nearly 10 m depth (Figure 2.13, arrow #5). At about 10 m there is a positive spike to -13.55‰ (Figure 2.13, arrow #6). Such a large excursion signals a change in the soil matrix that caused slowing of the freezing front (Michel, 1982). The $\delta^{18}O$ values below 10 m gradually become more depleted until they read around -18‰ near the bottom of the core (Figure 2.13, arrow #7). These $\delta^{18}O$ values form a slanted profile, but they are more variable than those values from 5.38 m to 9.81 m and may represent a more slowly freezing mixing zone. There are large shifts in data at 12 m and 16 m, possibly fractionation peaks from a change in soil texture or density.

There is another positive spike, -14.50‰ at 19.11 m, the very bottom of the core (Figure 2.13, arrow #8). This peak represents the fractionation that occurred when the freezing front moved from the unconsolidated lake bed material into the denser substrate at the bottom of the lake bed (made of consolidated material with less pore space), a change in texture of the substrate.

Additional information from deuterium values can help explain the relationship

between core H1 and core H2. Deuterium values can be extremely sensitive to minor

environmental changes so the data may be very noisy compared to $\delta^{18}O$ data, which is

remarkably precise for specific changes in water. The deuterium analyses in this study

are no different than the norm, and are noisy. We can, however, use deuterium in

comparison with the $\delta^{18}O$ data in order to establish a water line and a deuterium-excess

value.

The deuterium values in the two cores are statistically similar (Tables 2A-10 and

2A-12), even though the t-test reveals they have different mean distributions. The chart

profiles of the data vary greatly (Figure 2.6), and do not appear to match any other data

anomalies. The deuterium profiles as a whole do not appear similar, but the data patterns

are difficult to interpret. However, the relationship of deuterium to oxygen in the isotope

data presents some interesting results.

The general equation of the meteoric water line is $\delta D = 8\ \delta^{18}O + 10$ (Criss,

1999). The "+10" intercept is referred to as deuterium excess. Local meteoric water

lines have different intercepts, producing different deuterium excess values. As an

example, tap water from the University in Fairbanks comes from a well and has an

isotopic signature of $\delta^{18}O = -19.5‰ \pm 0.3$, $\delta D = -157‰ \pm 4$ which results in a deuterium

excess of approximately 0. For meteoric waters, a difference in deuterium excess may be

related to local conditions or fractionation that sometimes occurs in the evaporation

process, or may relate to groundwater that was charged by waters with different

deuterium excess (Criss, 1999). There is a difference in the deuterium excess for the two

cores. For core H1 the general equation of the average $\delta^{18}O$ to δD yields a deuterium excess very near to a value of 0, similar to Fairbanks well water. For core H2, the general equation of the average $\delta^{18}O$ to δD yields a value of approximately -9, considerably different from core H1 and Fairbanks well water. Evaporation, such as happens in lakes, results in isotopic enrichment of the water (Gibson, 2002; Gonfiantini, 1986) and a larger deuterium-excess value in the evaporated moisture (Gat, 1996), which results in a smaller deuterium-excess value in the lake water itself. The lower deuterium excess value for core H2 than for core H1 seems to be evidence for a greater evaporation effect on the core H2 pore water.

Another oxygen-deuterium relationship also suggests a difference in the two cores. Plotting δD vs. $\delta^{18}O$ shows the distribution of data around the meteoric water line. Figure 2.14 shows these data for core H1 plotted on a Global Meteoric Water Line graph scaled for the data. This is a tight cluster of data points, and the slope of the regression line is 5.5, quite different from the global meteoric water line slope of 8. This cluster shows that the water sources for the data have very similar isotopic signatures, not as varied as the precipitation normally associated with temperate zone meteoric waters.

Figure 2.15 shows the isotopic data for core H2. Two differences from Figure 2.14 are apparent from this plot; core H2 source water has more varied isotopic signatures than core H1, and the slope of the regression line for core H2 is less than that of core H1. The commonly found slope for evaporated waters in nature is between 4 and 6 on the standard plot of δD vs. $\delta^{18}O$ (Criss, 1999; Gibson, 2002). The slope of 5.52 for
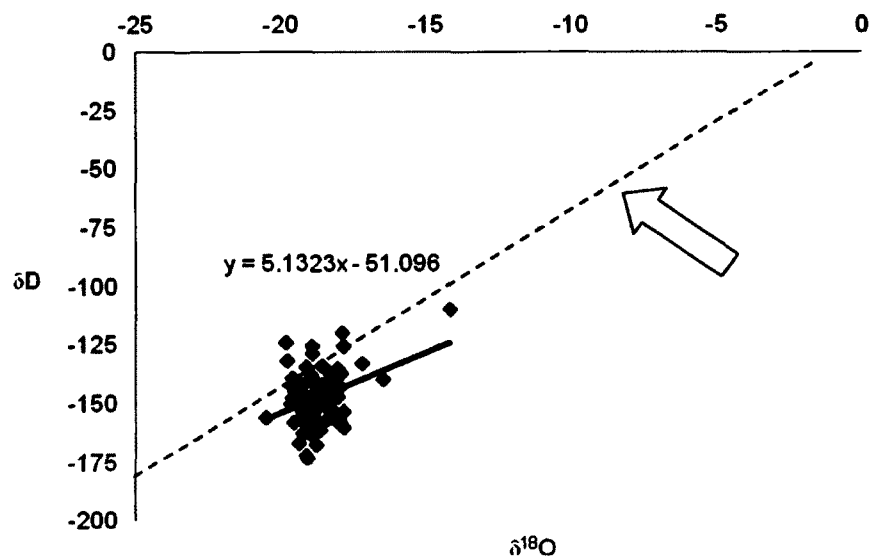
Figure 2.14 Lake Atna core H1 pore water isotopes, values in per mil, compared
with the Global Meteoric Water Line (arrow). "y" is trendline
formula.
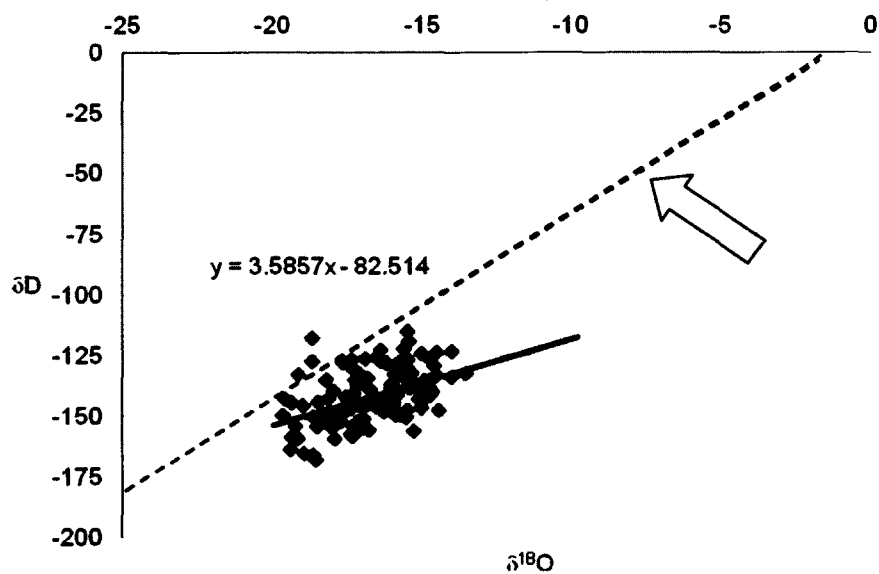
Figure 2.15 Lake Atna core H2 pore water isotopes, values in per mil, compared
with the Global Meteoric Water Line (arrow). "y" is trendline
formula.

the δD vs. $\delta^{18}O$ plot for core H1 is consistent with that of evaporated water (which is not surprising for Lake Atna water). The slope of 3.68 for the H2 plot is even smaller, which could suggest that the water experienced even more evaporation than water from core H1, or it may have a different source.

The oxygen-deuterium graphs suggest that core H2 pore water underwent more evaporation than core H1 before it was absorbed into the lake bed. The enriched column of $\delta^{18}O$ values between 5.38 m and 9.81 m depth (Figure 2.13B) show that the source of core H2 water at that depth was more enriched than Lake Atna water. This would be true for a small lake or pond being fed by meteoric water over some period after the initial drainage of Lake Atna.

If core H2 came from a site at a lower elevation than core H1 it would be tempting to suggest that Lake Atna drained slowly and core H2 shows climatic changes that took place and are reflected by the changes in water chemistry of a residual lake at the core H2 site. However, core H2 is located at a (slightly) higher elevation than core H1, and so should have drained earlier than core H1, even if the drainage were slow. A residual lake may have originated with Lake Atna water that was captured in a depression and prevented from draining by the saturated lake bed. As the lake bed water table lowered, however, the residual lake should have drained as well. It is unlikely that such a lake would have existed long enough to develop the enriched signatures found at 5.38 m to 9.81 m depth in core H2. Furthermore, it is hard to explain the pattern of $\delta^{18}O$ signatures down the length of core H2 if a sequestered lake, formed prior to permafrost

development, had been the source of the signatures. (For example, the signatures should have formed a mixing zone from the surface all the way to the bottom of the lake bed.)

The column of enriched data suggests that standing water existed at the site at some time after Lake Atna drained. There are several possible types of pond that could have formed other than a residual lake; there are lakes formed by damming action of moraines and fans, there are those formed in river valleys such as ox-bow ponds, and there are thaw lakes which are formed by depressions in permafrost (Livingstone et al., 1958). The site of core H2 is not near a river, nor are there morphological structures that would have formed dams. There is significant permafrost at the site, and that suggests a thaw lake could have formed there.

A thaw lake scenario requires the initial formation of permafrost (Yoshikawa and Hinzman, 2003). When Lake Atna first drained, the water table would have dropped because of the heterogeneity of the lake bed material, and permafrost would have started to form as soon as the residual heat from the lake bed had dissipated.

The istotopic signatures below 5.38 m depth in core H2 are all consistent with thaw lake formation and draining, but the necessary signatures for the initial surface disturbance to form such a lake are no longer available because of a secondary disturbance, probably a fire, that occurred later in the history of this site which destroyed early isotopic evidence. A consequence of reworked permafrost after fire is that earlier permafrost isotope history is erased to the depth of thaw. This secondary disturbance has left an isotopic signature on both cores where double peaks mark the freezing front that passed through thawed permafrost and met the aggrading permafrost table (Figure 2.13,

arrow 2). Since fire is one of the primary disturbances that initiate thaw lakes

(Yoshikawa et al., 2002), the very evidence of a likely fire that occurred after the thaw

lake drained suggests the possibility that an earlier fire may have provided the

disturbance that produced the thaw lake. If this is true for the creation of the thaw lake,

the fire could not have occurred until after vegetation cover had become established at a

density that would have helped insulate the permafrost. The vegetation would also have

fueled a fire hot enough to thaw the established permafrost deep enough for the ground

surface to subside. This is conjecture for the site but wildfire is a common event in

interior Alaska.

Whatever the initial disturbance, it would have produced subsidence in the lake

bed surface at the core H2 site that allowed the collection of runoff from snowmelt and

rain that did not drain away because of the unthawed permafrost beneath the newly

forming thaw lake. The lake could exist only as long as the permafrost existed. The

water source for the lake is likely to have been a combination of snowmelt and rain.

Isotopically the lake water would have become progressively heavier as the meteoric

water experienced evaporation on a greater relative scale than Lake Atna. The enriched

isotopic signature of the pore water in the lake bed supports the idea that input to the lake

was probably limited to snow melt in spring plus summer rain, producing an evaporation-

dominated lake (Brock et al., 2009). It is unlikely that glacial-fed streams would have

been a source for this lake since the isotope signature is enriched, not depleted. In

Fairbanks, there are several thaw ponds and lakes that have $\delta^{18}O$ signatures similar to (or

even more enriched than) those found between 5.38 m and 9.81 m depth of core H2 (Table 2A-18).

Permafrost under a thaw lake thaws slowly due to heat flux from the lake water (Yoshikawa and Hinzman, 2003; Hinkel et al., 2003). The consistent $\delta^{18}O$ signature from 5.38 m to 9.81 m is not a mixing zone and it suggests standing water penetrating the lake bed down to 9.81 m depth. There would have been much more water from the thaw lake than from the permafrost water in the lake bed ice so the signature became enriched and constant as the thaw lake water replaced the pore ice. Those consistent signatures show that the permafrost was frozen to 9.81 m depth when the thaw lake formed, which stopped the advance of the permafrost freezing front. The permafrost below the thaw lake allowed water to accumulate without draining, but the lake prevented permafrost from continuing to form below 9.81 m depth. The spike at 9.81 m marks stalling of the freezing front (Michel, 1982) when new permafrost formed from the top down at the thaw lake site after it had drained and the new freezing front reached the depth in the core which had never been frozen. Below 9.81 m the signatures are somewhat more variable than those for core H1 at the same depths, and they become gradually more depleted, suggesting a mixing zone of thaw lake water with original lakebed water.

There does not seem to be topological evidence of a thaw lake at the site of core H2. This may be because of frost heave forcing the lake bed upwards. When the permafrost below the lake thawed and the thaw lake drained, meteoric sources alone would have been insufficient to maintain the lake. As the lake became shallower, water would freeze in contact with the surface of the lake bed. Permafrost would begin to

reform in the lakebed from the base of the thaw lake downward (Ehlmann et al., 2005). As the freezing front descended down the soil column, segregation ice lenses could have formed sequentially in ice bands (Figure 2.4B). This would have resulted in frost heaving, forming an upward bulge preventing the collection of new water in the no-longer-existing lake depression (Williams and Smith, 1989). Permafrost would then continue to form down the soil column and the little lake would completely disappear, although the isotopic signature showing that it had existed would be frozen in the permafrost beneath it. There may also have been hydro-chemical indications of lake-bottom frost heave (Hyatt, 1998) when the thaw lake froze completely, but if so that has been subsumed by the surface disturbance common to both core locations that occurred after the thaw lake was gone.

Wildfire seems the most likely candidate to have caused the surface disturbance at the sites over an area that would have affected both cores at the same intensity and to the same depth. Thaw lakes are started by some surface disturbance in a permafrost zone that thaws the permafrost resulting in subsidence of the ground surface (Yoshikawa and Hinzman, 2003). Current depth to permafrost in undisturbed areas at the core sites is about 1 m, but the removal of the insulating surface vegetation on permafrost-rich soils can cause thawing and increased active layer depth (Osterkamp et al., 2000; Romanovsky, 2009; Shur and Jorgenson, 2007; Shur and Zhestkova, 2003). Wildfires are widespread and a natural phenomenon in the boreal forests of Alaska (Shur and Jorgenson, 2007; Yoshikawa et al., 2002) which can remove varying amounts of surface vegetation. Heat conduction to permafrost is not significant during a fire, but removal of

surface organic matter can increase heat conductivity up to 10-fold depending on fire intensity, which increases the active layer depth by removing thermal insulation and thawing permafrost ice. The active layer may continue to increase in depth for over ten years after a severe fire, producing a talik as much as 4 m in depth (Yoshikawa et al., 2002). Such a talik may or may not refreeze, depending on local climatic conditions (Shur and Jorgenson, 2007). In the case of ecosystem-driven permafrost such as that in the Copper River Basin, permafrost can recover from fire, though it may take hundreds of years (Shur and Jorgenson, 2007; Viereck, 1973). When permafrost thaws, the porewater is replaced by active layer groundwater. The isotope signature of the groundwater reflects the current groundwater source and if the talik and active layer refreeze, the "new" permafrost will have the isotope signature of the groundwater present at the time of refreezing. The different isotope signature is an indication of disturbance to the permafrost after it had originally formed.

Assuming that prior to disturbance $\delta^{18}O$ isotopic signatures of both cores reflected their respective pore water $\delta^{18}O$ values from a depth of 1m downward, the depleted signature followed by an enriched spike (a double peak) between 1.5 m and 2.7 m would reflect that the permafrost between 1.5 m and 2.7 m depth formed from groundwater present in the soil after the fire. The fractionation peak at 2.7 m depth marks where the refreezing permafrost met the old permafrost table aggrading upward.

After surface disturbance, groundwater would have penetrated into the thawed permafrost zone so that newly aggrading permafrost would freeze in signatures of the mixing zone in both cores. The difference in signatures between the more modern water

and the thawed water down to about 3 m to 5 m depth in core H1 was not very great so

the mixing zone is not apparent. The difference in core H2, however, was large and the

mixing zone from 3 m to 5 m depth is the dominant feature in the data profile.

The lighter pore water signatures below 9.81 m depth in core H2 as well as water

content spikes throughout most of the core suggest that the more enriched water which

drained from the thaw lake added to, mixed with, and was slowly displacing the original

ground water when it froze. This is indicated by the most depleted $\delta^{18}O$ value at about

14 m depth in core H2 of around -17‰ (thaw lake water mixed with Lake Atna water),

being not as depleted as at the bottom of core H1 (around 14 m depth) which has a

signature of about -20‰ (meteoric water mixing with Lake Atna water).

Below 10 m depth there are two spikes in core H1; one at a depth of 11.84 m

(-16.5‰) and one very near the bottom of the core (about -18‰). These spikes are deep

in the lake bed and so probably indicate changes in the freezing front rate due to a

physical change in the soil matrix. It is not possible to be specific without more

evidence. The data for core H2 is more scattered than for core H1 below 10 m depth and

there seem to be repeated shifts downcore, including two possible spikes at about 12 m

and 16 m depth. The general profile for both cores below 10 m depth is slanted, evidence

of mixing zones to the depth of the lake bed

In summary, two permafrost cores taken from the Copper River Basin near the

HAARP Permafrost Observatory provide two different paleoenvironment histories

although they are within 400 m of each other. Approximately 10,000 yr BP ice dams that

formed Lake Atna in the Copper River Basin failed, allowing the lake to drain. Once

Lake Atna drained, permafrost began to form in the basin lake bed

At the location of core H1, permafrost continued to freeze downward without

evidence of interruption, although the freezing front occasionally slowed, possibly due to

changes in the soil matrix, allowing some fractionation double peaks to form.

At the location of core H2, a relatively small thaw lake began to form at the time

the permafrost freezing front had reached 10 m depth. It is likely that the thaw lake

formation was due to a fire burning off insulating vegetation which allowed the surface of

the frozen Lake Atna lakebed to thaw and subside at that location. The thaw lake water

eventually thawed the 10 m of permafrost below it and the lake drained. The drained

thaw lake bed froze and the ice-rich lake bed expanded by frost heaving so that water

could no longer collect at that location. A new permafrost freezing front advanced,

freezing in the thaw lake isotope signatures to a depth of 10 m, and the signatures of the

mixed residual Lake Atna water and thaw lake water below 10 m. After permafrost had

reformed at the H2 site, another surface disturbance (possibly fire) removed the surface

vegetation.

Without the insulation provided by the vegetation cover, permafrost thawed to a

depth of at least 3 m at core H1, and to a depth of about 5 m at core H2 over a period of

several years. At both locations, new freezing fronts from the ground surface met the

aggrading freezing front from the permafrost table moving upward, to refreeze the lake

bed permafrost.

At both locations, but at different times (since the H2 site permafrost formation was delayed by the creation of the thaw lake), the permafrost freezing front eventually advanced beyond the depth of the water-permeable lakebed and into the consolidated base rock of the basin and remains in that state today.

LITERATURE CITED

Bennett, M.R., D. Huddart, G.S.P. Thomas. 2002. Facies architecture within a regional glaciolacustrine basin: Copper River, Alaska. Quat. Sci. Rev. 21, 2237-2279.

Brock, B.E., Y.Yi, K.P. Clogg-Wright, T.W.D. Edwards and B.B. Wolfe. 2009. Multi-year landscape-scale assessment of lakewater balances in the Slave River Delta, NWT, using water isotope tracers. Journal of Hydrology 379: 81-91.

Connor, C.L. 1984. Late Quaternary glaciolacustrine and vegetational history of the Copper River Basin, South-Central Alaska, Ph.D. disseration, University of Montana. 121 pages.

Coplen, T.B. 1988. Normalization of oxygen and hydrogen isotope data. Chem. Geol. 72: 293-297.

Criss, R.E. 1999. Isotope hydrology. *In: Principles of Stable Isotope Distribution.* Oxford University Press. New York. pp 89-138.

Davis, T.N. 2000. *Permafrost, A Guide to Frozen Ground in Transition.* University of Alaska Press. Fairbanks. 351 pages.

Ehlmann, B.L., R.E. Arvidson, B.L. Jolliff, S.S. Johnson, B. Ebel, N. Lovendusko, J.D. Morris, J.A. Byers, N.O. Snider and R.E. Criss. 2005. Hydrologic and isotopic modeling of alpine Lake Waiau, Mauna Kea, Hawai'i. Pac. Sci. 59:1, 1-15.

Ferrians, O.J. 1984. Pleistocene glacial history of the northeastern Copper River Basin, Alaska. Geological Society of America Abstracts with Programs 16:5, p. 282.

Ferrians, O.J. 1989. Glacial Lake Atna, Copper River Basin, Alaska. *In:* Carter, L.D., T.D. Hamilton, and J.P. Galloway, (eds), Late Cenozoic History of the Interior Basins of Alaska and the Yukon. United States Geological Survey, Circular 1026, 85-88.

Gat, J.R. 1996. Oxygen and hydrogen isotopes in the hydrologic cycle. Annual Review of Earth Planet Science 24, 225-262.

Gonfiantini, R. 1986. Environmental isotopes in lake studies. *In:* Fritz, P. and J.C. Fontes, (eds), *Handbook of Environmental Isotope Geochemistry.* The Terrestrial Environment, Vol.2. Elsevier, New York. pp 113-168.

Gibson, J.J. 2002. Short-term evaporation and water budget comparisons in shallow Arctic lakes using non-steady isotope mass balance. Journal of Hydrology 264, 242-261.

Hinkel, K.M., W.R. Eisner, J.G. Bockheim, F.E. Nelson, K.M. Peterson and X. Dai. 2003. Spatial extent, age, and carbon stocks in drained thaw lake basins on the Barrow Peninsula, Alaska. Arctic, Antarctic, and Alpine Research 35:3, 291-300.

Hyatt, J.A. 1998. The origin of lake-bed ground ice at Water Supply Lake, Pond Inlet, Nunavut, Canada. *In*: Permafrost – Seventh International Conference (Proceedings), Yellowknife (Canada), Collections Nordicana 55, 487-493.

Jackson, M.L. 1958. *Soil Chemical Analysis*. Prentice-Hall, Englewood Cliffs, NJ. 498 pages.

Jouzel, J. and R. Souchez. 1982. Melting-refreezing at the glacier sole and the isotopic composition of ice. J. Glaciol. 28:98, 35-42.

Kaufman, D.S. and W.F. Manley. 2004. Pleistocene maximum and Late Wisconsinan glacier extents across Alaska, U.S.A. *In*: Ehlers, J. and P.L. Gibbard, (eds) *Quaternary Glaciations-Extent and Chronology*. Volume 2: Part II: Developments in Quaternary Sciences 2. Amsterdam: Elsevier. 9-28.

Koehler, G., L.I. Wassenaar and M.J. Hendry. 2000. An automated technique for measuring δD and $\delta^{18}O$ values of porewater by direct CO_2 and H_2 equilibration. Analytical Chemistry 72:22, 5659-5664.

Lindsay, W.L. 1979. Carbonate Equilibria. *In*: *Chemical Equilibria in Soils*. John Wiley and Sons. New York. 79-88.

Livingstone, D.A., K. Bryan Jr. and R.G. Leary. 1958. Effects of an Arctic environment on the origin and development of freshwater lakes. Limnol. Oceanogr. 3:2, 192-214.

Lorrain, R., S. Sleewaegen, S. Fitzsimons and M. Stievenard. 2002. Ice formation in an Antarctic glacier-dammed lake and implications for glacier-lake interactions. Arctic, Antarctic and Alpine Research, 34:2, 150-158.

Mackay, J.R. 1983. Oxygen isotope variations in permafrost, Tuktoyaktuk Peninsula area, Northwest Territories. Project 680047. *In*: Current Research, Part B, Geological Survey of Canada, Paper 83-1B. 87-74.

Michel, F.A. 1982. Isotope investigations of permafrost waters in northern Canada. Ph.D. dissertation, University of Waterloo, Waterloo, Ontario. 424 pages.

Nichols, D.R. 1989. Pleistocene glacial events, Southeastern Copper River Basin, Alaska. *In*: Carter, L.D., T.D. Hamilton, and J.P. Galloway, (eds). Late Cenozoic History of the Interior Basins of Alaska and the Yukon. United States Geological Survey, Circular 1026, 78-80.

Osterkamp, T.E., L. Viereck, Y. Shur, M.T. Jorgenson, C. Racine, A. Doyle and R.D. Boone. 2000. Observations of thermokarst and its impact on boreal forests in Alaska, U.S.A. Arctic, Antarctic and Alpine Research 32:3, 300-315.

Pearson, R.W. and M. Hermans, eds. 2008. *Alaska in Maps: A Thematic Atlas*. CD-ROM. Fairbanks: University of Alaska Fairbanks.

Rhoades, J.D. 1982. Soluble salts. *In*: A.L. Page (ed.) *Methods of Soil Analysis*. Part 2. Chemical and Microbiological Properties. 2nd ed. 167-180.

Riordan, B., D. Verbyla and A.D. McGuire. 2006. Shrinking ponds in subarctic Alaska based on 1950-2002 remotely sensed images. J. Geophys. Res., 111, G04002, doi:10.1029/2005JG000150. 11 pages.

Romanovsky, V. 2009. Establishing permafrost observatory at the HAARP site. Final report to the ONR. 22 pages.

Rubin, M. and C. Alexander. 1960. U.S. Geological Survey radiocarbon dates 5: Am. Jour. Sci. Radiocarbon Supp. 2, 129-185.

Schrader, F.C. 1900. A reconnaissance of a part of Prince William Sound and the Copper River district, Alaska. United States Geological Survey 20th Annual Report, Part VII – Exploration in Alaska in 1898, 1898-99. 341-423.

Scrimgeour, C.M. 1995. Measurement of plant and soil water isotope composition by direct equilibration methods. Journal of Hydrology 172, 261-274.

Shur, Y.L. and M.T. Jorgenson. 2007. Patterns of permafrost formation and degradation in relation to climate and ecosystems. Permafrost and Periglacial Processes 18, 7-19.

Shur, Y. and T. Zhestkova. 2003. Cryogenic structure of a glacio-lacustrine deposit. Proceedings of the Eighth International Conference on Permafrost, 21-25 July 2003, Zurich, Switzerland. 2, 1051-1056.

Taber, S. 1929. Frost heaving. J. Geol. 37, 428-461.

Taber, S. 1930. The mechanics of frost heaving. J. Geol. 38, 303-317.

Viereck, L.A. 1973. Ecological effects of river flooding and forest fires on permafrost in the taiga of Alaska. *In*: Permafrost: The North American contribution to the Second International Conference. National Academy of Sciences. Washington, D.C. 60-67.

Wiedmer, M., D.R. Montgomery, A.R. Gillespie and H. Greenberg. 2010. Late Quaternary megafloods from Glacial Lake Atna, Southcentral Alaska, U.S.A. Quaternary Research 73, 413-424.

Williams, J.R. 1989. A working glacial chronology for the Western Copper River Basin, Alaska. *In*: Carter, L.D., T.D. Hamilton and J.P. Galloway (eds). Late Cenozoic History of the Interior Basins of Alaska and the Yukon. United States Geological Survey, Circular 1026, 81-84.

Williams, J.R. and J.P. Galloway. 1986. Map of western Copper River Basin, Alaska, showing lake sediments and shorelines, glacial moraines, and location of stratigraphic sections and radiocarbon-dated samples. United States Geological Survey Open-File Report 86:390, 30 pages.

Williams, P.J. and M.W. Smith. 1989. *The Frozen Earth, Fundamentals of Geocryology*. Cambridge University Press. Cambridge. 306 pages.

Yoshikawa, K., W.R. Bolton, V.E. Romanovsky, M. Fukuda and L.D. Hinzman. 2003. Impacts of wildfire on the permafrost in the boreal forests of Interior Alaska. Journal of Geophysical Research, vol. 107, 8148 doi:10.1029/2001JD000438, FFR 4:1, 4-14.

Yoshikawa, K. and L.D. Hinzman. 2003. Shrinking thermokarst ponds and groundwater dynamics in discontinuous permafrost near Council, Alaska. Permafrost and Periglacial Processes. 14:2, 151-160.

APPENDIX 2A

Table 2A-1. Lake Atna Core H1 % Gravimetric Water Content

Depth m	H$_2$O	Depth m	H$_2$O	Depth m	H$_2$O	Depth m	H$_2$O
1.575	27.04%	5.638	12.89%	9.904	13.18%	13.664	14.46%
1.676	20.88%	5.740	12.97%	9.957	9.03%	13.767	17.61%
1.778	77.01%	5.841	11.95%	10.108	10.66%	13.868	11.83%
1.980	27.14%	5.943	20.80%	10.210	11.96%	14.020	15.18%
2.031	21.56%	6.147	14.51%	10.312	17.41%	14.122	11.29%
2.133	19.98%	6.248	12.01%	10.719	29.57%	14.223	9.45%
2.234	22.99%	6.400	15.46%	10.820	22.40%	14.375	10.28%
2.337	31.88%	6.502	10.42%	10.972	24.10%	14.529	11.21%
2.438	19.65%	6.603	11.13%	11.074	19.90%	14.630	11.17%
2.590	18.24%	6.705	24.58%	11.175	17.47%	14.782	12.67%
2.692	19.87%	6.909	12.26%	11.277	21.54%		
3.099	21.56%	7.010	11.11%	11.408	19.44%		
3.200	26.26%	7.112	15.98%	11.481	19.33%		
3.352	23.13%	7.264	20.28%	11.582	21.62%		
3.454	20.04%	7.365	11.03%	11.734	15.79%	Average	16.34%
3.555	25.71%	7.467	11.20%	11.836	14.80%	Std Dev	7.91
3.657	24.28%	7.618	16.56%	12.243	12.48%	High Value	77.01%
3.798	19.29%	7.671	13.16%	12.344	13.09%	Low Value	9.03%
3.861	15.57%	7.772	10.28%	12.446	15.25%		
3.962	16.21%	7.924	10.27%	12.598	12.37%		
4.114	21.10%	8.026	12.64%	12.699	14.08%		
4.216	16.09%	8.127	9.45%	12.700	9.61%		
4.317	14.57%	8.329	9.89%	12.802	10.41%		
4.459	17.30%	8.433	16.37%	12.851	9.53%		
4.623	13.31%	8.534	10.85%	12.953	9.73%		
4.774	13.33%	9.195	20.21%	13.005	13.79%		
4.876	17.52%	9.296	12.64%	13.055	10.94%		
4.978	14.51%	9.448	10.73%	13.157	10.83%		
5.079	16.00%	9.550	9.90%	13.309	11.48%		
5.385	12.02%	9.651	13.80%	13.410	11.78%		
5.486	17.17%	9.803	12.26%	13.512	15.27%		

Table 2A-2. Lake Atna Core H2 % Gravimetric Water Content

Depth m	H$_2$O	Depth m	H$_2$O	Depth m	H$_2$O	Depth m	H$_2$O
0.051	64.58%	5.800	18.25%	9.651	14.50%	14.680	20.02%
0.152	17.90%	5.901	18.12%	9.813	17.08%	14.782	20.79%
0.254	21.13%	6.003	16.72%	9.957	18.92%	14.884	17.37%
0.356	25.76%	6.104	25.17%	10.058	19.63%	14.985	20.60%
0.507	22.33%	6.147	19.37%	10.210	30.05%	15.087	16.58%
1.575	18.86%	6.248	12.37%	10.719	15.96%	15.238	14.34%
1.676	30.30%	6.350	19.37%	10.820	24.40%	15.291	12.87%
1.828	21.54%	6.452	20.81%	10.922	20.22%	15.392	15.26%
1.930	22.38%	6.553	15.03%	11.074	80.69%	15.544	14.83%
2.031	18.58%	6.705	20.61%	11.175	13.69%	15.646	15.88%
2.183	17.11%	6.806	17.92%	11.327	12.08%	15.747	19.35%
2.337	19.18%	6.909	15.13%	11.481	18.55%	15.849	15.27%
2.488	16.25%	7.010	21.12%	11.582	13.41%	15.900	22.35%
2.590	19.31%	7.172	19.55%	11.684	13.88%	16.002	25.91%
2.692	10.03%	7.274	45.21%	11.846	12.88%	16.154	12.44%
3.099	20.95%	7.373	15.49%	11.947	20.89%	16.255	13.44%
3.250	26.09%	7.537	24.51%	12.049	17.84%	16.357	13.84%
3.352	19.02%	7.671	9.45%	12.243	21.59%	16.358	13.51%
3.454	23.93%	7.832	19.25%	12.344	13.77%	16.459	13.90%
3.555	19.30%	7.934	13.71%	12.496	16.10%	16.508	16.02%
3.707	16.87%	7.985	29.56%	12.598	16.86%	16.611	15.64%
3.808	13.88%	8.036	19.73%	12.749	16.97%	16.712	15.79%
3.861	23.83%	8.137	24.31%	12.851	17.78%	16.815	10.95%
4.012	16.19%	8.239	87.00%	13.005	20.40%	16.874	30.90%
4.114	21.85%	8.400	18.64%	13.106	22.00%	16.916	15.59%
4.216	18.19%	8.433	18.30%	13.208	22.12%	17.018	13.23%
4.377	18.63%	8.534	13.18%	13.360	16.86%	17.180	18.45%
4.479	28.06%	8.636	20.22%	13.461	25.38%	17.281	14.55%
4.580	62.88%	8.738	20.71%	13.563	15.37%	17.383	12.92%
4.623	16.38%	8.907	16.66%	13.767	15.67%	17.424	13.14%
4.724	16.23%	9.011	15.71%	13.868	16.24%	17.526	13.51%
4.826	17.77%	9.112	18.53%	14.020	15.10%	17.628	14.66%
4.928	16.76%	9.195	22.79%	14.122	13.25%	17.729	10.75%
5.385	98.51%	9.296	12.28%	14.223	43.00%	17.831	13.80%
5.546	13.78%	9.398	29.29%	14.375	12.83%	17.882	6.53%
5.648	20.16%	9.550	28.04%	14.529	36.49%	17.982	13.25%

Table 2A-2 continued.

Depth m	H_2O
17.983	13.38%
18.084	14.11%
18.085	14.77%
18.186	18.90%
18.288	14.61%
18.339	11.59%
18.440	13.73%
18.440	11.13%
18.542	11.59%
18.694	11.65%
18.795	12.87%
18.897	11.27%
18.948	10.81%
18.997	11.89%
19.110	13.94%

Average	19.90%
Std Dev	12.26
High Value	98.51%
Low Value	6.53%

Table 2A-3. Lake Atna Core H1 Isotope Data
(Results in bold may be ambiguous due to low water content)

Depth m	δ ^{18}O Relative to VSMOW	δ D Relative to VSMOW	Depth m	δ ^{18}O Relative to VSMOW	δ D Relative to VSMOW
1.575	-19.2572‰	-163.0863‰	5.486	-19.0809‰	-149.9953‰
1.676	-20.5408‰	-155.9239‰	5.638	-18.2961‰	-140.6185‰
1.778	-19.0816‰	-173.3673‰	5.740	-18.5551‰	-148.5140‰
1.980	-18.8535‰	-156.3681‰	5.841	-17.8489‰	-125.8281‰
2.031	-19.6758‰	-150.5220‰	5.943	-18.0787‰	-147.3388‰
2.133	-19.4222‰	-167.2769‰	6.147	-18.2938‰	-145.0544‰
2.234	-19.1002‰	-160.1465‰	6.248	-19.0701‰	-132.9815‰
2.337	-19.1307‰	-172.5485‰	6.400	-18.1289‰	-152.2505‰
2.438	-18.0250‰	-156.4054‰	6.502	**-18.9412‰**	**-125.8573‰**
2.590	-17.9780‰	-158.0886‰	6.603	-18.9076‰	-153.0715‰
2.692	-17.4592‰	-161.7485‰	6.705	-18.3971‰	-156.8215‰
3.099	-18.1920‰	-140.2821‰	6.909	-18.3819‰	-144.0192‰
3.200	-18.2805‰	-137.6490‰	7.010	-18.8362‰	-140.7944‰
3.352	-18.4279‰	-157.8378‰	7.112	-18.3578‰	-149.9719‰
3.454	-18.8004‰	-164.6242‰	7.264	-18.8944‰	-153.2378‰
3.555	-18.0760‰	-135.4334‰	7.365	-19.6499‰	-142.3943‰
3.657	-18.5667‰	-162.5237‰	7.467	-19.4054‰	-144.5146‰
3.798	-18.0554‰	-157.8276‰	7.618	-18.8621‰	-145.4556‰
3.861	-18.3127‰	-152.8308‰	7.671	-19.5518‰	-147.8961‰
3.962	-17.8248‰	-146.9026‰	7.772	**-18.5062‰**	**-142.8419‰**
4.114	-18.6559‰	-156.7988‰	7.924	**-18.8394‰**	**-145.9520‰**
4.216	-18.9606‰	-163.3566‰	8.026	-19.2678‰	-154.1948‰
4.317	-17.8507‰	-160.1990‰	8.127	**-19.7315‰**	**-145.4372‰**
4.459	-18.4895‰	-152.4583‰	8.329	**-19.5138‰**	**-145.0329‰**
4.623	-18.9411‰	-128.6954‰	8.433	-17.8467‰	-153.6025‰
4.774	-18.3411‰	-151.9087‰	8.534	**-16.4771‰**	**-105.7322‰**
4.876	-18.9863‰	-137.6537‰	9.195	-17.9899‰	-143.0559‰
4.978	-18.7169‰	-153.1863‰	9.296	-19.2169‰	-152.7580‰
5.079	-18.5543‰	-147.4442‰	9.448	**-19.4067‰**	**-147.8288‰**
5.385	-18.2612‰	-143.4477‰	9.550	**-19.3503‰**	**-145.5319‰**

Table 2A-3 continued.

Depth m	δ¹⁸O Relative to VSMOW	δD Relative to VSMOW	Depth m	δ¹⁸O Relative to VSMOW	δD Relative to VSMOW
9.651	-19.2499‰	-146.0606‰	13.309	-19.6271‰	-139.3587‰
9.803	-19.8406‰	-123.8425‰	13.410	-19.7418‰	-153.6506‰
9.904	-18.9257‰	-153.8011‰	13.512	-19.2987‰	-156.8292‰
9.957	**-14.2022‰**	**-110.0638‰**	13.664	-19.2416‰	-156.1935‰
10.108	**-17.3452‰**	**-143.6134‰**	13.767	-19.7992‰	-132.0626‰
10.210	-18.6724‰	-161.3069‰	13.868	-18.5980‰	-134.1948‰
10.312	-19.2195‰	-157.1786‰	14.020	-19.3931‰	-146.6511‰
10.719	-18.7634‰	-153.0954‰	14.122	-19.6091‰	-152.0208‰
10.820	-19.1058‰	-158.4777‰	14.223	**-19.2811‰**	**-152.0208‰**
10.972	-19.1253‰	-154.9334‰	14.375	**-19.5105‰**	**-148.1878‰**
11.074	-19.3550‰	-156.6269‰	14.529	-17.9484‰	-137.4170‰
11.175	-18.9846‰	-155.8918‰	14.630	-19.6165‰	-147.6030‰
11.277	-18.6849‰	-159.1584‰	14.782	-19.0525‰	-140.2092‰
11.408	-19.0270‰	-151.7861‰			
11.481	-19.3632‰	-156.6209‰			
11.582	-18.8076‰	-167.8338‰			
11.734	-17.8858‰	-119.8747‰	Average	**-18.7066‰**	**-147.8880‰**
11.836	-16.4773‰	-139.8927‰	Std Dev	**0.8236**	**11.6823**
12.243	-18.6449‰	-146.7086‰	High Value	**-14.2022‰**	**-105.7322‰**
12.344	-18.6363‰	-149.3716‰	Low Value	**-20.5408‰**	**-173.3673‰**
12.446	-19.2873‰	-153.6642‰			
12.598	-18.7227‰	-147.7118‰			
12.699	-18.8266‰	-140.2462‰	Excluding low water content samples		
12.700	**-18.5740‰**	**-143.9260‰**			
12.802	**-19.1585‰**	**-134.7485‰**	Average	-18.7584‰	-149.8118‰
12.851	**-18.6023‰**	**-141.8949‰**	Std Dev	0.6561	10.5341
12.953	**-18.0711‰**	**-135.1644‰**	High Value	-16.4773‰	-119.8747‰
13.005	-17.1995‰	-132.8211‰	Low Value	-20.5408‰	-173.3673‰
13.055	**-19.1654‰**	**-147.7380‰**			
13.157	**-17.6376‰**	**-136.8861‰**			

Table 2A-4. Lake Atna Core H2 Isotope Data
(Results in bold may be ambiguous due to low water content)

Depth m	$\delta^{18}O$ Relative to VSMOW	δD Relative to VSMOW	Depth m	$\delta^{18}O$ Relative to VSMOW	δD Relative to VSMOW
0.051	-18.6328‰	-166.3614‰	5.546	-15.8217‰	-141.6040‰
0.152	-17.9854‰	-155.1138‰	5.648	-16.1847‰	-128.6381‰
0.254	-18.5351‰	-168.0018‰	5.800	-14.8183‰	-138.9738‰
0.356	-18.6570‰	-127.5495‰	5.901	-15.8873‰	-129.2073‰
0.507	-18.2881‰	-149.2749‰	6.003	-15.4772‰	-126.8045‰
1.575	-19.5427‰	-143.2689‰	6.104	-15.0120‰	-124.2196‰
1.676	-19.2762‰	-158.2152‰	6.147	-14.9483‰	-143.3434‰
1.828	-19.9440‰	-156.8205‰	6.248	-15.4142‰	-136.7823‰
1.930	-19.3488‰	-159.1034‰	6.350	-14.8795‰	-138.0075‰
2.031	-19.6532‰	-149.9957‰	6.452	-15.1750‰	-138.0078‰
2.183	-18.4783‰	-154.6790‰	6.553	-15.2709‰	-136.4877‰
2.337	-19.5688‰	-153.9556‰	6.705	-15.8759‰	-139.6029‰
2.488	-18.9050‰	-165.4366‰	6.806	-15.4021‰	-138.7809‰
2.590	-17.0859‰	-130.5456‰	6.909	-15.4967‰	-130.3143‰
2.692	**-17.3436‰**	**-126.7635‰**	7.010	-15.8881‰	-146.7408‰
3.099	-19.2104‰	-154.4173‰	7.172	-15.1062‰	-143.4435‰
3.250	-19.1416‰	-159.6321‰	7.274	-14.8229‰	-147.9021‰
3.352	-19.8000‰	-162.3613‰	7.373	-15.5218‰	-150.9754‰
3.454	-19.0110‰	-162.7721‰	7.537	-14.9771‰	-143.9624‰
3.555	-19.6061‰	-148.3403‰	7.671	**-18.4517‰**	**-144.4736‰**
3.707	-19.4022‰	-163.9723‰	7.832	-15.2632‰	-156.5738‰
3.808	-19.6051‰	-158.9891‰	7.934	-15.6911‰	-150.0702‰
3.861	-19.1484‰	-133.0151‰	7.985	-15.0414‰	-148.2673‰
4.012	-19.3307‰	-144.9745‰	8.036	-15.0285‰	-146.5721‰
4.114	-18.9453‰	-145.7963‰	8.137	-15.4880‰	-148.0555‰
4.216	-18.6454‰	-150.5474‰	8.239	-14.7518‰	-137.9734‰
4.377	-18.6850‰	-117.7595‰	8.400	-14.4904‰	-133.6896‰
4.479	-17.7120‰	-152.5533‰	8.433	-14.7782‰	-141.4070‰
4.580	-16.9813‰	-154.7728‰	8.534	-15.4422‰	-138.2926‰
4.623	-17.1676‰	-142.9280‰	8.636	-14.6149‰	-129.6709‰
4.724	-17.2902‰	-130.7665‰	8.738	-14.7033‰	-141.8658‰
4.826	-16.1794‰	-144.5618‰	8.907	-15.6438‰	-127.1705‰
4.928	-16.4073‰	-142.5931‰	9.011	-14.7735‰	-135.6283‰
5.385	-14.6806‰	-136.5937‰	9.112	-14.9232‰	-135.6050‰

Table 2A-4 continued

Depth m	$\delta^{18}O$ Relative to VSMOW	δD Relative to VSMOW	Depth m	$\delta^{18}O$ Relative to VSMOW	δD Relative to VSMOW
9.195	-15.4367‰	-119.2069‰	13.868	-15.0298‰	-137.4454‰
9.296	-15.0694‰	-123.8899‰	14.020	-16.7999‰	-134.7087‰
9.398	-15.6245‰	-122.5607‰	14.122	-15.4116‰	-133.4721‰
9.550	-15.7857‰	-133.4820‰	14.223	-17.1057‰	-132.8142‰
9.651	-15.8348‰	-132.4651‰	14.375	-16.7031‰	-139.0777‰
9.813	-14.6473‰	-139.9823‰	14.529	-16.5098‰	-126.0018‰
9.957	-13.5452‰	-132.6944‰	14.680	-16.7193‰	-157.1782‰
10.058	-13.9836‰	-134.0198‰	14.782	-16.2701‰	-148.3029‰
10.210	-13.9894‰	-123.1969‰	14.884	-17.1453‰	-152.4027‰
10.719	-16.3255‰	-144.7018‰	14.985	-16.2772‰	-146.9600‰
10.820	-15.9086‰	-132.9007‰	15.087	-17.0376‰	-134.5794‰
10.922	-15.4908‰	-115.3606‰	15.238	-17.6467‰	-160.0369‰
11.074	-16.3712‰	-151.6179‰	15.291	-17.2827‰	-140.6689‰
11.175	-16.5842‰	-142.6537‰	15.392	-16.9643‰	-146.1808‰
11.327	-16.8825‰	-126.3644‰	15.544	-16.9210‰	-151.6271‰
11.481	-15.9563‰	-145.5295‰	15.646	-17.4921‰	-146.0703‰
11.582	-17.0356‰	-143.9130‰	15.747	-16.6729‰	-144.1694‰
11.684	-17.2441‰	-154.7315‰	15.849	-17.5614‰	-148.1894‰
11.846	-16.7072‰	-144.5675‰	15.900	-14.7638‰	-126.4300‰
11.947	-16.1916‰	-152.2365‰	16.002	-15.9822‰	-137.0918‰
12.049	-15.3593‰	-145.0869‰	16.154	-17.3364‰	-157.5655‰
12.243	-14.4220‰	-147.7503‰	16.255	-17.1205‰	-137.3563‰
12.344	-17.1185‰	-156.0325‰	16.357	-16.9319‰	-136.4654‰
12.496	-16.3787‰	-127.2306‰	16.358	-15.8857‰	-150.1199‰
12.598	-15.3518‰	-132.3533‰	16.459	-17.2103‰	-135.0766‰
12.749	-16.0138‰	-138.5061‰	16.508	-17.4483‰	-157.1733‰
12.851	-16.5723‰	-146.5324‰	16.611	-16.8233‰	-145.2361‰
13.005	-15.9328‰	-145.1288‰	16.712	-16.9699‰	-145.8979‰
13.106	-16.3420‰	-144.1870‰	16.815	-16.4490‰	-147.9609‰
13.208	-16.5252‰	-146.3658‰	16.874	-17.1623‰	-150.4733‰
13.360	-15.9738‰	-147.9725‰	16.916	-17.9358‰	-139.6618‰
13.461	-14.9685‰	-141.9893‰	17.018	-18.2176‰	-134.9059‰
13.563	-15.9568‰	-144.8849‰	17.180	-18.0540‰	-152.8726‰

Table 2A-4 continued

Depth m	δ ^{18}O Relative to VSMOW	δ D Relative to VSMOW	Depth m	δ ^{18}O Relative to VSMOW	δ D Relative to VSMOW
17.383	-18.0648‰	-148.4046‰	18.542	-17.9182‰	-159.4115‰
17.424	-18.1870‰	-144.9830‰	18.694	-18.4419‰	-144.1079‰
17.526	-17.3418‰	-146.6585‰	18.795	-17.8666‰	-149.0448‰
17.628	-17.3104‰	-158.3442‰	18.897	-17.5077‰	-142.4017‰
17.729	**-18.1106‰**	**-142.6498‰**	18.948	**-16.6380‰**	**-142.4363‰**
17.831	-18.2115‰	-139.9209‰	18.997	-16.7636‰	-155.7366‰
17.882	**-18.4069‰**	**-152.4080‰**	19.110	-14.4996‰	-123.6648‰
17.982	-17.0582‰	-146.0425‰			
17.983	-16.3697‰	-122.6760‰			
18.084	-18.8264‰	-153.7364‰			
18.085	-18.2234‰	-151.1299‰	Average	**-16.7547‰**	**-143.1763‰**
18.186	-17.2744‰	-154.3610‰	Std Dev	1.4787	10.7821
18.288	-17.6504‰	-127.9162‰	High Value	**-13.5452‰**	**-115.3606‰**
18.339	-17.4284‰	-144.8658‰	Low Value	**-19.9440‰**	**-168.0018‰**
18.440	-17.2771‰	-157.2803‰			
18.440	-17.2313‰	-143.1918‰			

Excluding low water content samples		
Average	-16.7229‰	-143.1918‰
Std Dev	1.4899	10.8786
High Value	-13.5452‰	-115.3606‰
Low Value	-19.9440‰	-168.0018‰

Table 2A-5. Lake Atna Core H1 Cations: Ca, Fe, K and Mg.

Depth m	Ca mg/l	Fe mg/l	K mg/l	Mg mg/l	Depth m	Ca mg/l	Fe mg/l	K mg/l	Mg mg/l
1.575	0.4046	0.3426	0.1572	0.1600	7.010	0.4143	0.2180	0.2115	0.1589
1.676	0.6775	0.0849	0.1045	0.1273	7.112	0.4614	0.2699	0.1886	0.1705
1.778	0.5220	0.0112	0.1712	0.2019	7.264	0.4465	0.2263	0.2137	0.1551
1.980	0.5827	0.2055	0.1815	0.1839	7.365	0.4156	0.2357	0.2144	0.1564
2.031	0.6932	0.3042	0.2283	0.2489	7.467	0.4274	0.2446	0.2305	0.1567
2.133	0.3728	0.0480	0.1051	0.1070	7.618	0.4716	0.2719	0.2617	0.1684
2.234	0.8057	0.7035	0.3326	0.4074	7.671	0.4341	0.2546	0.2664	0.1634
2.337	0.4314	0.2680	0.1656	0.2052	7.772	0.3769	0.2036	0.2022	0.1286
2.438	0.4278	0.3162	0.1684	0.2344	7.924	0.3893	0.2240	0.2054	0.1377
2.590	0.5467	0.4535	0.2432	0.3068	8.026	0.4872	0.2117	0.2411	0.1567
2.692	0.3797	0.2153	0.1465	0.2034	8.127	0.4154	0.2538	0.3170	0.1446
3.099	0.6352	0.5437	0.2375	0.2884	8.329	0.3909	0.2348	0.2386	0.1395
3.200	0.5061	0.4052	0.2207	0.2511	8.433	0.6480	0.3146	0.4457	0.2128
3.352	0.5684	0.4842	0.2368	0.2797	8.534	0.7385	0.1937	0.3630	0.1751
3.454	0.4477	0.3671	0.2081	0.2437	9.195	0.3733	0.2615	0.2042	0.1321
3.555	0.4812	0.4627	0.2071	0.2487	9.296	0.3383	0.2464	0.1875	0.1228
3.657	0.4275	0.3468	0.1798	0.2126	9.448	0.3564	0.2640	0.1712	0.1346
3.798	0.4434	0.3714	0.1942	0.2256	9.550	0.3529	0.2396	0.1965	0.1326
3.861	0.6387	0.6078	0.2555	0.3285	9.651	0.3954	0.2764	0.2243	0.1424
3.962	0.8474	1.2836	0.5501	0.5653	9.803	0.3954	0.2516	0.2354	0.1328
4.114	0.8587	1.4599	0.5752	0.6239	9.904	0.3732	0.2558	0.2442	0.1335
4.216	0.5049	0.5084	0.2599	0.2555	9.957	0.2695	0.0120	0.1979	0.0507
4.317	0.7891	0.9994	0.3509	0.4573	10.108	0.2273	0.0193	0.1864	0.0468
4.459	0.7889	0.9439	0.3320	0.4182	10.210	0.2782	0.0542	0.3284	0.0656
4.623	0.2894	0.2163	0.1376	0.1324	10.312	0.2086	0.2099	0.3150	0.1070
4.774	0.3502	0.2179	0.1336	0.1473	10.719	0.2974	0.5275	0.3163	0.2292
4.876	0.2726	0.1709	0.1067	0.1180	10.820	0.2788	0.3533	0.2543	0.1687
4.978	0.3621	0.3210	0.1601	0.1706	10.972	0.2495	0.2849	0.2475	0.1382
5.079	0.3000	0.2443	0.1123	0.1272	11.074	0.2817	0.3574	0.3074	0.1685
5.385	0.4349	0.3214	0.2021	0.1918	11.175	0.2763	0.6181	0.2919	0.2533
5.486	0.4399	0.2961	0.2004	0.1868	11.277	0.5058	0.5495	0.3573	0.2533
5.638	0.4192	0.3328	0.1878	0.1928	11.408	0.5713	0.2654	0.2389	0.1460
5.740	0.4898	0.4169	0.2277	0.2163	11.481	0.4802	0.1810	0.1964	0.1267
5.841	0.4700	0.3758	0.2190	0.2107	11.582	0.4875	0.2735	0.2713	0.1728
5.943	0.4809	0.4135	0.2043	0.2154	11.734	0.5104	0.3936	0.2359	0.2055
6.147	0.6989	0.6930	0.2952	0.3262	11.836	0.5137	0.2953	0.2114	0.1725
6.248	0.6651	0.5864	0.2983	0.2959	12.243	0.4448	0.2990	0.2362	0.1574
6.400	0.6013	0.5146	0.2430	0.2583	12.344	0.4564	0.1942	0.2450	0.1152
6.502	0.6838	0.6164	0.2701	0.3037	12.446	0.4124	0.2894	0.2496	0.1530
6.603	0.5407	0.3974	0.2305	0.2200	12.598	0.4663	0.2975	0.2367	0.1551
6.705	0.5656	0.4762	0.2283	0.2302	12.699	0.4836	0.2555	0.2081	0.1413
6.909	0.3079	0.2574	0.2113	0.1487	12.700	0.4512	0.2712	0.1897	0.1400

Table 2A-5 continued

Depth m	Ca mg/l	Fe mg/l	K mg/l	Mg mg/l
12.802	0.4650	0.2858	0.2044	0.1634
12.851	0.4796	0.2340	0.2278	0.1814
12.953	0.3298	0.2377	0.2169	0.1562
13.005	0.3286	0.2334	0.1917	0.1458
13.055	0.6001	0.2776	0.2857	0.1629
13.157	0.4621	0.3394	0.2045	0.1699
13.309	0.5610	0.4776	0.2556	0.2274
13.410	0.4366	0.3860	0.2008	0.1731
13.512	0.4388	0.4061	0.2050	0.1851
13.664	0.5251	0.4549	0.2531	0.2173
13.767	0.3229	0.2320	0.1726	0.1106
13.868	0.4121	0.3110	0.1851	0.1452
14.020	0.4856	0.3556	0.2319	0.1752
14.122	0.4432	0.3555	0.2159	0.1675
14.223	0.4310	0.3661	0.2056	0.1748
14.375	0.3944	0.2868	0.2103	0.1408
14.529	0.1877	0.0047	0.2947	0.0279
14.630	0.3423	0.3585	0.2291	0.1607
14.782	0.1488	0.0280	0.1661	0.0291

	Ca	Fe	K	Mg
Average	0.4583	0.3436	0.2332	0.1914
Std Dev	0.1421	0.2221	0.0739	0.0920
High Value	0.8587	1.4599	0.5752	0.6239
Low Value	0.1488	0.0047	0.1045	0.0279

Table 2A-6. Lake Atna Core H2 Cations: Ca, K, Fe and Mg

Depth m	Ca mg/l	Fe mg/l	K mg/l	Mg mg/l	Depth m	Ca mg/l	Fe mg/l	K mg/l	Mg mg/l
0.051	0.3999	0.0219	1.2401	0.1343	6.003	0.4570	0.2192	0.2380	0.1910
0.152	0.9869	0.4956	0.1885	0.3164	6.104	0.3932	0.1990	0.1625	0.1533
0.254	0.7979	0.5897	0.2358	0.2847	6.147	0.4457	0.2850	0.3266	0.1980
0.356	0.6970	0.4538	0.2683	0.2472	6.248	0.5478	0.4819	0.2436	0.2583
0.507	0.4809	0.2530	0.1584	0.1654	6.350	0.4893	0.4115	0.2137	0.2152
1.575	0.5632	0.1054	0.2186	0.1861	6.452	0.5038	0.4767	0.2363	0.2354
1.676	0.6398	0.1876	0.1463	0.2194	6.553	0.5468	0.4603	0.2287	0.2380
1.828	0.6742	0.2461	0.1726	0.2154	6.705	0.5245	0.3387	0.2199	0.2151
1.930	0.5590	0.2167	0.4428	0.2183	6.806	0.5217	0.4032	0.2463	0.2122
2.031	0.4549	0.2014	0.4801	0.2086	6.909	0.6005	0.3650	0.2262	0.2294
2.183	0.5073	0.2939	0.1682	0.2245	7.010	0.5152	0.2475	0.1938	0.1926
2.337	0.5049	0.3524	0.1823	0.2439	7.172	0.4757	0.1926	0.1927	0.1718
2.488	0.3778	0.2306	0.1308	0.1953	7.274	0.5095	0.2405	0.1778	0.1703
2.590	0.4058	0.2317	0.1363	0.2024	7.373	0.4742	0.1935	0.1984	0.1607
2.692	0.4101	0.1933	0.1583	0.2275	7.537	0.4856	0.1811	0.1916	0.1528
3.099	0.5559	0.2101	0.2125	0.2367	7.671	0.3529	0.2119	0.2168	0.1287
3.250	0.4851	0.1615	0.1751	0.2033	7.832	0.3905	0.2093	0.1582	0.1379
3.352	0.4996	0.1634	0.1879	0.2086	7.934	0.3621	0.1984	0.1590	0.1385
3.454	0.5397	0.1718	0.1969	0.2155	7.985	0.3723	0.1967	0.1471	0.1318
3.555	0.5513	0.2074	0.2339	0.2262	8.036	0.3636	0.1929	0.1619	0.1276
3.707	0.5549	0.2013	0.2137	0.2218	8.137	0.3546	0.2275	0.2290	0.1556
3.808	0.4638	0.1642	0.2057	0.2032	8.239	0.3596	0.2829	0.1544	0.1505
3.861	0.4888	0.2703	0.1955	0.2035	8.400	0.4011	0.2354	0.2470	0.1676
4.012	0.4880	0.2174	0.2235	0.2092	8.433	0.3744	0.3019	0.2796	0.1993
4.114	0.5000	0.2018	0.2089	0.2120	8.534	0.4562	0.1960	0.2445	0.1656
4.216	0.4725	0.1888	0.1955	0.1942	8.636	0.4513	0.2376	0.2063	0.1655
4.377	0.4785	0.1979	0.1962	0.1898	8.738	0.4431	0.2936	0.2066	0.1809
4.479	0.5489	0.1866	0.2213	0.2053	8.907	0.4439	0.2890	0.2267	0.1725
4.580	0.4622	0.2031	0.1626	0.1641	9.011	0.4098	0.2686	0.2003	0.1617
4.623	0.4434	0.2641	0.1811	0.1799	9.112	0.4102	0.2444	0.1999	0.1542
4.724	0.4530	0.2456	0.1766	0.1740	9.195	0.5291	0.4041	0.2507	0.2260
4.826	0.4560	0.2283	0.1702	0.1777	9.296	0.4000	0.2582	0.1912	0.1650
4.928	0.3567	0.3190	0.3523	0.1904	9.398	0.4217	0.2783	0.2138	0.1725
5.385	N/S	N/S	N/S	N/S	9.550	0.5367	0.2686	0.2508	0.1737
5.546	0.4363	0.2224	0.1913	0.1793	9.651	0.4427	0.2723	0.2139	0.1811
5.648	0.4700	0.2232	0.2419	0.1836	9.813	0.4533	0.2525	0.2217	0.1797
5.800	0.3986	0.3106	0.1300	0.1712	9.957	0.4548	0.3132	0.2413	0.2054
5.901	0.4400	0.3636	0.1665	0.1923	10.058	0.4972	0.3955	0.3123	0.2143

Table 2A-6 continued

Depth m	Ca mg/l	Fe mg/l	K mg/l	Mg mg/l	Depth m	Ca mg/l	Fe mg/l	K mg/l	Mg mg/l
10.210	0.4246	0.3069	0.2417	0.1890	15.291	0.2584	0.2283	0.1537	0.1214
10.719	0.3759	0.2820	0.2716	0.1869	15.392	0.3055	0.2602	0.2354	0.1464
10.820	0.3542	0.2781	0.2640	0.1760	15.544	0.2978	0.3363	0.2352	0.1700
10.922	0.3814	0.3608	0.2752	0.1995	15.646	0.3210	0.3554	0.2629	0.1750
11.074	0.4295	0.4333	0.2110	0.2147	15.747	0.3474	0.3491	0.2463	0.1827
11.175	0.2855	0.3152	0.1881	0.1570	15.849	0.2965	0.2907	0.2333	0.1544
11.327	0.4814	0.2285	0.1969	0.1908	15.900	0.4581	0.5240	0.3187	0.2657
11.481	0.4591	0.3855	0.3133	0.2428	16.002	0.1749	0.0635	0.2173	0.0617
11.582	0.3615	0.2463	0.2346	0.1692	16.154	0.4726	0.4934	0.3099	0.2398
11.684	0.3083	0.2644	0.2349	0.1561	16.255	0.3356	0.3512	0.2471	0.1686
11.846	0.4501	0.3120	0.2929	0.2074	16.357	0.3328	0.4487	0.2755	0.2033
11.947	0.3597	0.3215	0.2393	0.1948	16.358	0.0838	0.0223	0.1824	0.0329
12.049	0.4485	0.1292	0.2376	0.1804	16.459	0.1366	0.1045	0.2256	0.0691
12.243	0.3049	0.2078	0.2158	0.1414	16.508	0.1391	0.1205	0.2020	0.0696
12.344	0.2735	0.2127	0.2069	0.1408	16.611	0.0819	0.0258	0.1601	0.0370
12.496	0.4170	0.3627	0.2939	0.2171	16.712	0.1327	0.0608	0.1789	0.0534
12.598	0.4682	0.3921	0.3147	0.2373	16.815	0.3229	0.3395	0.2021	0.1686
12.749	0.3618	0.2831	0.2985	0.1787	16.874	0.1613	0.0321	0.1733	0.0452
12.851	0.3228	0.2721	0.2502	0.1671	16.916	0.1997	0.1609	0.1517	0.0945
13.005	0.4022	0.3334	0.2930	0.2066	17.018	0.3603	0.4172	0.2436	0.2020
13.106	0.4008	0.3576	0.2778	0.2068	17.180	0.3419	0.4337	0.2467	0.2033
13.208	0.3421	0.3056	0.2323	0.1781	17.281	0.4588	0.5505	0.2945	0.2527
13.360	0.3889	0.3523	0.2370	0.1988	17.383	0.4602	0.5813	0.3161	0.2535
13.461	0.4399	0.4771	0.2956	0.2520	17.424	0.3017	0.4174	0.3127	0.2073
13.563	0.3083	0.2638	0.2265	0.1567	17.526	0.2976	0.3446	0.3775	0.1890
13.767	0.3460	0.2379	0.2135	0.1588	17.628	0.2750	0.2514	0.2528	0.1473
13.868	0.3419	0.2418	0.2291	0.1641	17.729	0.3083	0.2333	0.1994	0.1289
14.020	0.3979	0.3307	0.2817	0.2048	17.831	0.3375	0.3547	0.2685	0.1718
14.122	0.4162	0.5503	0.3540	0.2711	17.882	0.4507	0.4828	0.2979	0.2572
14.223	0.3586	0.4071	0.3079	0.2061	17.982	0.3164	0.3764	0.2481	0.1802
14.375	0.5313	0.2444	0.2502	0.1492	17.983	0.3540	0.4439	0.2829	0.2174
14.529	0.3038	0.3886	0.2854	0.1845	18.084	0.2263	0.2647	0.2298	0.1309
14.680	0.3035	0.3173	0.2463	0.1448	18.085	0.3446	0.3348	0.2512	0.1740
14.782	0.3067	0.3506	0.2318	0.1619	18.186	0.3502	0.3576	0.3334	0.1860
14.884	0.2881	0.3523	0.2471	0.1580	18.288	0.4092	0.4206	0.2940	0.2109
14.985	0.3537	0.4227	0.3204	0.1930	18.339	0.2911	0.2593	0.2203	0.1357
15.087	0.2939	0.2947	0.2469	0.1537	18.440	0.3488	0.3204	0.2484	0.1620
15.238	0.2939	0.2852	0.2461	0.1478	18.440	0.5907	0.7064	0.3252	0.3058

Table 2A-6 continued

Depth m	Ca mg/l	Fe mg/l	K mg/l	Mg mg/l
18.542	0.3054	0.2654	0.1868	0.1362
18.694	0.2879	0.2491	0.1899	0.1304
18.795	0.2961	0.2971	0.2524	0.1458
18.897	0.3032	0.2486	0.1853	0.1373
18.948	0.3836	0.0979	0.2734	0.1056
18.997	0.3500	0.3319	0.2160	0.1668
19.110	0.3557	0.0880	0.3580	0.1192

	Ca	Fe	K	Mg
Average	0.4065	0.2881	0.2400	0.1813
Std Dev	0.1205	0.1160	0.0981	0.0468
High Value	0.9869	0.7064	1.2401	0.3164
Low Value	0.0819	0.0219	0.1300	0.0329

Table 2A-7. Lake Atna Core H1 pH Values
(1:1 dilution, water to soil).

Depth m	pH	Depth m	pH	Depth m	pH	Depth m	pH
1.575	7.36	5.841	8.19	10.312	7.84	14.375	8.71
1.676	7.54	5.943	8.15	10.719	7.99	14.529	7.76
1.778	7.82	6.147	8.17	10.820	8.10	14.630	8.45
1.980	7.89	6.248	8.08	10.972	8.03	14.782	7.88
2.031	7.77	6.400	8.21	11.074	8.06		
2.133	7.87	6.502	8.05	11.175	8.36		
2.234	7.87	6.603	8.06	11.277	8.11		
2.337	7.95	6.705	8.16	11.408	8.08		
2.438	8.07	6.909	8.44	11.481	8.15	Average	8.15
2.590	8.10	7.010	8.12	11.582	8.21	Std Dev	0.24
2.692	8.02	7.112	8.20	11.734	8.18	High Value	8.74
3.099	8.17	7.264	8.08	11.836	8.26	Low Value	7.36
3.200	8.09	7.365	8.08	12.243	8.24		
3.352	8.16	7.467	8.07	12.344	8.16		
3.454	8.10	7.618	8.09	12.446	8.23		
3.555	8.13	7.671	8.02	12.598	8.21		
3.657	8.17	7.772	8.02	12.699	8.37		
3.798	8.14	7.924	8.15	12.700	8.42		
3.861	8.05	8.026	8.13	12.802	8.52		
3.962	8.08	8.127	8.05	12.851	8.45		
4.114	8.02	8.329	8.08	12.953	8.56		
4.216	8.09	8.433	7.74	13.005	8.14		
4.317	8.09	8.534	7.81	13.055	8.13		
4.459	8.16	9.195	8.11	13.157	8.60		
4.623	8.21	9.296	8.21	13.309	8.56		
4.774	8.14	9.448	8.13	13.410	8.74		
4.876	8.20	9.550	8.12	13.512	8.62		
4.978	8.28	9.651	8.11	13.664	8.58		
5.079	8.32	9.803	8.14	13.767	8.40		
5.385	8.26	9.904	8.11	13.868	8.60		
5.486	8.23	9.957	7.88	14.020	8.49		
5.638	8.18	10.108	7.88	14.122	8.53		
5.740	8.18	10.210	7.73	14.223	8.65		

Table 2A-8. Lake Atna Core H2 pH Values
(1:1 dilution, water to soil)

Depth m	pH	Depth m	pH	Depth m	pH	Depth m	pH
0.051	6.23	5.800	8.53	9.651	8.35	14.680	8.30
0.152	7.03	5.901	8.57	9.813	8.27	14.782	8.27
0.254	7.64	6.003	8.17	9.957	8.12	14.884	8.32
0.356	7.71	6.104	8.29	10.058	8.15	14.985	8.28
0.507	7.89	6.147	7.88	10.210	8.35	15.087	8.25
1.575	7.83	6.248	8.04	10.719	8.12	15.238	8.27
1.676	8.24	6.350	7.99	10.820	8.12	15.291	8.50
1.828	7.86	6.452	8.14	10.922	8.08	15.392	8.36
1.930	7.97	6.553	8.10	11.074	8.30	15.544	8.38
2.031	8.56	6.705	8.04	11.175	8.16	15.646	8.40
2.183	8.70	6.806	7.99	11.327	8.27	15.747	8.31
2.337	8.09	6.909	8.20	11.481	8.16	15.849	8.46
2.488	8.06	7.010	8.13	11.582	8.27	15.900	8.24
2.590	8.01	7.172	8.04	11.684	8.26	16.002	8.31
2.692	7.99	7.274	8.11	11.846	8.23	16.154	8.32
3.099	7.76	7.373	7.86	11.947	8.13	16.255	8.33
3.250	7.83	7.537	7.77	12.049	7.74	16.357	8.36
3.352	7.88	7.671	8.09	12.243	8.16	16.358	8.26
3.454	7.83	7.832	8.12	12.344	8.61	16.459	8.21
3.555	7.96	7.934	8.10	12.496	8.60	16.508	8.28
3.707	8.00	7.985	8.07	12.598	8.82	16.611	8.23
3.808	7.96	8.036	8.12	12.749	8.84	16.712	8.26
3.861	8.03	8.137	8.10	12.851	7.89	16.815	8.43
4.012	7.97	8.239	8.33	13.005	8.28	16.874	8.10
4.114	8.02	8.400	8.05	13.106	8.29	16.916	8.39
4.216	8.03	8.433	8.20	13.208	8.33	17.018	8.39
4.377	8.11	8.534	8.21	13.360	8.32	17.180	8.38
4.479	7.97	8.636	8.24	13.461	8.34	17.281	8.42
4.580	8.24	8.738	8.26	13.563	8.31	17.383	8.45
4.623	7.93	8.907	8.23	13.767	8.11	17.424	8.49
4.724	8.10	9.011	8.23	13.868	8.20	17.526	8.50
4.826	8.05	9.112	8.24	14.020	8.17	17.628	8.51
4.928	7.96	9.195	8.29	14.122	8.34	17.729	8.62
5.385	N/S	9.296	8.26	14.223	8.29	17.831	8.52
5.546	8.15	9.398	8.24	14.375	8.28	17.882	8.55
5.648	8.17	9.550	8.23	14.529	8.21	17.982	8.54

Table 2A-8 contunuted

Depth m	pH
17.983	8.63
18.084	8.48
18.085	8.58
18.186	8.17
18.288	8.20
18.339	8.60
18.440	8.38
18.440	8.73
18.542	8.61
18.694	8.64
18.795	8.45
18.897	8.66
18.948	8.31
18.997	8.53
19.110	8.21

Average	8.21
Std.Dev	0.29
High Value	8.84
Low Value	6.23

Table 2A-9. Lake Atna Core H1 μS/cm Conductivity
(2:1 dilution, water to soil)

Depth m	μS/cm	Depth m	μS/cm	Depth m	μS/cm	Depth m	μS/cm
1.575	175	5.841	137	10.312	192	14.375	193
1.676	248	5.943	134	10.719	85	14.529	243
1.778	164	6.147	166	10.820	71	14.630	168
1.980	129	6.248	174	10.972	140	14.782	224
2.031	186	6.400	169	11.074	164		
2.133	176	6.502	178	11.175	212		
2.234	236	6.603	158	11.277	144		
2.337	173	6.705	167	11.408	158		
2.438	86	6.909	180	11.481	142	Average	189
2.590	168	7.010	203	11.582	169	Std Dev	47
2.692	156	7.112	192	11.734	268	High Value	348
3.099	135	7.264	242	11.836	217	Low Value	71
3.200	182	7.365	239	12.243	201		
3.352	169	7.467	235	12.344	348		
3.454	147	7.618	266	12.446	322		
3.555	116	7.671	209	12.598	213		
3.657	152	7.772	191	12.699	245		
3.798	162	7.924	195	12.700	198		
3.861	153	8.026	190	12.802	209		
3.962	242	8.127	207	12.851	192		
4.114	168	8.329	218	12.953	191		
4.216	168	8.433	N/S	13.005	178		
4.317	216	8.534	N/S	13.055	200		
4.459	144	9.195	241	13.157	177		
4.623	186	9.296	222	13.309	184		
4.774	205	9.448	221	13.410	138		
4.876	182	9.550	201	13.512	183		
4.978	177	9.651	172	13.664	179		
5.079	151	9.803	207	13.767	256		
5.385	150	9.904	203	13.868	146		
5.486	123	9.957	307	14.020	234		
5.638	122	10.108	286	14.122	232		
5.740	126	10.210	259	14.223	206		

Table 2A-10. Lake Atna Core H2 µS/cm Conductivity
(2:1 dilution, water to soil)

Depth m	µS/cm	Depth m	µS/cm	Depth m	µS/cm	Depth m	µS/cm
0.051	134	5.385	N/S	9.011	250	13.461	253
0.152	538	5.546	112	9.112	238	13.563	218
0.254	177	5.648	164	9.195	214	13.767	227
0.356	189	5.800	113	9.296	216	13.868	166
0.507	167	5.901	124	9.398	287	14.020	195
1.575	357	6.003	142	9.550	240	14.122	210
1.676	259	6.104	150	9.651	177	14.223	204
1.828	182	6.147	168	9.813	216	14.375	203
1.930	119	6.248	149	9.957	150	14.529	147
2.031	122	6.350	157	10.058	226	14.680	171
2.183	92	6.452	139	10.210	207	14.782	187
2.337	157	6.553	187	10.719	175	14.884	206
2.488	174	6.705	129	10.820	180	14.985	188
2.590	163	6.806	110	10.922	170	15.087	148
2.692	179	6.909	212	11.074	118	15.238	67
3.099	195	7.010	219	11.175	171	15.291	222
3.250	209	7.172	242	11.327	219	15.392	224
3.352	244	7.274	196	11.481	226	15.544	258
3.454	244	7.373	205	11.582	226	15.646	247
3.555	203	7.537	163	11.684	253	15.747	232
3.707	287	7.671	234	11.846	191	15.849	240
3.808	239	7.832	245	11.947	235	15.900	283
3.861	223	7.934	221	12.049	69	16.002	255
4.012	227	7.985	218	12.243	174	16.154	254
4.114	165	8.036	239	12.344	218	16.255	248
4.216	204	8.137	272	12.496	233	16.357	261
4.377	199	8.239	131	12.598	258	16.358	264
4.479	151	8.400	262	12.749	248	16.459	268
4.580	155	8.433	173	12.851	241	16.508	316
4.623	288	8.534	238	13.005	254	16.611	267
4.724	222	8.636	216	13.106	186	16.712	224
4.826	235	8.738	268	13.208	206	16.815	226
4.928	203	8.907	252	13.360	168	16.874	326

Table 2A-10 continued

Depth (cm)	μS/cm
16.916	229
17.018	187
17.180	247
17.281	183
17.383	228
17.424	259
17.526	182
17.628	204
17.729	174
17.831	204
17.882	273
17.982	182
17.983	265
18.084	218
18.085	212
18.186	349
18.288	171
18.339	226
18.440	229
18.440	177
18.542	207
18.694	226
18.795	144
18.897	216
18.948	223
18.997	267
19.110	N/S

Average	209
Std Dev	56
High Value	538
Low Value	67

Table 2A-11. Lake Atna Core H1 meq/l Bicarbonate

Depth m	HCO₃ meq/l	Depth m	HCO₃ meq/l	Depth m	HCO₃ meq/l
1.575	0.090	6.400	0.220	11.481	0.500
1.676	0.320	6.502	0.510	11.582	0.600
1.778	0.380	6.603	0.210	11.734	0.370
1.980	0.500	6.705	0.010	11.836	0.390
2.031	0.550	6.909	0.380	12.243	0.470
2.133	0.350	7.010	0.310	12.344	0.660
2.234	0.700	7.112	0.280	12.446	0.520
2.337	0.340	7.264	0.340	12.598	0.460
2.438	0.390	7.365	0.310	12.699	0.460
2.590	0.470	7.467	0.340	12.700	0.410
2.692	0.350	7.618	0.280	12.802	0.330
3.099	0.330	7.671	0.450	12.851	0.400
3.200	0.420	7.772	0.430	12.953	0.320
3.352	0.500	7.924	0.420	13.005	0.580
3.454	0.430	8.026	0.440	13.055	0.330
3.555	0.230	8.127	0.500	13.157	0.090
3.657	0.360	8.329	0.440	13.309	0.480
3.798	0.370	8.433	0.630	13.410	0.520
3.861	0.640	8.534	0.560	13.512	0.460
3.962	0.670	9.195	0.340	13.664	0.590
4.114	0.660	9.296	0.360	13.767	0.440
4.216	0.530	9.448	0.400	13.868	0.190
4.317	0.650	9.550	0.350	14.020	0.500
4.459	0.660	9.651	0.370	14.122	0.440
4.623	0.230	9.803	0.450	14.223	0.340
4.774	0.300	9.904	0.420	14.375	0.380
4.876	0.220	9.957	0.390	14.529	0.280
4.978	0.290	10.108	0.290	14.630	0.460
5.079	0.280	10.210	0.360	14.782	0.340
5.385	0.410	10.312	0.390		
5.486	0.370	10.719	0.510		
5.638	0.350	10.820	0.410		
5.740	0.420	10.972	0.450		
5.841	0.410	11.074	0.620	Average	0.413
5.943	0.340	11.175	0.430	Std Dev	0.130
6.147	0.410	11.277	0.660	High Value	0.700
6.248	0.500	11.408	0.550	Low Value	0.010

Table 2A-12. Lake Atna Core H2 meq/l Bicarbonate

Depth m	HCO$_3$ meq/l	Depth m	HCO$_3$ meq/l	Depth m	HCO$_3$ meq/l	Depth m	HCO$_3$ meq/l	Depth m	HCO$_3$ meq/l
0.051	0.100	6.147	0.360	11.074	0.280	15.900	0.570	18.542	0.460
0.152	0.550	6.248	0.600	11.175	0.480	16.002	0.660	18.694	0.450
0.254	0.350	6.350	0.360	11.327	0.310	16.154	0.660	18.795	0.580
0.356	0.350	6.452	0.350	11.481	0.540	16.255	0.660	18.897	0.350
0.507	0.230	6.553	0.430	11.582	0.340	16.357	0.490	18.948	0.560
1.575	0.400	6.705	0.560	11.684	0.360	16.358	0.440	18.997	0.480
1.676	0.330	6.806	0.450	11.846	0.630	16.459	0.500	19.110	0.590
1.828	0.360	6.909	0.620	11.947	0.410	16.508	0.520		
1.930	0.400	7.010	0.470	12.049	0.360	16.611	0.360		
2.031	0.440	7.172	0.460	12.243	0.490	16.712	0.450	Average	0.459
2.183	0.510	7.274	0.400	12.344	0.560	16.815	0.560	Std Dev	0.118
2.337	0.310	7.373	0.370	12.496	0.500	16.874	0.410	High Value	0.720
2.488	0.310	7.537	0.470	12.598	0.630	16.916	0.580	Low Value	0.100
2.590	0.310	7.671	0.490	12.749	0.550	17.018	0.640		
2.692	0.350	7.832	0.390	12.851	0.600	17.180	0.650		
3.099	0.570	7.934	0.440	13.005	0.480	17.281	0.600		
3.250	0.600	7.985	0.350	13.106	0.470	17.383	0.300		
3.352	0.400	8.036	0.280	13.208	0.470	17.424	0.520		
3.454	0.470	8.137	0.350	13.360	0.410	17.526	0.510		
3.555	0.510	8.239	0.200	13.461	0.500	17.628	0.550		
3.707	0.150	8.400	0.350	13.563	0.460	17.729	0.460		
3.808	0.480	8.433	0.560	13.767	0.440	17.831	0.630		
3.861	0.420	8.534	0.560	13.868	0.610	17.882	0.660		
4.012	0.480	8.636	0.590	14.020	0.510	17.982	0.530		
4.114	0.450	8.738	0.460	14.122	0.570	17.983	0.540		
4.216	0.420	8.907	0.490	14.223	0.600	18.084	0.490		
4.377	0.390	9.011	0.400	14.375	0.600	18.085	0.540		
4.479	0.450	9.112	0.560	14.529	0.460	18.186	0.660		
4.580	0.360	9.195	0.380	14.680	0.480	18.288	0.620		
4.623	0.310	9.296	0.230	14.782	0.550	18.339	0.520		
4.724	0.310	9.398	0.400	14.884	0.650	18.440	0.540		
4.826	0.300	9.550	0.450	14.985	0.720	18.440	0.560		
4.928	0.320	9.651	0.370	15.087	0.520				
5.385	N/S	9.813	0.440	15.238	0.620				
5.546	0.460	9.957	0.430	15.291	0.360				
5.648	0.420	10.058	0.440	15.392	0.550				
5.800	0.260	10.210	0.390	15.544	0.470				
5.901	0.370	10.719	0.400	15.646	0.620				
6.003	0.390	10.820	0.410	15.747	0.540				
6.104	0.310	10.922	0.420	15.849	0.670				

Table 2A-13. Lake Atna Core H1 %Nitrogen and %Carbon Content

Depth m	%N	%C	Depth m	%N	%C	Depth m	%N	%C
1.575	0.170	2.216	6.705	0.044	0.699	12.446	0.079	0.846
1.676	0.111	1.757	6.909	0.058	0.844	12.598	0.070	1.064
1.778	N/S	N/S	7.010	0.055	1.028	12.699	0.063	0.771
1.980	0.021	1.293	7.112	0.024	0.763	12.700	0.033	0.784
2.031	0.042	1.122	7.264	0.046	0.786	12.802	0.045	0.726
2.133	0.036	1.044	7.365	0.042	0.801	12.851	0.054	0.814
2.234	0.054	1.137	7.467	0.040	0.828	12.953	0.051	0.794
2.337	0.117	1.251	7.618	0.076	0.744	13.005	0.043	0.829
2.438	0.055	1.256	7.671	0.069	0.831	13.055	0.043	0.724
2.590	0.084	1.232	7.772	0.076	0.829	13.157	0.030	1.814
2.692	0.072	1.208	7.924	0.055	0.769	13.309	0.055	0.732
3.099	0.045	0.915	8.026	0.076	0.814	13.410	0.038	0.600
3.200	0.077	0.961	8.127	0.068	0.739	13.512	0.038	0.734
3.352	0.065	0.886	8.329	0.078	0.690	13.664	0.039	0.706
3.454	0.074	0.948	8.433	0.053	0.783	13.767	0.055	0.883
3.555	0.045	0.827	8.534	0.052	0.768	13.868	0.036	0.693
3.657	0.118	0.873	9.195	0.049	0.829	14.020	0.047	0.835
3.798	0.066	0.925	9.296	0.056	0.822	14.122	0.075	0.783
3.861	0.048	0.830	9.448	0.060	0.897	14.223	0.047	0.751
3.962	0.043	0.828	9.550	0.053	0.772	14.375	0.065	0.683
4.114	0.060	0.860	9.651	0.072	0.830	14.529	0.041	0.730
4.216	0.053	0.831	9.803	0.072	0.818	14.630	0.042	0.689
4.317	0.045	0.841	9.904	0.069	0.807	14.782	0.043	0.729
4.459	0.040	1.578	9.957	0.053	0.797			
4.623	0.075	0.797	10.108	0.073	0.878			
4.774	0.069	0.805	10.210	0.056	0.777			
4.876	0.055	0.834	10.312	0.091	0.384			
4.978	0.042	0.812	10.719	0.109	0.452	Average	0.060	0.860
5.079	0.019	0.715	10.820	0.114	0.378	Std Dev	0.025	0.283
5.385	0.036	0.928	10.972	0.107	0.496	High Value	0.170	2.216
5.486	0.064	0.812	11.074	0.094	0.467	Low Value	0.017	0.131
5.638	0.055	0.750	11.175	0.082	0.377			
5.740	0.053	0.763	11.277	0.103	0.899			
5.841	0.053	0.877	11.408	0.069	1.148			
5.943	0.047	0.773	11.481	0.091	0.719			
6.147	0.017	0.700	11.582	0.082	0.664			
6.248	0.037	0.740	11.734	0.047	1.166			
6.400	0.023	0.725	11.836	0.068	1.189			
6.502	0.044	0.732	12.243	0.076	1.427			
6.603	0.034	0.833	12.344	0.020	0.131			

Table 2A-14. Lake Atna Core H2 %Nitrogen and %Carbon Content

Depth m	%N	%C	Depth m	%N	%C	Depth m	%N	%C
0.051	0.623*	14.257*	5.648	0.053	0.863	9.398	0.051	0.867
0.152	0.123	2.136	5.800	0.016	0.678	9.550	0.053	1.075
0.254	0.053	1.032	5.901	0.021	0.610	9.651	0.034	0.829
0.356	0.056	1.057	6.003	0.050	1.081	9.813	0.045	0.828
0.507	0.039	0.831	6.104	0.025	0.754	9.957	N/S	N/S
1.575	0.017	0.856	6.147	0.045	0.876	10.058	N/S	N/S
1.676	0.044	0.900	6.248	0.052	0.670	10.210	0.052	0.684
1.828	0.038	0.866	6.350	0.044	0.699	10.719	0.094	0.765
1.930	0.048	0.905	6.452	0.031	0.958	10.820	0.066	0.761
2.031	0.026	0.873	6.553	0.047	0.746	10.922	0.078	1.156
2.183	0.037	0.747	6.705	0.062	1.024	11.074	N/S	N/S
2.337	0.045	0.943	6.806	0.066	0.991	11.175	0.068	0.774
2.488	0.048	0.994	6.909	0.038	0.888	11.327	0.063	0.727
2.590	0.051	0.995	7.010	0.086	0.957	11.481	0.023	0.588
2.692	0.074	0.940	7.172	0.062	0.705	11.582	0.031	0.645
3.099	0.043	0.941	7.274	N/S	N/S	11.684	0.041	0.724
3.250	0.050	0.882	7.373	0.026	0.828	11.846	0.045	0.595
3.352	0.067	0.833	7.537	0.060	0.884	11.947	0.054	0.661
3.454	0.061	0.962	7.671	0.072	0.861	12.049	0.061	0.625
3.555	0.056	0.965	7.832	0.066	0.868	12.243	0.050	0.667
3.707	0.063	0.939	7.934	0.050	0.845	12.344	0.037	0.583
3.808	0.033	0.844	7.985	N/S	N/S	12.496	0.048	0.580
3.861	0.062	0.705	8.036	0.025	0.681	12.598	0.045	0.694
4.012	0.073	0.909	8.137	0.038	0.620	12.749	0.049	0.722
4.114	0.052	0.896	8.239	0.043	0.677	12.851	0.074	0.706
4.216	0.046	0.476	8.400	0.048	0.716	13.005	0.081	0.989
4.377	0.058	0.848	8.433	0.072	0.621	13.106	0.073	0.828
4.479	0.061	1.007	8.534	0.072	1.078	13.208	0.061	0.732
4.580	N/S	N/S	8.636	0.058	0.948	13.360	0.061	0.782
4.623	0.068	0.958	8.738	0.062	0.841	13.461	0.046	0.910
4.724	0.073	0.867	8.907	0.053	0.865	13.563	0.064	0.614
4.826	0.089	0.883	9.011	0.065	0.825	13.767	0.083	0.798
4.928	0.073	1.069	9.112	0.047	0.830	13.868	0.082	0.746
5.385	N/S	N/S	9.195	0.039	0.812	14.020	0.065	0.764
5.546	0.052	0.859	9.296	0.046	0.761	14.122	0.072	1.196

*Not included in statistics, see text.

Table 2A-14 continued

Depth m	%N	%C	Depth m	%N	%C
14.223	N/S	N/S	17.729	0.043	0.725
14.375	0.076	0.642	17.831	0.073	0.817
14.529	N/S	N/S	17.882	0.055	1.048
14.680	0.059	0.637	17.982	0.046	0.742
14.782	0.066	0.835	17.983	0.075	0.781
14.884	0.073	0.782	18.084	0.093	0.779
14.985	0.077	1.022	18.085	0.057	0.745
15.087	0.078	0.630	18.186	0.060	0.866
15.238	0.082	0.776	18.288	0.053	0.732
15.291	0.067	0.785	18.339	0.065	0.948
15.392	0.061	0.772	18.440	0.038	0.830
15.544	0.085	0.749	18.440	0.056	0.686
15.646	0.072	0.788	18.542	0.055	1.018
15.747	0.087	0.770	18.694	0.047	0.787
15.849	0.077	0.704	18.795	0.066	0.848
15.900	0.056	0.760	18.897	0.039	0.788
16.002	0.051	0.708	18.948	0.037	0.992
16.154	0.057	0.768	18.997	0.046	0.782
16.255	0.040	0.728	19.110	0.052	0.817
16.357	0.076	0.754			
16.358	0.059	0.724			
16.459	0.060	0.763			
16.508	0.048	0.755			
16.611	0.050	0.681	Average	0.057	0.824
16.712	0.047	0.720	Std Dev	0.017	0.170
16.815	0.053	0.753	High Value	0.123	2.136
16.874	0.077	0.815	Low Value	0.016	0.476
16.916	0.063	1.071			
17.018	0.055	0.898			
17.180	0.037	0.735			
17.281	0.040	0.690			
17.383	0.057	0.724			
17.424	0.083	0.750			
17.526	0.068	0.743			
17.628	0.070	1.071			

Table 2A-15. Lake Atna Core H1 Chemistry Correlations
Results in under lined and bold type reflect correlation coefficients greater than 0.70.

	Depth	H₂O	δ¹⁸O	δD	N	C	Ca	Fe	K	Mg	pH	Conductivity	Bicarbonate
Depth	1.000	-0.436	-0.092	0.292	-0.095	-0.389	-0.382	-0.243	0.058	-0.451	0.534	0.314	0.065
H₂0	-0.436	1.000	-0.065	-0.478	0.440	0.232	0.135	0.027	-0.048	0.201	-0.347	-0.289	0.012
δ¹⁸O	-0.092	-0.065	1.000	0.389	-0.189	0.074	0.054	0.045	0.112	0.092	-0.117	0.050	-0.045
δD	0.292	-0.478	0.389	1.000	-0.325	-0.093	-0.063	-0.132	-0.029	-0.201	0.161	0.259	-0.130
N	-0.095	0.440	-0.189	-0.325	1.000	0.217	-0.236	-0.100	-0.021	-0.105	-0.352	-0.114	0.004
C	-0.389	0.232	0.074	-0.093	0.217	1.000	0.276	0.023	-0.208	0.122	-0.292	-0.045	-0.191
Ca	-0.382	0.135	0.054	-0.063	-0.236	0.276	1.000	0.681	0.518	**0.793**	-0.092	-0.094	0.421
Fe	-0.243	0.027	0.045	-0.132	-0.100	0.023	0.681	1.000	0.686	**0.946**	0.119	-0.223	0.426
K	0.058	-0.048	0.112	-0.029	-0.021	-0.208	0.518	0.686	1.000	0.638	-0.146	0.057	0.586
Mg	-0.451	0.201	0.092	-0.201	-0.105	0.122	**0.793**	**0.946**	0.638	1.000	-0.010	-0.268	0.443
pH	0.534	-0.347	-0.117	0.161	-0.352	-0.292	-0.092	0.119	-0.146	-0.010	1.000	-0.077	-0.031
Conductivity	0.314	-0.289	0.050	0.259	-0.114	-0.045	-0.094	-0.223	0.057	-0.268	-0.077	1.000	0.040
Bicarbonate	0.065	0.012	-0.045	-0.130	0.004	-0.191	0.421	0.426	0.586	0.443	-0.031	0.040	1.000

Table 2A-16. Lake Atna Core H2 Chemistry Correlations.
Results in underlanded bold type reflect correlation coefficients greater than 0.70.

	Depth	H₂O	δ¹⁸O	δD	N	C	Ca	Fe	K	Mg	pH	Conductivity	Bicarbonate
Depth	1.000	-0.278	0.131	0.059	0.182	-0.300	-0.674	0.199	0.049	-0.358	0.632	0.165	0.480
H₂0	-0.278	1.000	0.147	-0.024	-0.100	0.006	0.116	-0.082	0.198	-0.002	-0.302	-0.200	-0.343
δ¹⁸O	0.131	0.147	1.000	0.504	-0.033	-0.167	-0.121	0.092	-0.071	-0.125	0.116	-0.086	-0.015
δD	0.059	-0.024	0.504	1.000	-0.025	-0.069	-0.004	0.138	-0.077	0.054	0.191	-0.080	0.023
N	0.182	-0.100	-0.033	-0.025	1.000	0.349	-0.072	0.101	0.090	0.006	-0.160	0.224	0.200
C	-0.300	0.006	-0.167	-0.069	0.349	1.000	0.452	0.103	-0.019	0.288	-0.438	0.291	0.017
Ca	-0.674	0.116	-0.121	-0.004	-0.072	0.452	1.000	0.339	0.019	**0.776**	-0.440	-0.003	-0.096
Fe	0.199	-0.082	0.092	0.138	0.101	0.103	0.339	1.000	0.104	**0.733**	0.254	-0.038	0.305
K	0.049	0.198	-0.071	-0.077	0.090	-0.019	0.019	0.104	1.000	0.141	-0.339	-0.112	0.023
Mg	-0.358	-0.002	-0.125	0.054	0.006	0.288	**0.776**	**0.733**	0.141	1.000	-0.134	-0.078	0.125
pH	0.632	-0.302	0.116	0.191	-0.160	-0.438	-0.440	0.254	-0.339	-0.134	1.000	-0.044	0.359
Conductivity	0.165	-0.200	-0.086	-0.080	0.224	0.291	-0.003	-0.038	-0.112	-0.078	-0.044	1.000	0.138
Bicarbonate	0.480	-0.343	-0.015	0.023	0.200	0.017	-0.096	0.305	0.023	0.125	0.359	0.138	1.000

Table 2A-17. Statistical Comparisons of Significant Differences in Chemical Parameters Between Core H1 and Core H2.

H1 and H2 Core Data Significantly Different

Parameter	H_2O	$\delta^{18}O$	δD	Ca	Conductivity 2:1 dilution	HCO_3
F-test =	3.40E-06	1.15E-09	0.364	0.063	0.0587	0.246
T-test =	0.00232	1.21E-32	0.00048	0.00088	0.00123	0.00162

H1 and H2 Core Data Not Significantly Different

Parameter	N	C	Fe	K	Mg	pH 1:1 dilution
F-test =	1.02E-12	7.16E-36	2.81E-13	0.00223	3.37E-14	0.0208
T-test =	0.37355	0.42190	0.01048	0.26364	0.15191	0.04915

Table 2A-18. Fairbanks Area Thaw Lake and Groundwater Isotopes.

Summary Data, Fall 2009

Site	Designation	$\delta^{18}O$	δD
Ballaine Lake	Thaw Lake	-16.658‰	-140.926‰
Smith Lake	Thaw Lake	-12.319‰	-124.227‰
Hagelbarger Pond	Thaw Lake	-16.235‰	-137.093‰
Tap Water	Ground Water	-19.601‰	-149.904‰
Well Water	Ground Water	-18.972‰	-145.773‰

Chapter 3

Characterization of Loess Deposition and Permafrost Development by Chemical and Isotopic Analysis of a Soil Core from Northeast of Fairbanks, Alaska

INTRODUCTION

Fairbanks, Alaska is located in central Alaska at the northern extent of the Tanana River valley floodplain (Figure 3.1; Pearson and Hermans, 2008) and is built on the combined floodplains of the Chena and Tanana Rivers (Péwé and Reger, 1989). The floodplain itself is bounded by the Alaska Range to the south and by hills to the north that are part of the Yukon-Tanana upland (Péwé, 1977).

Central Alaska has been glaciated in small local mountain passes, but glaciers never advanced closer than 80 km of Fairbanks on the Tanana floodplain (Péwé, 1977). However, glacial outflows into rivers deposited over two hundred meters of silt, sand and gravel in the Tanana Valley and a large amount of silt was subsequently transported by wind to surrounding hills where it accumulated to depths of over 100m in valleys and over 60 m on hillsides (Péwé, 1977; Péwé and Reger, 1989). A loess bed (known as Gold Hill Loess) to the west of Fairbanks is a popular research area because nearly the full depth of the loess was exposed during gold mining operations. The bed is as much as 55 m thick at some locations (Preece et al., 1999). Research on tephrochronology in the bed indicates that loess deposition may have begun as early as 3 Ma ago in interior
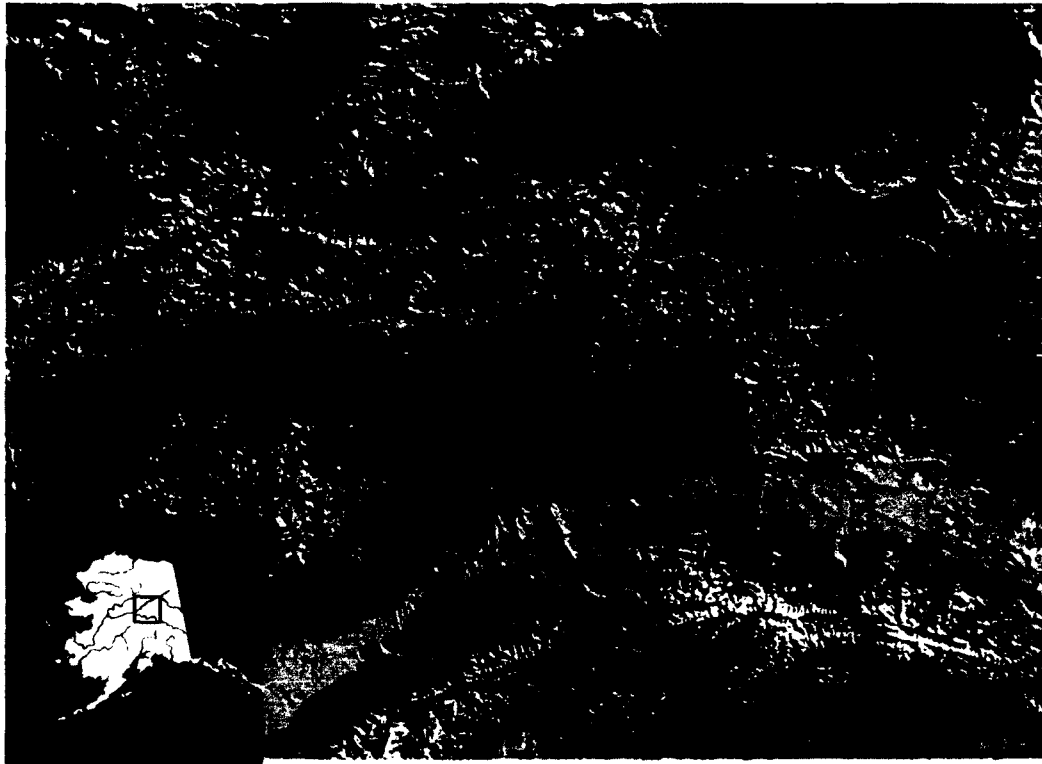
**Figure 3.1 Hagelbarger site. The dot is Fairbanks location. The box above
the dot is the study site location.**

Alaska (Westgate and Stemper, 1990) and that loess has been deposited in the Fairbanks

area during several glaciations. Chemical and mineralogical analyses of loess from

various sites in central Alaska confirm that loess deposition was episodic (Muhs et al.,

2003), and also that at different times loess was blown in from different outwash sources,

such as the Tanana River to the south, the Yukon River to the north and the Nenana River

to the southeast (Muhs and Budahn, 2006).

Loess deposits are interspersed at most locations with thin beds of paleosols,

which indicate periods between heavy loess deposition when the landscape was stable

enough for plant material to produce soils by pedogenesis (Höfle and Ping, 1996; Muhs

et al., 2003; Verosub et al., 1993). There is evidence that the deep loess deposits in the

Fairbanks area are the result of the presence of trees and large shrubs which facilitate the

accumulation of windblown silt, even during periods of lower loess production, such as

interglacials. The competing processes of loess deposition and pedogenesis occur during

both glacial and interglacial periods (Beget, 1996; Muhs et al., 2003). This suggests that

loess deposits are a stratigraphic archive from which climate records can be

reconstructed. Loess deposits are unconsolidated and subject to many kinds of downhill

transport such as soil creep, solifluction and slumping, as well as removal by erosional

processes. Many loess deposits in valleys have been found to have been retransported

after their original deposition. However, upland loess sites that have not been disturbed

are more likely to be mostly or wholly air-fall silt (Beget, 2001; Muhs et al., 2003).

About half the uplands in the Fairbanks area are underlain by permafrost, but

Fairbanks is in the discontinuous permafrost zone and the ground is relatively warm

(typically between -1.0° and 0° C) so the permafrost is sensitive to disturbance (Péwé and Reger, 1989). Present permafrost in the area is thought to be the result of the severe climate of the latest glacial stage (Péwé, 1977; French, 1999) although a short warming interval thought to have occurred about 5000 to 8000 years ago caused the permafrost table to be lowered (Péwé, 1977). In more recent times there have been several episodes of alternating colder and warmer periods, ending with the warming trend of the 1980's which is continuing to the current time (Jorgenson et al., 2001; Romanovsky et al., 2007; Smith et al., 2010). In some areas the upper boundary of permafrost lies below the depth of the seasonally frozen layer, indicating residual or relict permafrost. The thaw layer above permafrost, known as a talik, is an unfrozen layer that was formerly permafrost which lies between the active layer above and the actual permafrost body below.

Permafrost presence and extent depends on site factors such as geologic materials, soil properties, vegetation cover, slope angle and aspect and the history of disturbance. Depth to the permafrost table ranges from less than 1 m to over 27 m where permafrost is still extant, and known thickness of permafrost ranges from 3 m to more than 80 m in the Fairbanks area (Péwé, 1977; Toniolo et al., 2009).

With proper interpretation chemical and isotopic changes that occur in the silt and pore water of the loess deposits can reveal environmental processes that occurred in the past. The record in the silt reaches back further, but has less resolution than the permafrost pore ice isotope record.

RESEARCH AREA

The field site (Figure 3.2) is a nearly square 4-acre lot on the north side of

Hagelbarger Avenue 6 miles (10 km) northeast of Fairbanks, Alaska (-147.621°,

64.909°). To the south of the lot and about 100 m south of Hagelbarger Avenue is a ridge

that runs east to west. On the north side of the site is an unimproved area that has bog

vegetation and usually has very wet soil in the summer. The site is at approximately

300 m asl and slopes to the northwest about 10 degrees. The land was unimproved until it

was purchased for a house site in 1971. In 1977 a water well log recorded frozen silt

from 0' to 8' depth (0 - 2.4 m), mud from 8' to 15' depth (2.4 - 4.6 m), frozen silt from

15' to 97' depth (4.6 - 29.6 m) and schist from 97' to 130' depth (29.6 - 40 m). Depth to

the permafrost table beneath a house on a lot about half a mile east on Hagelbarger

Avenue was approximately 6 meters in the mid 1990's (Davis, 2000).

Excavation for a house basement on the lot exposed charcoal fragments at several

depths one or two meters below the surface, indicating the area had been burned several

times in the past. Unfortunately no record was made of the depths or concentrations of

these fragments. However, in 2010 trenches were dug on the north and south sides of

that basement in order to install piers. At a consistent depth of 60 cm to 75 cm there were

numerous small (about 0.5 cm diameter) rounded grey spots scattered at average spacing

of approximately 30 cm apart. These were spots of ash that had no charcoal in them but

that seemed to mark the location of organic material, probably roots, that burned in place.

These grey spots were located the full length and on both sides of both trenches.
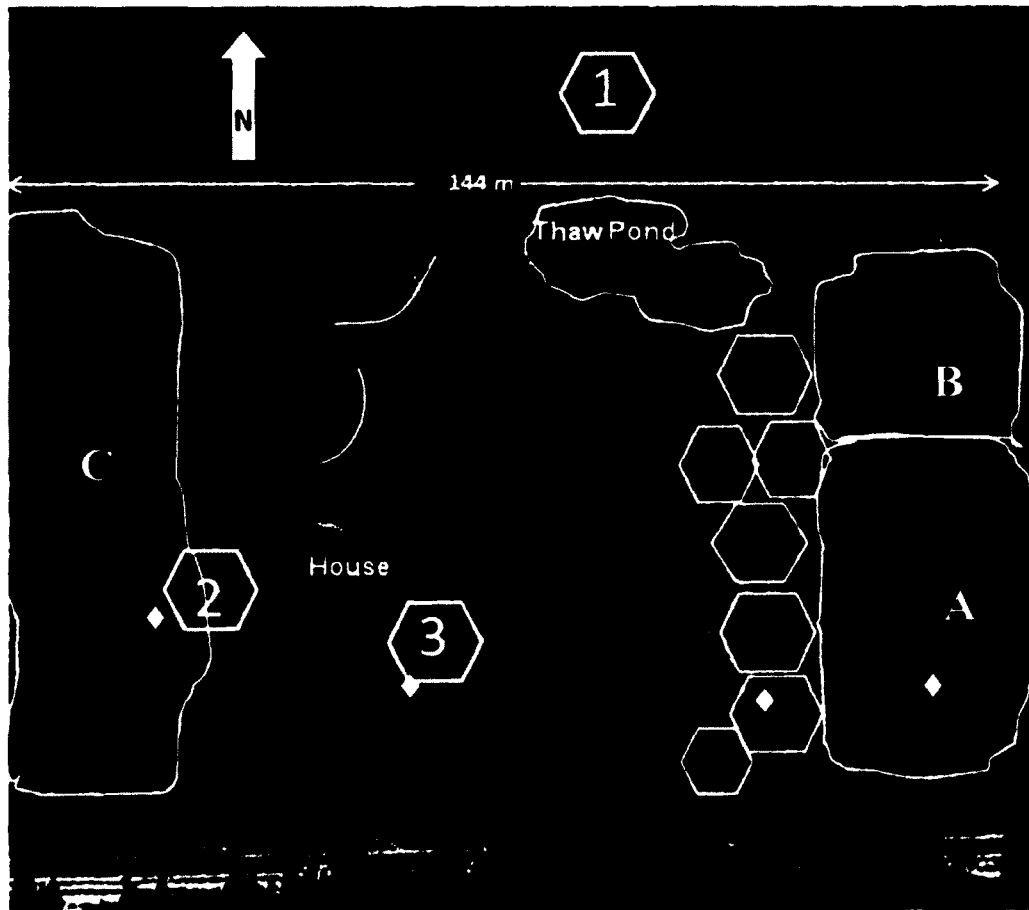
Scraped, covered with fill	A
Scraped, not covered, swampy area	B
Undisturbed	C
Pilot hole location (to top of permafrost)	◇
Polygons in scraped, not covered, area	⬡⬡
Sunken trenches	⌐
Shallow core	1
Auger core	2
Hagelbarger core	3

Figure 3.2 Research site, Hagelbarger Avenue, Fairbanks.

There was no air temperature, rainfall or snowfall record for this site prior to

coring, but it is known to benefit from thermal inversion. Spring bud break is delayed by

about two weeks compared with south aspect or level sites and winter temperatures range

from 5° C to 10° C warmer than the official airport temperatures. Temperature

measurements made at the site from 2009-2011 (Figure 3.3) confirm this.

Vegetation on the site in 1977 was mostly black spruce (*Picea mariana*), young

(20- to 30-year-old) paper birch (*Betula papyrifera*), Labrador tea (*Ledum*

groenlandicum), alder (*Alnus tenufolia*), willow (*Salix*), wild rose (*Rosa acicularis*), and

mosses. Plant cover on the eastern half of the site at that time was a moss and black

spruce bog. In 1980 the two acres on the east half of the site were bull-dozed clear of all

vegetation down to mineral soil. The following summer approximately one-half acre (the

southeast-most part) of the cleared area was covered with old roadbed material to a depth

of from one-third to one-half meter. The roadbed material consisted of silt and rocks

with very little sand or gravel. Two years later an additional acre just west of the cleared

area had alder and small black spruce removed, but was not scraped down to mineral soil.

Ground cover in this thinned area was mostly horsetail (*Equisetum*) rather than moss, and

birch and large black spruce were left standing. The rest of the site (the west-most acre),

vegetated to the south by a dense stand of black spruce and moss and to the north

by mixed shrubs, mosses and larch (*Larix laricina*), was left alone. Over 30 years the

scraped area has developed extensive thermokarst depressions more than 2 m in depth, as

well as polygons and ponds, while the area that was covered by road material has
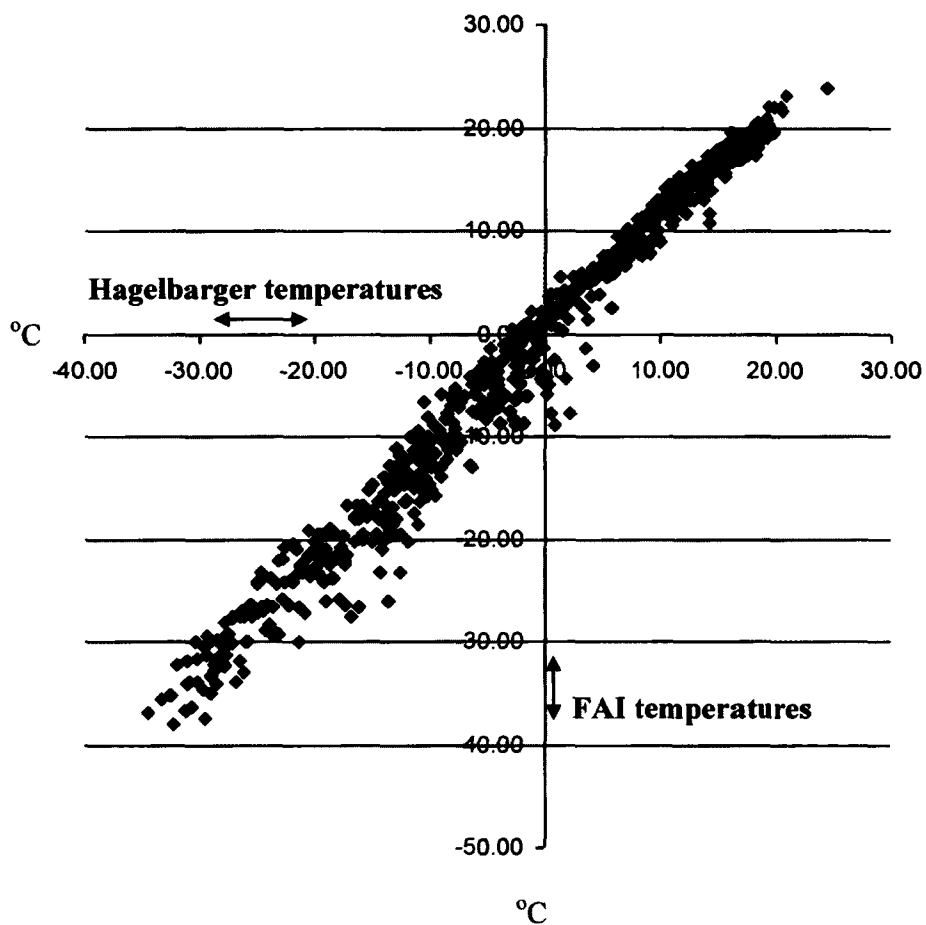
**Figure 3.3 Comparison of air temperatures at Hagelbarger site (horizontal axis)
with Fairbanks International Airport (FAI) air temperatures
(vertical axis), 2009-2011 (*Figure courtesy of V.E. Romanovsky*).**

maintained an even surface but that surface has sunk relative to the surrounding terrain by nearly half a meter.

The thinned area appeared unchanged for nearly 15 years, but eventually developed several thermokarst depressions. The undisturbed site has shown no change. A permafrost pilot hole was drilled in each of the four areas (scraped, scraped then covered, thinned and undisturbed) in the summer and fall of 2005. The holes were located at a distance of at least 20 m from any structure, and about 30 m north of the southern boundary of the site (Figure 3.2). The drill was water lubricated and penetrated the silt easily. The drill was determined to have encountered permafrost when the rate of descent slowed dramatically or stopped. Three pilot holes drilled in the disturbed areas encountered permafrost at depths of around 6 meters, but the pilot hole at the undisturbed site penetrated only about 1 meter before it met permafrost. Depth of moss at the undisturbed site was approximately 15 cm.

SAMPLING AND SAMPLE PROCESSING

There were three separate sample sets collected from the site, and they were sampled at three different intensities. In February 2007 the first sample set was collected from the main core (Hagelbarger core) that was drilled from the "thinned but not scraped" area within a few meters of the pilot hole that had been drilled in 2005 (Figure 3.2). Samples were collected from 6.1 m down to 25.6 m depth. Depth to permafrost as determined by change of drilling speed was 6.1 m, and at about 25 m another change in drill speed indicated the full depth of permafrost had been penetrated.

Temperature data taken from the core borehole later confirmed the drill log indicators for

permafrost (Figure 3.4). For the first 3 m of permafrost drilled (6.1 m to 9.1 m) samples

were taken at 30 cm intervals from the drill auger when it was raised from the borehole,

and placed directly into labeled WhirlPak™ bags. This interval was calculated to allow

for the stretching of the soil as it was pulled along the auger flights during drilling so that

the actual sample interval was 15 cm. For samples below 9.1 m depth, a corer was used

that was able to bring up sample cores intact, and when those cores were removed from

their casing, samples were taken at actual 15 cm intervals. The samples taken from the

core sections were cut off the core with a dull knife and placed into Whirlpak™ bags as

soon as the core was removed from the casing. The cores were frozen to a point of

plasticity when they came out of the ground, and if samples were taken immediately

before they froze solid, it was possible to cut through the core easily. The core sampling

method was used for the rest of the drilling down to 25.6 m depth.

For the core sampling method the loess cores had to be pushed out of a casing.

The casing was heated briefly with a propane torch in order to thaw a thin layer of mud

between the casing wall and the core itself, and the core was pushed out before the

thawed mud could refreeze. The core that was taken at 19.52 m (from 19.52 to 21.35 m)

was especially difficult to remove and eventually only part of the core was collected and

that part was completely thawed. Therefore, although there were four samples collected

from the core, the values for water content and isotope analyses were not useable and so

those four samples were only used for chemical analysis. Data computations were

adjusted accordingly.
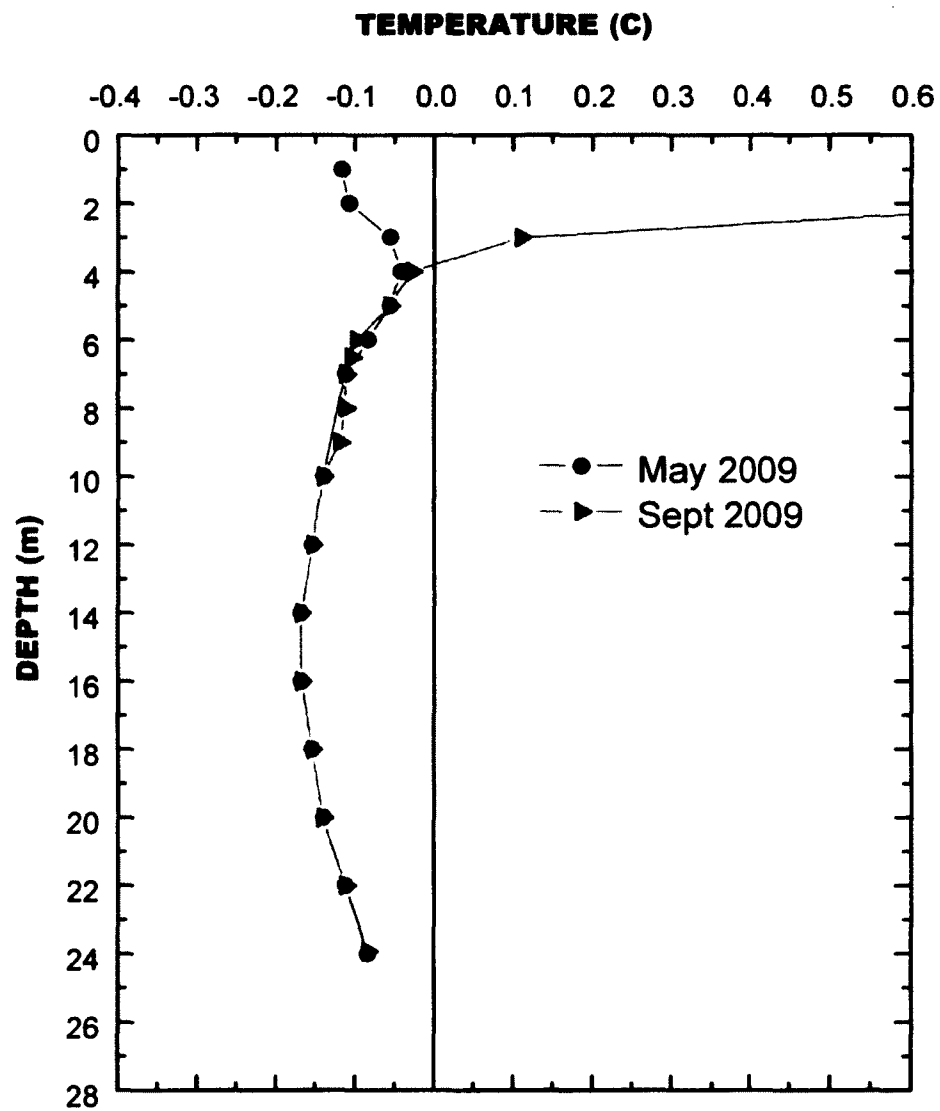
Figure 3.4 Borehole temperatures for Hagelbarger core. Freezing point depression is 0.08°C (*Figure courtesy of V.E. Romanovsky*).

At 25 m the drill penetrated through the bottom of the permafrost. The data for the last core, from 25.16 to 25.62 m, are included in the graphs of isotope and water content data but they should be noted as outside the permafrost data set, and they are not included in data processing.

The silt of the core was a dark tan color (while wet) throughout, except for light green material at 14.64 m and from 18.00 to 19.52 m. There was rust colored material at 19.52 m. From 22.57 to 25.62 m the entire core was greenish and had areas of darker material.

The second sample set (auger core) was taken in March, 2009, from a site approximately 30 m to the west-northwest of the first core. In order to install a temperature probe for the site, a borehole was augured at this location. It was convenient to take samples from the auger in order to check that the samples taken from the earlier Hagelbarger core actually reflected the depths assigned to them, especially the samples taken from the auger flights. A few samples were taken from the auger as the hole was drilled, using the same method to estimate the depth of sample source as had been done on the Hagelbarger core. This borehole was drilled on the very eastern edge of the west section of the site (Figure 3.2).

The west section is undisturbed and the permafrost table in the center of the site is at 1 meter. Just beyond the eastern edge is a driveway that is likely to have increased the depth of the active layer. This seems to be substantiated by the drill log for the auger borehole which showed the auger penetrated seasonal ice at 1.5 m and the drill appeared to enter permanently frozen material at 3 m below the surface. At slightly more than

24 m the drill began to seize, an indication of soft (thawed) material and drilling was stopped. Temperatures taken from the auger borehole later essentially confirmed the depth to permafrost table, and depth of permafrost at the site (Figure 3.5).

For the first and second sample sets all of the cores were drilled during < 0° C weather, and the core samples were immediately bagged and labeled as they were taken from the drilled hole. Samples were transferred to a freezer directly from the sub-freezing outdoor temperatures.

The third sample set (shallow core) was taken after freeze-up in the fall of 2009. The core was taken from the unimproved area north of the four-acre sample site, about 70 m north and 10 m east of the first core (Figure 3.2). This site has ground cover of mosses and low lying shrubs including bog blueberry (*Vaccinium uliginosum*), lowbush cranberry (*Vaccinium vitis-ideae*), Labrador tea (*Ledum groenlandicum*), and small black spruce trees (*Picea mariana*). In summer the ground is wet and boggy. Samples were collected using a SIPRE corer. Since depth to the permafrost table is at less than 1 m, the top 90 cm of the core were discarded as active layer soil. From 90 cm to 3.03 m there were 8 sequential cores taken, including a 2 cm section taken right at 90 cm. These eight cores were wrapped in foil and then in plastic, labeled and then taken to a freezer prior to processing. Sampling was stopped at 3.03 m because the corer was seizing and freezing in the ground.

Analytical samples from the shallow cores were processed differently from the earlier cores. The frozen sections were cut in half lengthwise, and one half was returned to the freezer for storage. The second half had three grooves cut lengthwise down the
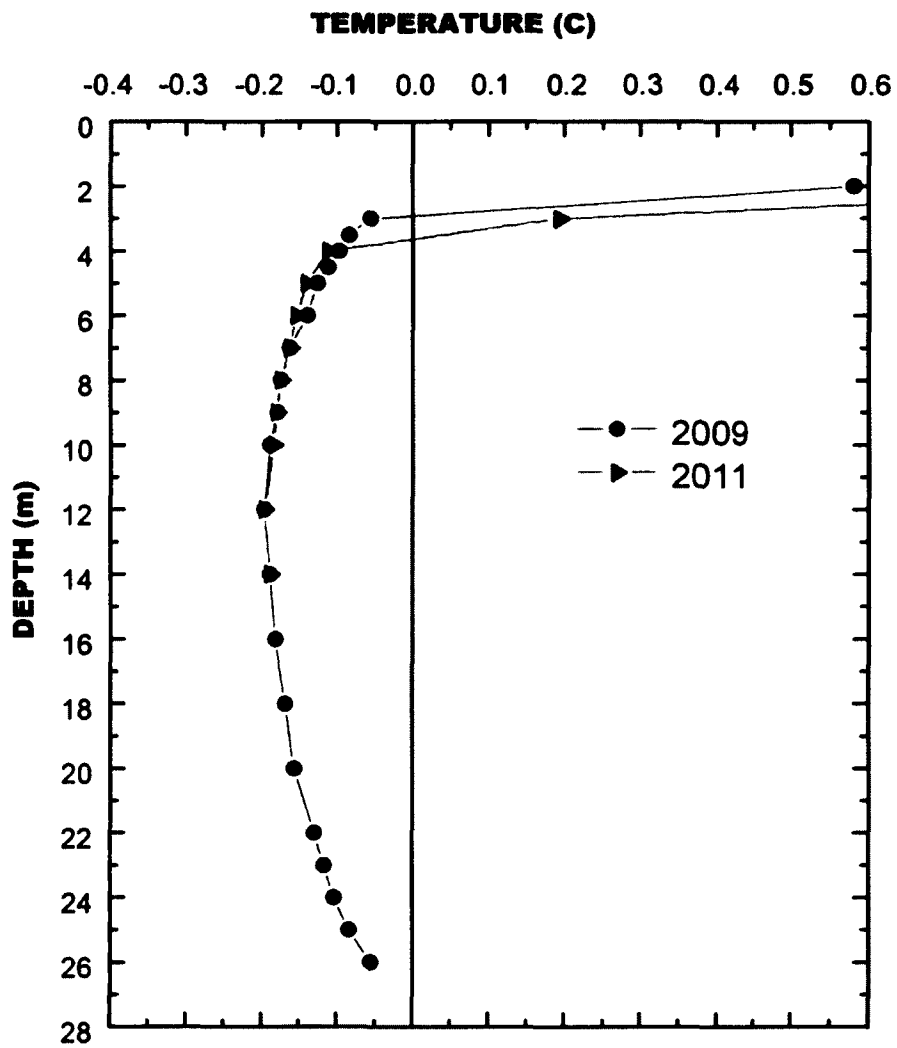
TEMPERATURE (C)

Figure 3.5 Borehole temperatures for auger core. Freezing point
depression is 0.08°C (*Figure courtesy of V.E Romanovsky*).

center of the core, about 1 cm apart. A chisel was used to cut across the three grooves at about 1 cm spacing. A narrow flexible spatula was used to pry the two samples from each 1 cm long section. This provided two samples for each centimeter of depth in the core. The sampling interval was 1 cm, and the sample size was 1 cm length so in effect the core was sampled continuously. There were occasional small roots and bits of charcoal or charred plant material at several locations in the core sections which were noted and logged. Aside from providing data from soils above the 6.1 m sampling depth of the first core, the shallow core samples were a test to see how much information may have been lost in the lower resolution of the Hagelbarger core compared to the shallow core.

In all three samplings the entire core consisted of silt. There were no rocks or gravel, nor any sand. There was neither clear ice nor ice lenses of a size to be seen without magnification.

For the Hagelbarger and auger cores the analytical methods were as described for cores from Lake Atna (see Chapter 2, this dissertation) but with the addition of magnetic susceptibility data for the Hagelbarger core. For the shallow cores, only the percent water content and water isotopes ($\delta^{18}O$ and δD) were analyzed, and that was also done as described for the Lake Atna cores in Chapter 2.

RESULTS

All statistical results exclude values between 19.52 and 21.49 m and below 24.99 m for percent water and isotope data as explained above.

<u>Percent Water Content</u>

The % gravimetric water content values for the Hagelbarger core are fairly consistent throughout the core (Figure 3.6A). They average 22.1% with a standard deviation of 2.5%, a high value of 30.52% and a low value of 15.28%. From the top of the core (6.10 m) the values decrease from generally around 25% to less than 19% at about 9.5 m depth (except for the very first value which is somewhat low at 21.42%). The values vary from 19% to 26% from 9.61 m to 20.13 m with only two exceptions; a value of 30.52% (the maximum value for the core) at 11.59 m and 27.79% at 16.78 m depth. Below 20 m depth water content values stabilize at very near 20% plus or minus 4% for the rest of the core. The two water content spikes, one over 30% and one at about 28%, are not especially different from the general values for the core, and probably don't indicate segregation ice. The water content at 25.01 m depth in the core drops to just over 15%, (Table 3A-1).

Percent water content for the auger core samples are similar to those for the Hagelbarger core samples at similar depths, and the pattern of the changes in percent water down the core is also similar (Figure 3.6B). Even though the augered samples were taken for the full depth of the core, including above 6.1 m, the data are still statistically similar. The average value is 21.8%, with a standard deviation of 2.7%. The maximum value is 25.6% at 3.05 m, and the minimum value is 17.2% at 1.8 m. There are no obvious peak values in the data (Table 3A-2).
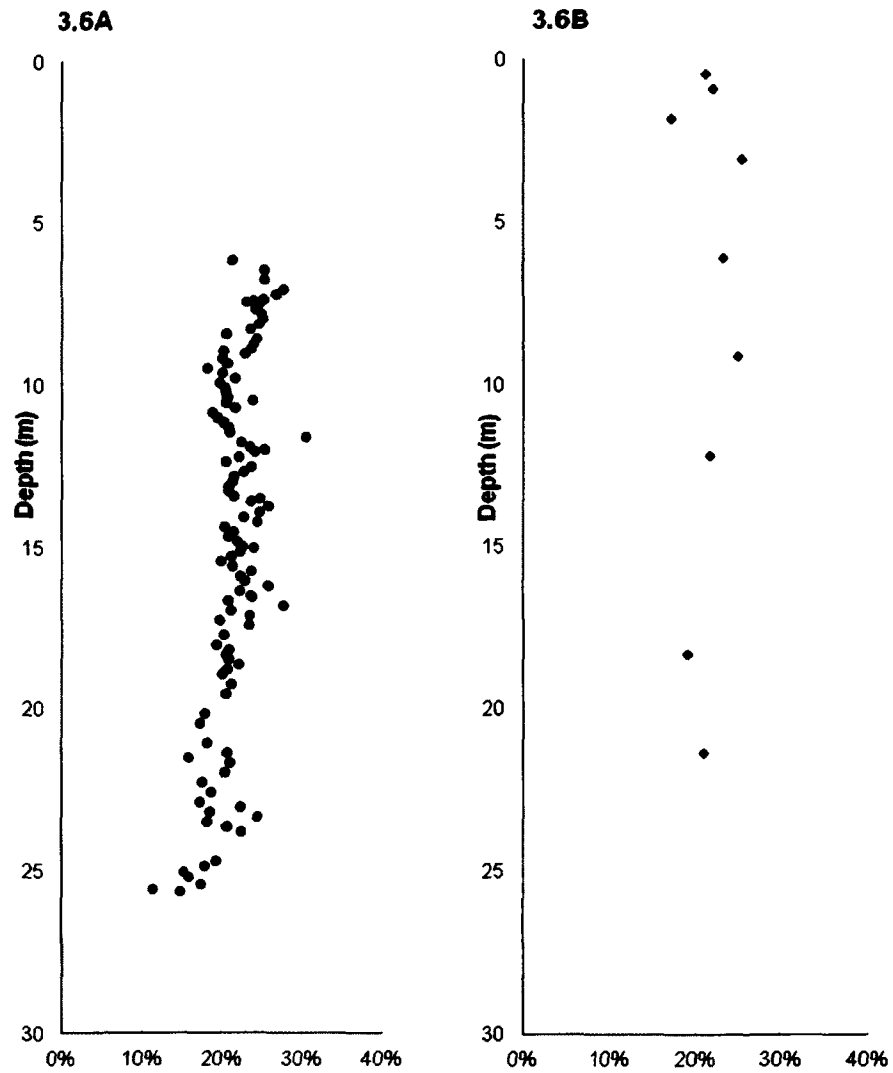
Figure 3.6 Gravimetric % water content for the Hagelbarger core (3.6A) and auger core (3.6B).

The soils from the shallow core are considerably wetter and more variable

(Figure 3.7). The percent water content average is 35.4% with a standard deviation of

6.2%. The maximum value is 69.92% and the minimum is 25.51%. This core is the most

shallow of the three examined, with samples taken from depths of 0.90 m to 3.03 m. The

maximum value is the 69.92% water spike at a depth of 1.25 m, which indicates possible

segregation ice. The majority of percent water contents are between about 30% and 40%,

considerably higher than the values for the other two cores. The higher standard

deviation reflects the fluctuations in water content in the first two meters depth of this

core. The water contents vary from around 25% to nearly 70% and do not seem to follow

a pattern down the core although the highest values (over 45% water content) are all

located above 1.5 m depth. Below 1.68 m the values no longer vary so widely. The next

low is 32.52% at 1.79 m, and the next high is 42.88% at 1.91 m. With only a few

fluctuations the values decrease slowly from that point on down the core. The last

sample water content value is 32.26% at 3.03 m. This core was drilled in a wetland area

which could explain the higher water content values (Table 3A-3).

Oxygen Isotopes

Hagelbarger core $\delta^{18}O$ data gradually decrease from about -17.4‰ at 6.1 m depth

to around -18.3‰ near 9.6 m depth (Figure 3.8A). At 10.07 m the $\delta^{18}O$ values rise

abruptly to -17.26‰ and then vary between -17‰ and -18‰ to a depth of 12.35 m. At
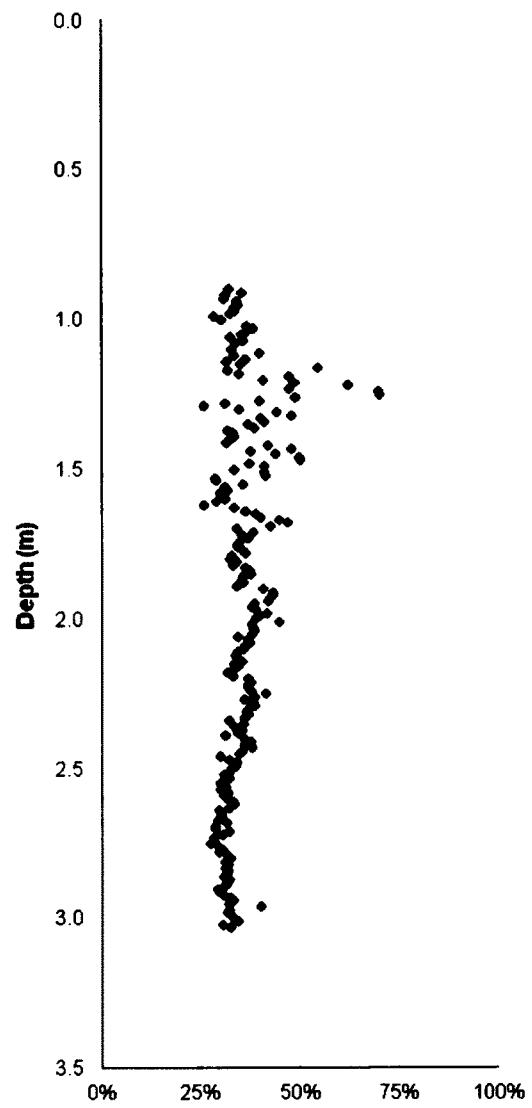
Figure 3.7 Gravimetric % water content, shallow core.
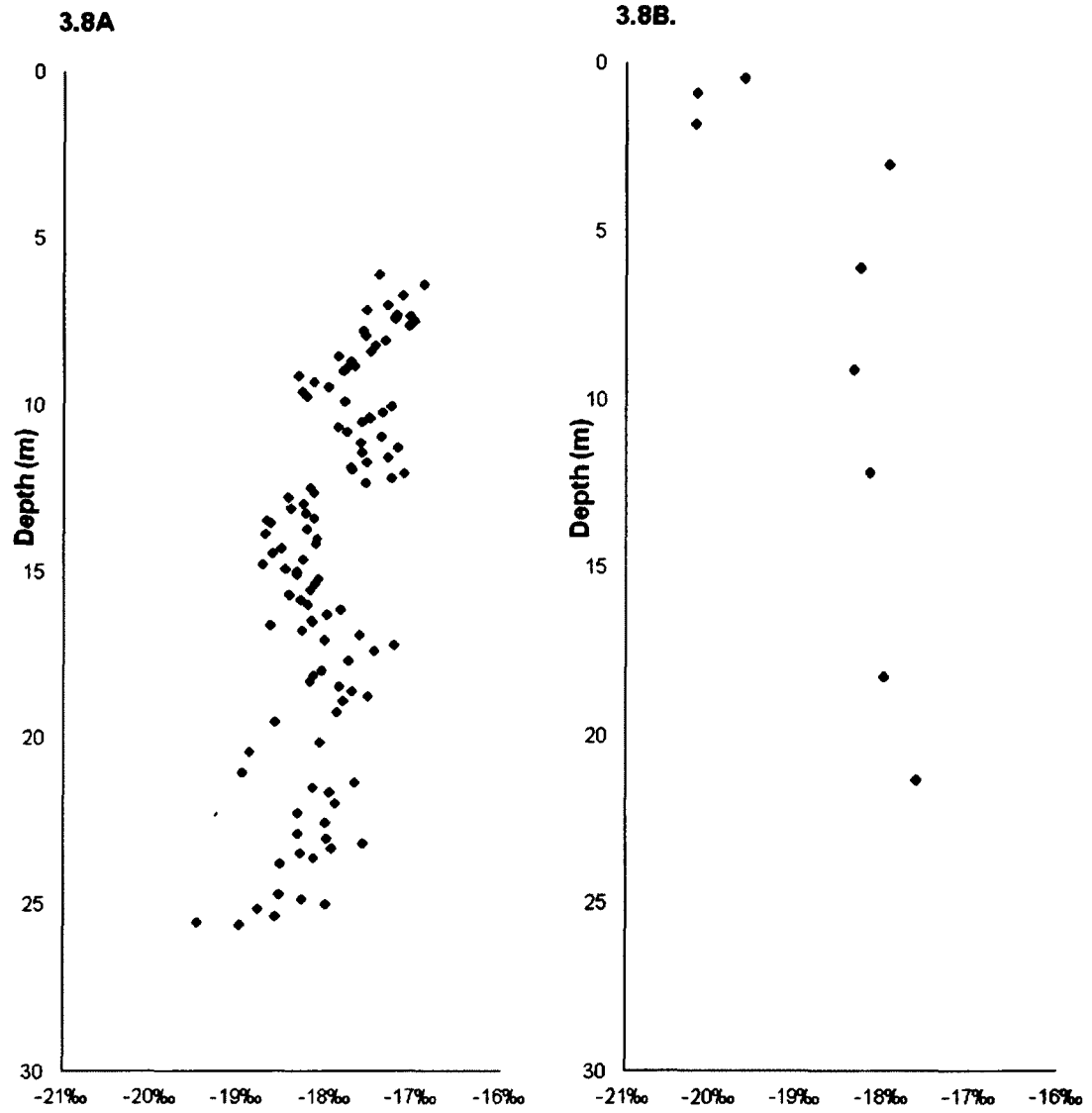
Figure 3.8 $\delta^{18}O$ values in ‰ relative to VSMOW for the Hagelbarger core (3.8A) and auger core (3.8B).

12.51 m $\delta^{18}O$ values drop abruptly to lower than -18‰ and from 12.51 m to 16.01 m the values vary randomly between -18‰ and -19‰. At 16.17 m depth the values zigzag through a double peak, going from -17.84‰ to -18.63‰ at 16.62 m, then back up to -17.23‰ at 17.23 m and back down to -18.18‰ at 18.30 m and then finally to -17.52‰ at 18.76 m. From 18.76 m to the bottom of the permafrost core the rest of the values vary randomly between -17.6‰ and -18.5‰. The average $\delta^{18}O$ value for this core is -17.9‰, the standard deviation is 0.5‰, the high value is -16.88‰, and the low value is -18.72‰ (Table 3A-1).

There are only nine data points from the auger sampling, so the statistics are skewed by larger differences from fewer samples (Figure 3.8B). The average value for the auger samples is -18.7‰, the standard deviation is 1.0‰, the high value is -17.62‰, and the low value is -20.18‰. However, the three most depleted samples (-19.62‰, -20.16‰, -20.18‰) were taken from above 6.1 m, the depth to the permafrost table for the Hagelbarger core, and the other six samples are all between -18.33‰ and -17.62‰, values similar to the Hagelbarger core (Table 3A-2).

The shallow core $\delta^{18}O$ values are more variable than those of either of the other cores (Figure 3.9). The average is -18.2‰, the standard deviation is 1.0‰, the high value is -15.50‰, and the low value is -20.90‰. Above 1.7 m depth the values are generally more depleted than those values below 1.7 m. The values above 1.7 m range from -17.27‰ to -20.90‰. Below 1.7 m depth, they range from -15.50‰ to -19.27‰. The difference between high values and adjacent lows above 1.7 m appear greater than those
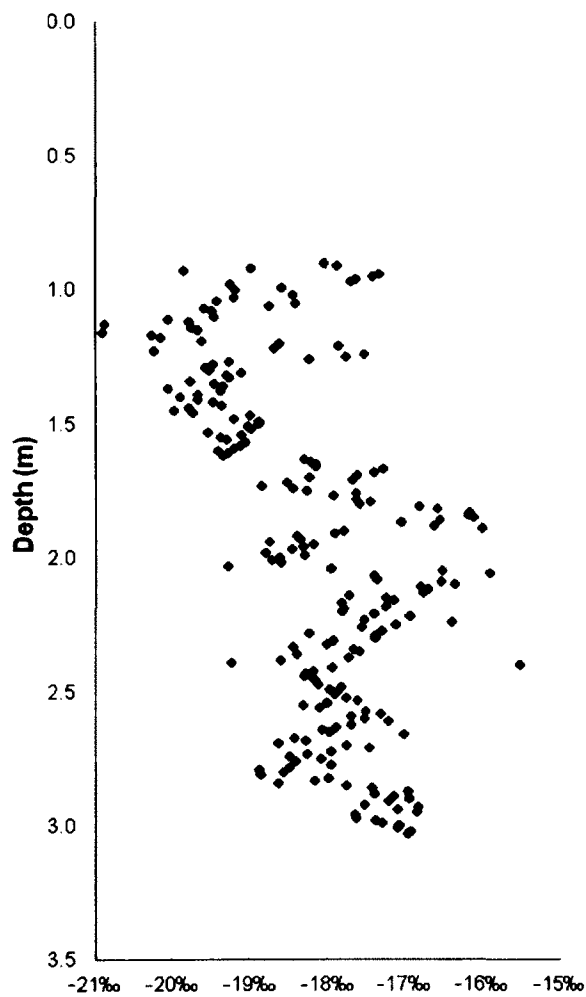
Figure 3.9 $\delta^{18}O$ values in ‰ relative to VSMOW for the shallow core.

below that level, although the values swing widely between highs and lows for the entire

length of the core (Table 3A-3).

<u>Deuterium</u>

δD values for the Hagelbarger core average -143.7‰ with a standard deviation of

5.2‰, a high value of -130.15‰ and a low value of -155.07‰ (Figure 3.10A). Between

6.10 and 10.06 m the δD values generally vary randomly between about -130‰ and

-140‰ with only a few values slightly lower. From 10.21 m to 15.01 m the values

decrease steadily to about -150‰. From 15.01 m to 17.07 m the values remain steady at

about -150‰, and below 17.22 m the values increase to about -145‰ and become more

variable for the rest of the core (Table 3A-1).

The auger deuterium values generally increase downcore except for the first

sample, -160.62‰ at 0.46 m (Figure 3.10B). The second sample, -190.40‰ at 0.91 m, is

the lowest of all nine values, and the deepest sample (at 21.34 m) is -154.52‰, only

slightly lower than the highest value of -152.85‰, located just above that sample at

18.29 m. Average value for the auger samples is -166.4‰ with a standard deviation of

11.4‰. The high value is -152.85‰ and low value is -190.40‰ (Table 3A-2).

Shallow core δD value average is -154.1‰ with a standard deviation of 9.5‰

(Figure 3.11). The maximum value is -126.59‰ and the minimum value is

-175.58‰. The initial values zigzag between low and high values from 0.9 to

1.25 m depth. Below that the values climb more gradually from -164.15‰ at 1.28 m to

-150.62‰ at 1.46 m, with only one spike of -146.69‰ at 1.37 m. The δD values down
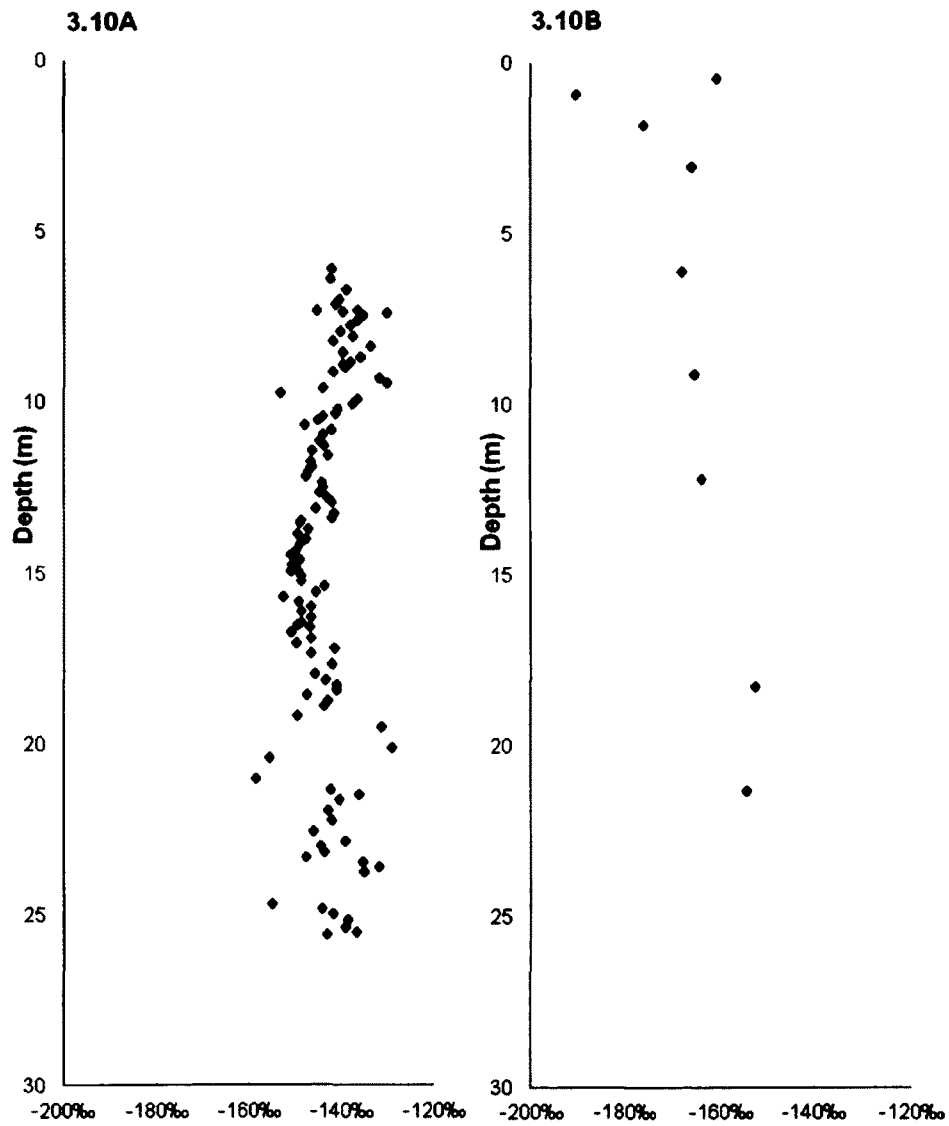
Figure 3.10 δD values in ‰ relative to VSMOW for the Hagelbarger core (3.10A) and auger core (3.10B).
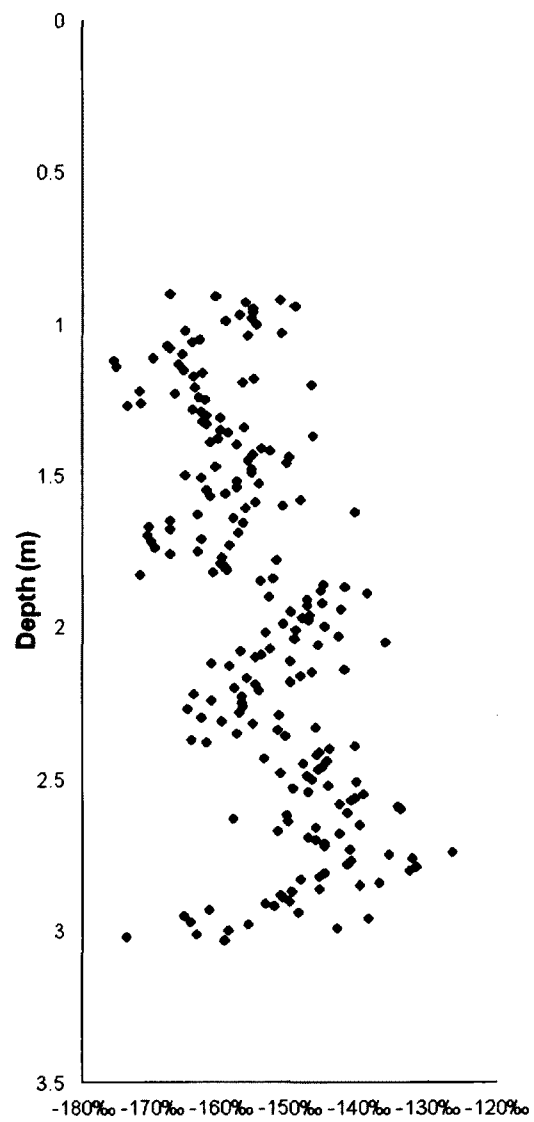
Figure 3.11 δD values in ‰ relative to VSMOW for the shallow core.

the length of the rest of the core form a more expanded zigzag pattern that is also more variable (Table 3A-3).

Nitrogen

Nitrogen and carbon are the only analyses that were done directly on the silt and not on the pore water or water extracts of the silt, therefore the values for nitrogen and carbon are a direct measure of the amount of element found in the silt, not the water.

The average nitrogen value in the Hagelbarger core data is 0.13% with a standard deviation of 0.06%. The high value is 0.376% and the low value is 0.064% (Table 3A-4).

The first few nitrogen values show a rapid increase in percent downcore, from 0.134% at 6.10 m to 0.376% at 7.35 m depth (Figure 3.12A). From 7.38 m to 9.00 m the values gradually drop to 0.186%, and then drop suddenly to 0.140% at 9.15 m depth. They continue at approximately 0.15% until a depth of 10.68 m except for one value of 0.202% at 10.43 m. Below 10.68 m to a depth of 13.42 m the values maintain a value of about 0.12% with minor variations. There is a jump from 0.153% at 13.73 m to 0.214% at 14.18 m before a drop to 0.105% at 14.34 m. The values stay at about 0.10% to a depth of 16.62 m and then there are two higher values, 0.151% at 16.62 m and 0.142% at 16.78 m. From a depth of 17.08 m (with a value of 0.107%) the values drop gradually and steadily down to 0.066% at the bottom of the core, 25.62 m.

Percent nitrogen values for the auger core are variable within the same range as the sample data from the Hagelbarger core (Table 3A-5). The data from sample depths that match or are close to the same depths as for the Hagelbarger core are very similar.
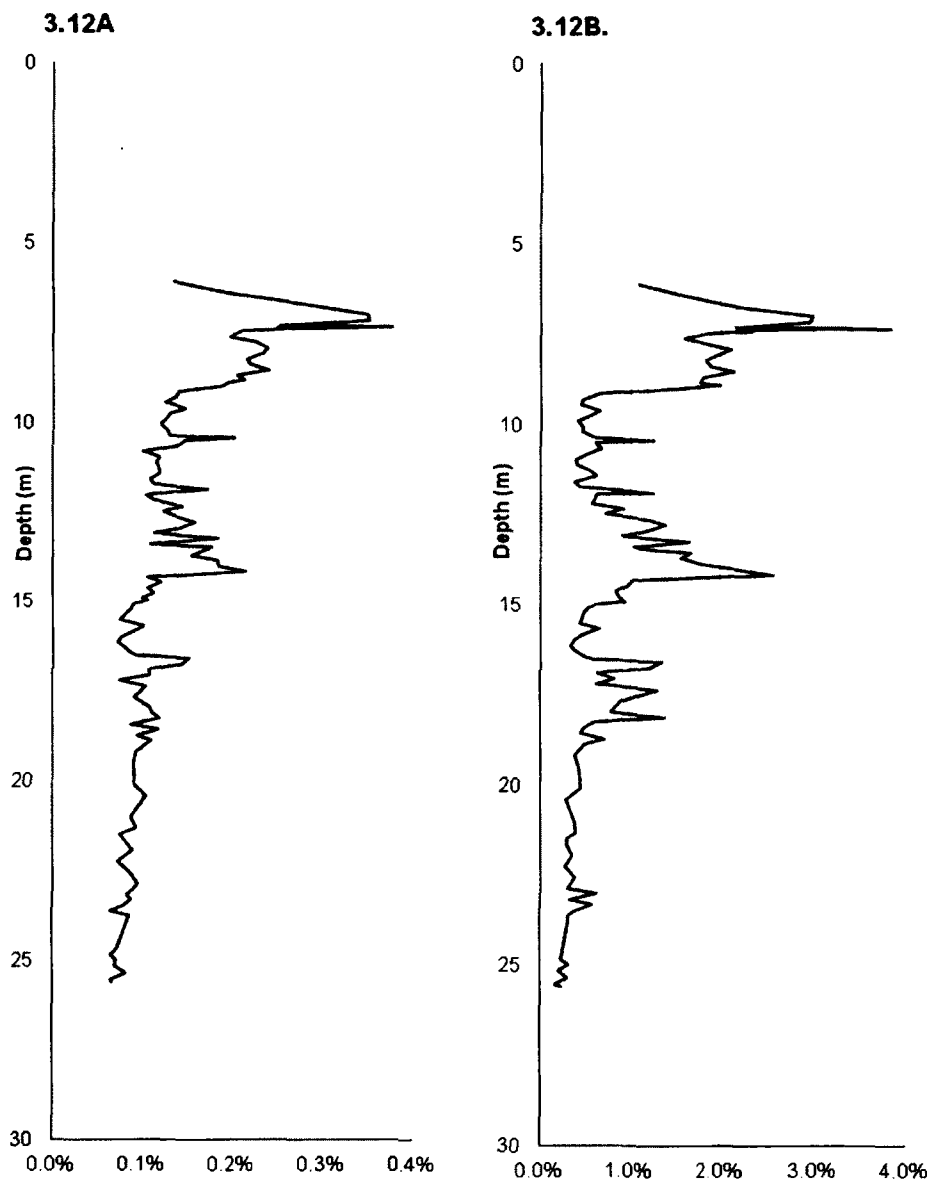
Figure 3.12 Percent N (3.12A) and percent C (3.12B) versus depth in the Hagelbarger core.

Carbon

The changes in the percent nitrogen presented above may seem very minor, but these relative changes and the graphical profile for nitrogen is almost exactly duplicated, though in larger scale, by the value changes in percent carbon (Figure 3.12B).

The average percent carbon value for the Hagelbarger core is 0.94% with a standard deviation of 0.72%. The high value is 3.825% and the low value is 0.165% (Table 3A-4). The first carbon value (at 6.10 m) is 1.088%, and climbs to 3.825% at 7.35 m before dropping to 1.581% at 7.63 m. The value then rises to 2.122% at 7.93 m and remains at slightly less than 2% for the next several centimeters until it drops suddenly to 0.655% at 9.15 m depth. With the exception of two spikes (1.256% at 10.43 m and 1.249% at 11.90 m) the values remain well below 1% down to 12.66 m, where there is a reading of 1.193%. The values remain around 1% down to 13.57 m but climb over 1.5% from 13.57 m to 13.88 m and then spike to 2.579% at 14.18 m. Abruptly, at 14.34 m, the values drop to around 1% and then steadily decrease downcore to less than 0.5% at 16.47 m. At 16.62 m depth there are two values over 1% (16.62 m and 16.78 m), then three values below 1% down to 17.39 m where the reading is 1.297%. Below, it drops to less than 1% again for two more readings before there is one more reading above 1% at 18.15 m. From that point down to the bottom of the core all the values are below 1% and most of them are below 0.5% C.

Data from the auger samples have the same relative values for percent carbon (higher, lower, highest, etc.) as those values for nitrogen (Table 3A-5). Those carbon values that come from depths similar to those of the Hagelbarger core generally have

similar percent carbon values as the Hagelbarger samples for the same or nearly the same depths.

Calcium

The average value for mg/l of water soluble calcium in the Hagelbarger core is 0.41 mg/l, with a standard deviation of 0.27 mg/l. The high value is 1.093 mg/l and the low value is 0.081 mg/l (Table 3A-4).

Calcium values vary widely with values from 0.544 mg/l to 1.093 mg/l between 6.10 m and 8.08 m depth (Figure 3.13). From 8.24 m to 13.42 m, the values stabilize and drop steadily from 0.686 mg/l down to around 0.372 mg/l with minor fluctuations. There is only one value spike of 0.692 mg/l which occurs at 11.90 m depth. At 13.48 m, the values climb abruptly from 0.621 to 1.043 mg/l at 14.03 m and just as abruptly drop to 0.344 mg/l at 15.10 m depth. The values are consistently in the 0.3-0.4 mg/l range down to 16.62 m where they once again spike to 0.909 mg/l and then drop to 0.234 mg/l at 17.69 m. There are two values, 0.387 and 0.354 mg/l, that occur at 18.00 and 18.15 m depth, respectively, but the rest of the calcium values down to the bottom of the core decrease steadily, from 0.247 mg/l at 18.30 m to 0.087 mg/l at 25.62 m.

Calcium values for the auger core are similar to values at similar depths where there are samples with similar depths (Table 3A-5).
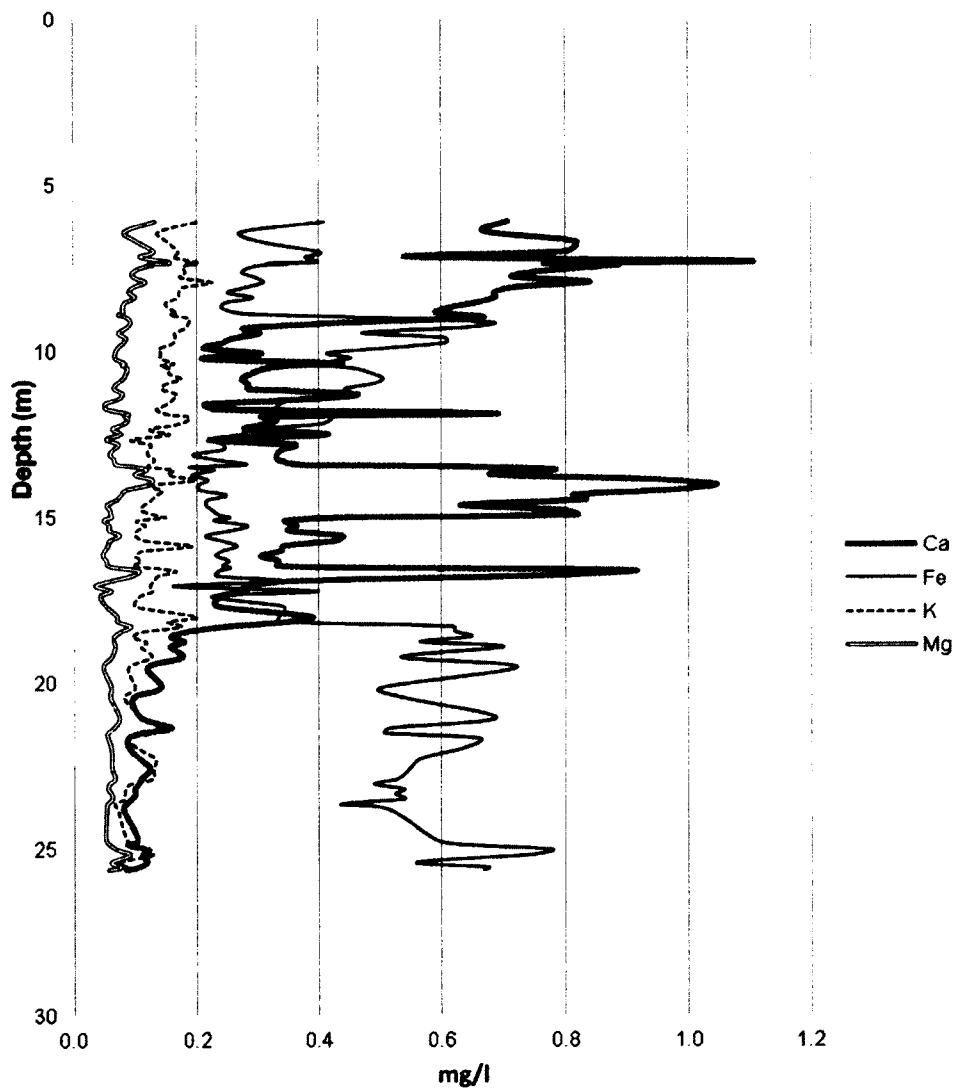
Figure 3.13 Mg/l Ca, Fe, K, and Mg versus depth in Hagelbarger core.

Potassium

Average value for potassium in the Hagelbarger core is 0.14 mg/l with a standard deviation of 0.03 mg/l (Table 3A-4). The high value is o.226 mg/l and the low value is 0.065 mg/l. The general trend of the entire potassium data set is to decrease in value from about 0.200 mg/l at the top of the core (6.10 m) to less than 0.08 mg/l at the bottom of the core (Figure 3.13). There are a few small spikes in the values. At 11.74 m the values shift from 0.134 mg/l to 0.185 mg/l at 11.96 m. At 13.42 m the values are 0.121 mg/l, but they spike to 0.199 mg/l at 13.88 m before dropping back down to 0.124 mg/l at 14.03 m. At 15.86 m there is a single point spike to 0.194 mg/l, and a second single point spike to 0.200 mg/l at 18.00 m. These variations are very small especially considering the low values of the potassium overall.

The potassium mg/l values for the auger samples are in general agreement with those samples that are from a comparable depth in the Hagelbarger core (Table 3A-5).

Magnesium

Average value for magnesium for the Hagelbarger core is 0.08 mg/l with a standard deviation of 0.02 mg/l. The high value is 0.157 mg/l and the low value is 0.035 mg/l (Table 3A-4).

For the most part the magnesium values down the length of the core are from one-half to two-thirds the value of the potassium data and the profile of the data generally echoes the profile of the potassium data (Figure 3.13). However, the magnesium data only has two spikes, both at the same depth as potassium spikes, but much smaller. At

13.42 m depth the Mg value is 0.070 mg/l, and at 13.88 m the value rises to 0.129 mg/l

before dropping back to 0.087 mg/l at 14.18 m depth. The second spike occurs at

18.30 m depth with a value of 0.094 mg/l, up from 0.053 mg/l at 17.69 m, and dropping

to 0.062 mg/l at 19.22 m.

The values of the auger core magnesium samples are also about half to two-thirds

the values of the auger sample potassium samples (Table 3A-5).

Iron

The average value for iron in the Hagelbarger core is 0.39 mg/l with a standard

deviation of 0.16 mg/l. The high value is 0.778 mg/l and the low value is 0.160 mg/l

(Table 3A-4).

The mg/l values for iron from 6.01 m to 7.02 m vary between 0.272 mg/l to

0.408 mg/l (Figure 3.13). From 7.35 m to 8.91 m the values are consistent around

0.3 mg/l (±0.06 mg/l), but at 8.91 m the values abruptly start to rise to 0.683 mg/l (at

9.15 m), and then nearly as suddenly drop to 0.397 mg/l at 10.37 m. There is another

small increase to 0.504 mg/l at 10.83 m, and then the values gradually drop to 0.192 mg/l

at 13.73 m depth. Between 13.88 and 16.78 m the values level off, ranging from 0.20 to

0.29 mg/l. Starting at 16.93 m the values begin to vary widely and they also increase in

value in a general way, going from 0.340 mg/l at 16.93 m to 0.699 mg/l at 18.91 m.

Below 18.91 m to the bottom of the core the values vary from 0.434 mg/l to 0.778 mg/l

randomly.

The auger sample values for iron are similar to those for the Hagelbarger core for those samples that were taken from similar depths (Table 3A-5).

Conductivity

The average value for conductivity for the length of the Hagelbarger core is 198 μS/cm with a standard deviation of 97 μS/cm (Table 3A-4). The high value is 425 μS/cm and the low value is 54 μS/cm. At 6.10 m the conductivity value is 309 μS/cm and it slowly drops to 157 μS/cm at 9.76 m depth, though there are two spikes in the data above 10 m (Figure 3.14A). The first spike, at 7.35 m is the high value for the core of 425 μS/cm. The second spike at 8.91 m is 401 μS/cm.

Below 10 m depth the values are fairly constant around 200 μS/cm down to 13.42 m except for two more small spikes, one of 264 μS/cm at 11.29 m, and one of 286 μS/cm at 11.90 m depth. At 13.42 m the values jump from 181 μS/cm to 288 μS/cm at 13.48 m. The values continue to climb as high as 418 μS/cm at 14.18 m and then decrease abruptly to 153 μS/cm at 15.25 m depth. The values increase to over 200 μS/cm two more times, once at 15.71 m (214 μS/cm) and once at 16.62 m (236 μS/cm). Below 16.78 m the conductivity values decrease steadily down the core until at the bottom of the core the values are well below 200 μS/cm, and most are below 100 μS/cm.

The conductivity values for the auger core samples are slightly different from those of the Hagelbarger values, but not so much that they could be considered to be from a different environment or soil type (Table 3A-5).
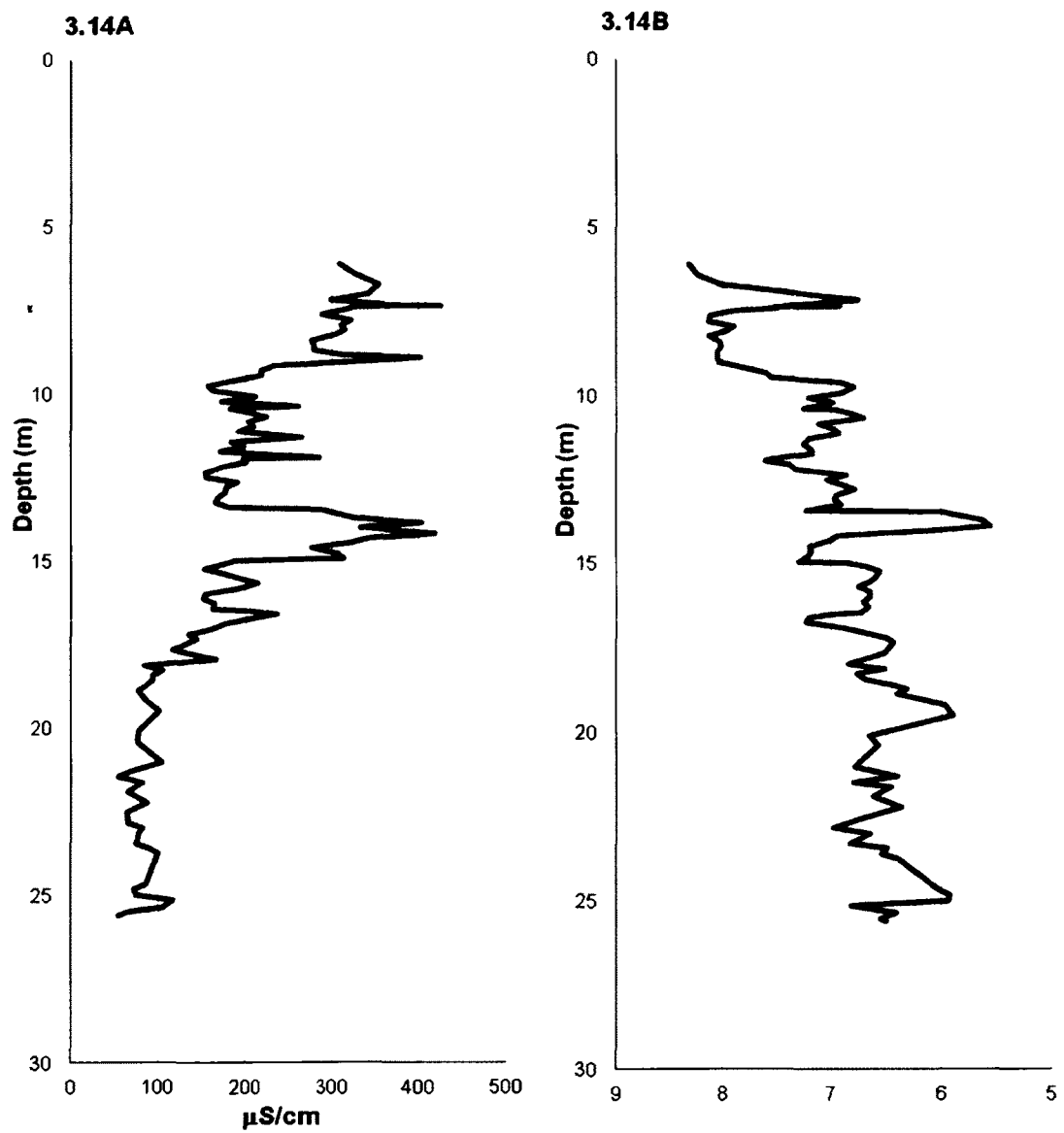
3.14A

3.14B

Figure 3.14 Conductivity in µS/cm (3.14A) and pH (3.14B) versus depth in Hagelbarger core.

pH

The pH values for the Hagelbarger core have an average value of 7.0 with a standard deviation of 0.6. The high value is 8.31 and the low value is 5.55 (Table 3A-4).

The pH values start at 8.31 (6.10 m) but drop rapidly to 6.75 at 7.17 m, and then just as rapidly increase to around 8.0 at 7.47 m and stay near that value down to 9.00 m depth (Figure 3.14B). Below 9.00 m the values drop steeply to a low of 6.79 at 9.76 m and remain near the 7.0 value down to 13.48 m where they drop again, this time to less than 6.0. At 14.34 m the values rise to over 7.0 for several samples, down to 15.01 m. At that point the values drop again, to around 6.7 (at 15.10 m) and stay near that value to 16.53 m where they increase to 7.2 at 16.78 m before dropping again to 6.50 at 17.23 m. For the rest of the core the pH values vary somewhat more from sample to sample, but remain generally near 6.5.

The pH values for the auger samples are similar to the values in the Hagelbarger core samples for those data from the same depths (Table 3A-5).

Bicarbonate

Bicarbonate was found in all but one of the samples. The average value for bicarbonate is 0.4 meq/l, with a standard deviation of 0.3 meq/l. The high value is 1.22 meq/l and the low value is 0.14 meq/l (Table 3A-4).

Although the values for bicarbonate decrease steadily down the depth of the core, variations from sample to sample are small (Figure 3.15A). At a depth of 7.32 m the values rise from less than 1.0 meq/l to over 1.0 meq/l but return to lower values at 7.63 m

3.15A   3.15B
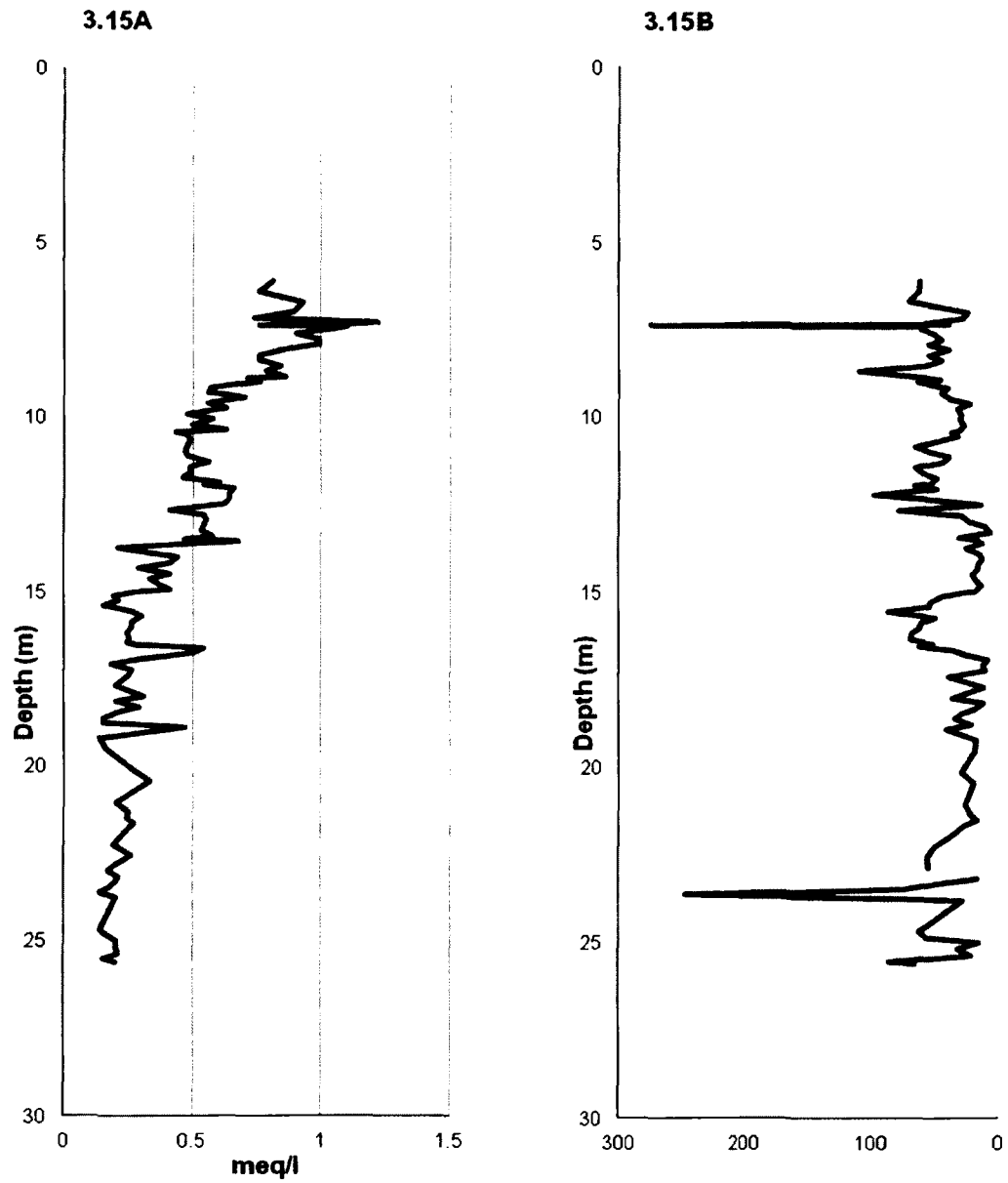
Figure 3.15 Bicarbonate in meq/l (3.15A) and magnetic susceptibility (3.15B)
versus depth in the Hagelbarger core.

depth. At 13.57 m the value of 0.68 meq/l is followed immediately by a lower value of

0.21 meq/l at 13.73 m and the values below that are generally below 0.30 meq/l except

for two very small spikes; one at 16.62 m (0.54 meq/l) and one at 18.91 m (0.47 meq/l).

The bicarbonate values for the auger samples are in a general way similar for

samples taken from similar depths (Table 3A-5).

Magnetic Susceptibility

Measurements of volume susceptibility were made on Hagelbarger samples using

a Bartington MS2 susceptibility meter and an MS2F microprobe. After subsamples for

chemical analysis had been taken from the original core samples, the remaining material

was kept frozen in Whirlpak™ bags. Those core samples were analyzed for susceptibility

while still frozen and in Whirlpak™ bags. Three readings were taken on each sample and

averaged for each depth. The data are in dimensionless volume susceptibility units and

have been left as recorded for ease of plotting; however to convert susceptibilities into SI

units they should be multiplied by 10^{-5} (Beget, 2006).

The overall average value for magnetic susceptibility is 44, with a standard

deviation of 36. The maximum value is 275, and the minimum value is 6. (Table 3A-4).

There are two values for susceptibility that arre at least twice the value of any

other reading. The first, at 7.38 m is 275, the second at 23.64 m is 247. All the other

values vary within a much smaller range, from about 6 to about 109 (Figure 3.15B).

Data vary fairly smoothly between relatively high and relatively low values down

the length of the core except for the two exceptionally high values mentioned above.

Excluding those two data points, the high values are: 70 at 6.71 m, a series of high values

from 7.41 m to 9.00 m with the highest being 63, a series of high values from 11.29 m to

12.51 m with the highest being 97, a series of high values from 15.10 m to 16.53 m with

the highest being 86, and a series of high values from 22.57 m to the bottom of the core

with the highest values being 86. The lows are: a 24 at 7.01 m, a 22 at 9.61 m, a series of

low values from 12.96 m to 15.01 m with the lowest being 12, a series of low values from

16.78 m to 18.45 m with the lowest value being 8 and a series of low values from

19.22 m to 21.66 m with the lowest being 16.

Magnetic susceptibility was not measured on the auger core samples.

Correlations

There are a number of significantly high (over 0.7) statistical correlations between

the analyses done for the Hagelbarger sample set (Table 3.1). The highest correlations

(greater than 0.9 correlation value) are between conductivity and calcium, and between

nitrogen and carbon. Other correlations with over 0.7 correlation value (greater than 0.5

coefficient of determination) are between depth and potassium, conductivity, bicarbonate

and nitrogen; between calcium and magnesium, conductivity, carbon and nitrogen;

between potassium, magnesium and bicarbonate; between magnesium and conductivity,

bicarbonate, nitrogen and carbon; between pH and bicarbonate; between conductivity and

bicarbonate, nitrogen and carbon; and between bicarbonate and nitrogen and carbon.

Table 3-1. Correlations of Chemical Analytical Results.

	Depth m	Ca mg/l	Fe mg/l	K mg/l	Mg mg/l
Depth	1.000	-0.658	0.477	_-0.739_	-0.575
Ca	-0.658	1.000	-0.636	0.596	_0.730_
Fe	0.477	-0.636	1.000	-0.217	-0.131
K	_-0.739_	0.596	-0.217	1.000	_0.707_
Mg	-0.575	_0.730_	-0.131	_0.707_	1.000
pH	-0.687	0.463	-0.254	0.559	0.351
Conductivity	_-0.789_	_0.922_	-0.590	0.648	0.689
Bicarbonate	_-0.843_	0.677	-0.313	_0.742_	_0.736_
N	_-0.733_	_0.723_	-0.347	0.605	_0.773_
C	-0.631	_0.804_	-0.493	0.524	_0.734_
Susceptibility	-0.096	0.014	-0.024	0.062	0.100

Correlations greater than ±0.7 are in bold and underlined.

pH	Conductivity μS/cm	Bicarbonate meq/l	%N	%C	Magnetic Susceptibility
-0.687	**-0.789**	**-0.843**	**-0.733**	-0.631	-0.096
0.463	**0.922**	0.677	**0.723**	**0.804**	0.014
-0.254	-0.590	-0.313	-0.347	-0.493	-0.024
0.559	0.648	**0.742**	0.605	0.524	0.062
0.351	0.689	**0.736**	**0.773**	**0.734**	0.100
1.000	0.537	**0.738**	0.492	0.407	0.240
0.537	1.000	**0.731**	**0.765**	**0.790**	0.081
0.738	**0.731**	1.000	**0.826**	**0.730**	0.142
0.492	**0.765**	**0.826**	1.000	**0.938**	0.078
0.407	**0.790**	**0.730**	**0.938**	1.000	0.047
0.240	0.081	0.142	0.078	0.047	1.000

The analyses that have less than 0.7 correlation with other analyses are percent water content, $\delta^{18}O$ isotope values, δD isotope values, mg/l iron values and magnetic susceptibility.

DISCUSSION

Chemical Data

Comparison of the augered core chemical data (Table 3A-5) with the Hagelbarger core chemical data (Table 3A-4) did not show major differences in any parameter values, (allowing for minor discrepancies in depths). This comparison was made to check that the samples from the Hagelbarger core that came from auger flights were from the depths calculated during drilling, and that the data was truly comparable between the cored samples and the auger flight samples. The results are comparable between the Hagelbarger core and the auger core (where there are similar depths), and the samples are also comparable whether the samples came from the auger flights or from the cored samples from the Hagelbarger core. These results make it possible to be confident about the depths from which the various samples have been taken.

The very high correlations between %N and %C and between conductivity and mg/l of soluble Ca (Table 3.1) suggest that these two sets of parameters may be dependent. Percents of carbon may reflect carbonate content or organic matter content. Nitrogen is a major component of organic tissues but is uncommon in mineral soil, so the very close relationship of the carbon content to nitrogen content strongly suggests that they both reflect changes in organic matter content at various depths in the core. There is

a high correlation between carbon and calcium (> 0.8) and between carbon and

magnesium (> 0.7), and since calcium and magnesium are also components of organic

matter, that is not unreasonable.

The peaks in percent nitrogen, percent carbon, mg/l calcium, and most of μS/cm

conductivity data occur at the same depths (Figure 3.16). In general, the magnesium

values follow the same profile as for carbon, nitrogen, calcium and conductivity, but the

magnesium values are much lower and the pattern is not as distinct. The values for

potassium are also very low, and only show a correlation greater than 0.7 with

magnesium (Table 3.1). Muhs et al., (2003) suggest that low potassium contents are a

result of the near-absence of K-feldspar in Alaskan loess.

Conductivity measures ion activity and so it is natural for the conductivity values

to follow the cation values (Ca, Mg, K and Fe). The peak that occurs in the conductivity

data at near 9 m depth that is not echoed by calcium, magnesium or potassium is echoed

by the iron data.

There is a peak in iron content near 9 m depth, and also an abrupt increase in iron

at about 18.3 m which does not decrease significantly further down the permafrost core.

Aside from the coincident peak at 9 m depth with conductivity, iron values do not

correlate with any of the other parameters in the data set and the distinct pattern to the

iron values is not comparable with any other pattern in the data set. Muhs et al. (2003)

suggest that high iron content may be due to the presence of larger amounts of iron rich

minerals compared to phyllosilicate clays. This indicates that clays present in the core at

depths where iron content is higher may be sedimentary, not alteration products of loess
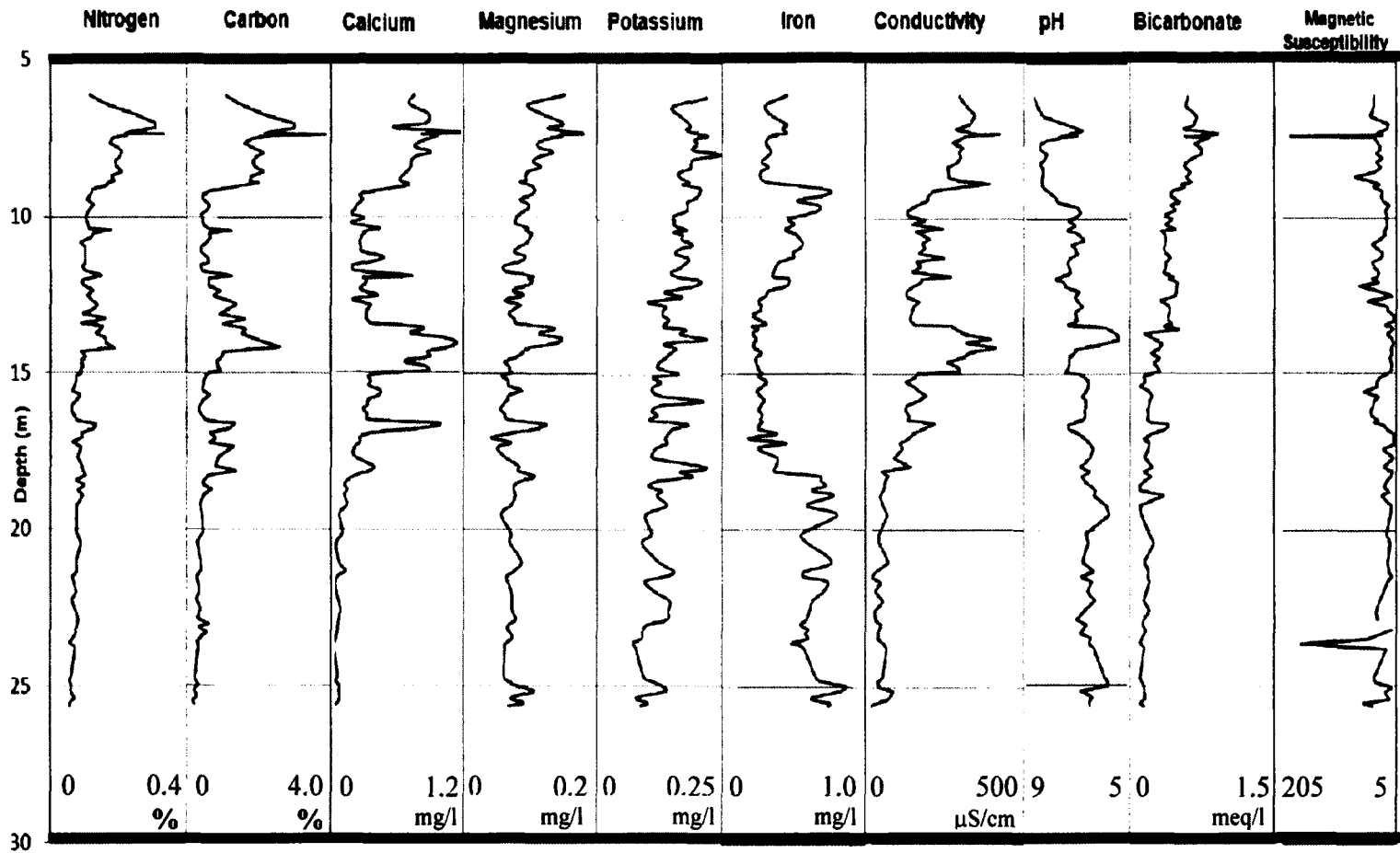
Figure 3.16 Comparison of graphed profiles of chemical analysis results from Hagelbarger core. Shaded sections indicate possible pedogensis depths. Note that pH and magnetic susceptibility peaks are reversed so that correlations with other peak values are more apparent.

(Muhs et al., 2003). This may also indicate that the loess origin at depths where the iron content is higher may be different from the loess origin where the iron content is lower.

Bicarbonate values are very low but are correlated with magnesium, conductivity, nitrogen and carbon, as well as pH. Bicarbonate also has a strong negative correlation with depth as do nitrogen, potassium and conductivity.

The pH values start at over 8 but drop to less than 7 at 7.3 m depth and fluctuate down the rest of the core, but generally the pH values slowly decrease until at the bottom of the permafrost the value is 5.94.

The fluctuations in pH seems to mimic the fluctuations in nitrogen and calcium. In Figure 3.16 pH has been plotted with low values on the right so that the correlations are more apparent. Soils become acidic when organic acids are produced during decomposition of forest litter (Pritchett and Fisher, 1987), so increased acidity would be an indication of soil formation during vegetative growth. In Figure 3.16, low pH values occur in the same locations as the highest carbon and nitrogen contents.

Loess deposition in interior Alaska is continuous, although the rate changes with intensity and direction of winds and frequency of dust storms at any given site (Beget, 1996). Fine-grained magnetic particles are included in loess produced during glacial periods. Strong katabatic winds off glaciers and associated storms are able to carry these heavier particles further during glacial intervals than during interglacials or interstadials. In interior Alaska this produces magnetic susceptibility variations that are lower during warmer periods when loess deposition is lower and pedogenesis occurs, and higher during colder periods when production is higher but soils are thin (Beget, 1996, 2001).

Magnetic susceptibility data from the Hagelbarger core has been plotted with low

values on the right (similar to the pH data) in order to more closely match high and low

peaks with other data in Figure 3.16. The magnetic susceptibility profile is in general

agreement with the %N and %C profiles at the significant depths of 7 m, 14 m and 17 m;

samples from those depths all have comparatively low magnetic susceptibilities. The two

extremely high values are anomalous and are so different from the other values around

them that they can be considered outliers. These two peaks have been truncated in

Figure 3.16.

Depth of loess at the Hagelbarger core location is comparable to other loess

deposits in the Fairbanks area, though not as deep as at some research areas such as Gold

Hill (Péwé, 1977; Péwé and Reger, 1989). The maximum possible length of time

required for the accumulation of this amount of material is bracketed by the 3 million

year age suggested for the earliest accumulation at the Gold Hill site (Westgate and

Stemper, 1990) and the present. Prior to permafrost development deeper parts of the core

experienced more chemical and biological activity, resulting in less obvious differences

in the parameters at depth; however, there are some traces that may indicate pedogenesis

even low in the core.

Core samples were collected from the Hagelbarger site from depths between

6.1 m and 25.6 m. Abrupt coincident changes in values for several of the chemical

parameters at different depths in the Hagelbarger core suggest several episodes of

pedogenesis. The stacked profiles for core chemistry in Figure 3.16 show the soil layers

as peaks in concurrent data parameters that are shaded. The depths for the layers are very

similar to those found by Beget et al., (1991) and Muhs et al., 2003. Muhs et al. in their

2003 paper thought they found at least eight paleosols in a 20 m section (measured from

the surface) at Gold Hill, including a welded paleosol couplet between 6.65 and 7.6 m, a

recognizable A horizon of soil at 14 m, and a pedocomplex at 18 m depth. The section

was not topographically the highest point in the local landscape, but it is well-drained

upland loess located well above the adjacent valley bottom (Muhs et al., 2003).

Calcium, carbon, nitrogen and bicarbonate have small spikes in value at about

16.5 m and pH increases slightly to just above 7.2 (Figure 3.16). The pH value drops

down to less than 7 and the other parameters drop to pre-peak values by 16.3 m depth.

The pH stays in the neutral-to-slightly-acid range when the nitrogen, carbon, calcium and

bicarbonate increase so this could be a pedogenesis event, though the evidence is not very

strong. The depth to these data is most similar to the pedocomplex Muhs et al. (2003)

found at 18 m depth in the 20 m section of Gold Hill.

The most convincing evidence for soil production is at around 14 m depth. The

pH drops below 6 and magnetic susceptibility is at a minimum. The bicarbonate value

also drops while conductivity, nitrogen, carbon and calcium jump in value (Figure 3.16).

The data at this depth show the expected changes that take place when organic matter

decays and produces organic acids. Decomposition of the plant material produces

increased levels of nitrogen, calcium and carbon. Organic acids lower the pH and

increased ion activity from cations released from the organic material increases

conductivity. Lower pH results in decreased bicarbonate. This section of the core has

the most convincing evidence for a major increase in plant production and resulting soil

development. The relatively low pH suggests increased pedogenesis from increased

vegetative growth and humic acid production, and the low magnetic susceptibility

suggests a warmer climate (decreased loess production from glaciation). Above about

13.5 m the parameter values return to near the values that preceded the change at 14 m.

As mentioned earlier, there was also an A horizon soil at 14 m depth found by Muhs et al.

(2003) at Gold Hill.

From 13.5 m to near 9 m depth there are only minor variations in the parameters

except that magnetic susceptibility increases between 12 and 10.5 m before dropping

again at about 10 m depth. At about 9.5 m calcium, carbon, nitrogen, bicarbonate and pH

all increase, and stay at higher values until about 7.5 m depth, where calcium, carbon,

conductivity and nitrogen abruptly increase even more and pH drops to less than 7

(Figure 3.16). Magnetic susceptibility decreases between 7.5 and 7 m depth.

Bicarbonate initially increases, but then drops back to the level it was at below 7.5 m.

This is once more the expected change in values with increased plant production

followed by decomposition. The pH value is not as low as for the event at 14 m, which

could mean that the increased plant production was not a forest, but another type of

vegetation, such as herb-shrub tundra or grassland. Since the top of the core is at 6.1 m,

this is the last organic soil collected. The depth to this horizon also matches that of one

of the Gold Hill soils found by Muhs et al. (2003). Since the depth to possible soils at

Hagelbarger and Gold Hill sites are similar in three cases (Figure 3.16, shaded sections),

the deposition rate at both Gold Hill and the Hagelbarger site could be similar as well.

Isotope Data

The changes in water isotope signatures in a permafrost soil column indicate either of two processes: fractionation, which is closely associated with changes due to the freezing process in the soil; or a change in the origin and history of the water itself (Michel, 1982, Michel and Fritz, 1978). Permafrost that thaws and is replaced by groundwater that has a different isotopic signature and then freezes again can be recognized by abrupt changes in signature, often accompanied by double-peaks in the signature where the change took place, indicating where two freezing fronts, one from the top and one from the bottom, have met during the refreezing process (Michel, 1982).

At the shallow core location there is no talik between the active layer and the permafrost table. The ground cover there is moss, low shrubs and black spruce, all of which insulate the cold soil from summer air temperatures and support below-freezing mean annual ground temperatures. Mean annual temperature measured at the ground surface at the shallow core site was -1 °C in 2009-2010 and -1.4 °C in 2010-2011 (V.E. Romanovsky, personal communication, November 3, 2011).

The shallow core samples were taken at high resolution of 1 cm spacing (Figure 3.9) in order to check the precision of the data from the Hagelbarger core taken at 15 cm spacing. A graph of the shallow core data with a spacing of 15 cm was also plotted for comparison (Figure 3.17). The plots show that variations in $\delta^{18}O$ over a short distance can easily be missed by the lower resolution sampling. In addition, if sample spacing happens to result in data points at the midrange of a spike without sampling the highest or lowest values, the data will appear less variable than the actual value of the
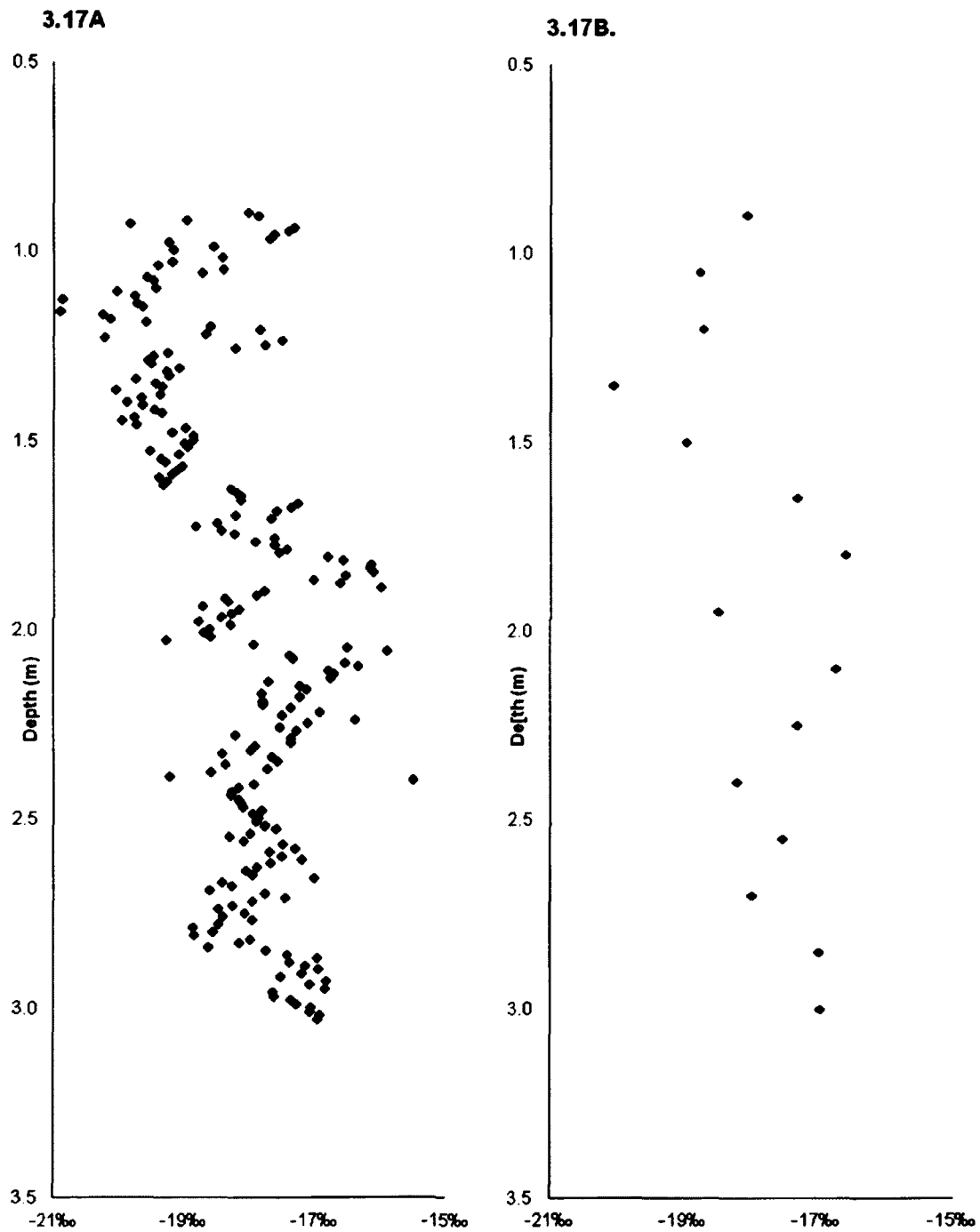
Figure 3.17 Shallow core $\delta^{18}O$ data at 1 cm spacing (3.17A) and 15 cm spacing (3.17B) versus depth.

spike would indicate, had it been part of the data. What the graphs demonstrate is that for oxygen isotope data taken at coarse resolution, variations in data may understate the actual variability of the isotopes in the sample. Still, even sampling at 15 cm resolution can show changes in isotope data profiles in a core; however, it should be recognized that greater sampling density would provide more information.

The high resolution sampling for isotopes from the shallow core shows the isotope signature changes in the permafrost very clearly (Figure 3.9). The isotope values for the entire depth of the shallow core vary widely, indicating several episodes of thawing and refreezing within the depth of the shallow core samples. It is almost certain that during repeated freeze-thaw cycles some mixing zone and double peak signatures have been at least partially replaced when the permafrost thawed and modern groundwater was able to mix with the thawed pore ice prior to refreezing. It is likely that some isotope information has been entirely erased during thaws, since the deeper a thaw penetrates, the more permafrost ice is replaced by groundwater which may have a different signature. When the replacement groundwater freezes, the "new" permafrost will have the more recent groundwater signature.

There are several mixing zone signatures that are very compressed so that the proper sequence of formation of these closely spaced multiple peaks is difficult to sort out. By applying statistical analysis to the data, the greatest differences, which are likely to be fractionation peaks formed each time the thawed permafrost refroze, can be isolated and then sorted by depth to separate discreet mixing zones.

Laboratory research on the fractionation process in soils has shown that the positive-negative isotope couplet (double peak) that is formed when the freezing front advance is slowed, such as when the active layer meets the permafrost table, is completely contained within a 5 to 10 cm interval (Michel, 1982). By comparing plots of "running" standard deviations for both 5 cm and 10 cm intervals of the shallow core $\delta^{18}O$ data to the plot of the data itself, it is possible to more easily separate the most variable data (double peaks) from the less variable but still changeable isotope signatures in the core. The running standard deviations were produced by taking the standard deviation of every 5 (or 10) cm section of the core for the length of the core, and then repeating the process for another series of 5 (or 10) cm sections, but starting 1 cm lower in the core. By doing this 5 (or 10) times for the core, standard deviations for all possible 5 cm (Table 3A-6), or 10 cm (Table 3A-7) sections of the core were taken. The standard deviations were then plotted and compared to the core data (Figure 3.18).

The best separation of data with highest variation is shown by the 5 cm spacing standard deviation chart (Figure 3.18B) although the 10 cm spacing chart (Figure 3.18A) reinforces that information, but with less clear separation. Aligning the 5 highest peaks in standard deviation from the Figure 3.18B chart with the data on the shallow $\delta^{18}O$ chart (Figure 3.18C) indicates the locations of double peaks in the shallow core. If the $\delta^{18}O$ data were not so noisy in this core, it would be easy to pick out these peaks, but with the amount of variation shown by the data, statistics are helpful.

The five peaks at or over 1 standard deviation on Figure 3.18B represent slowing of the freezing front and are most probably due to the refreezing thawed shallow
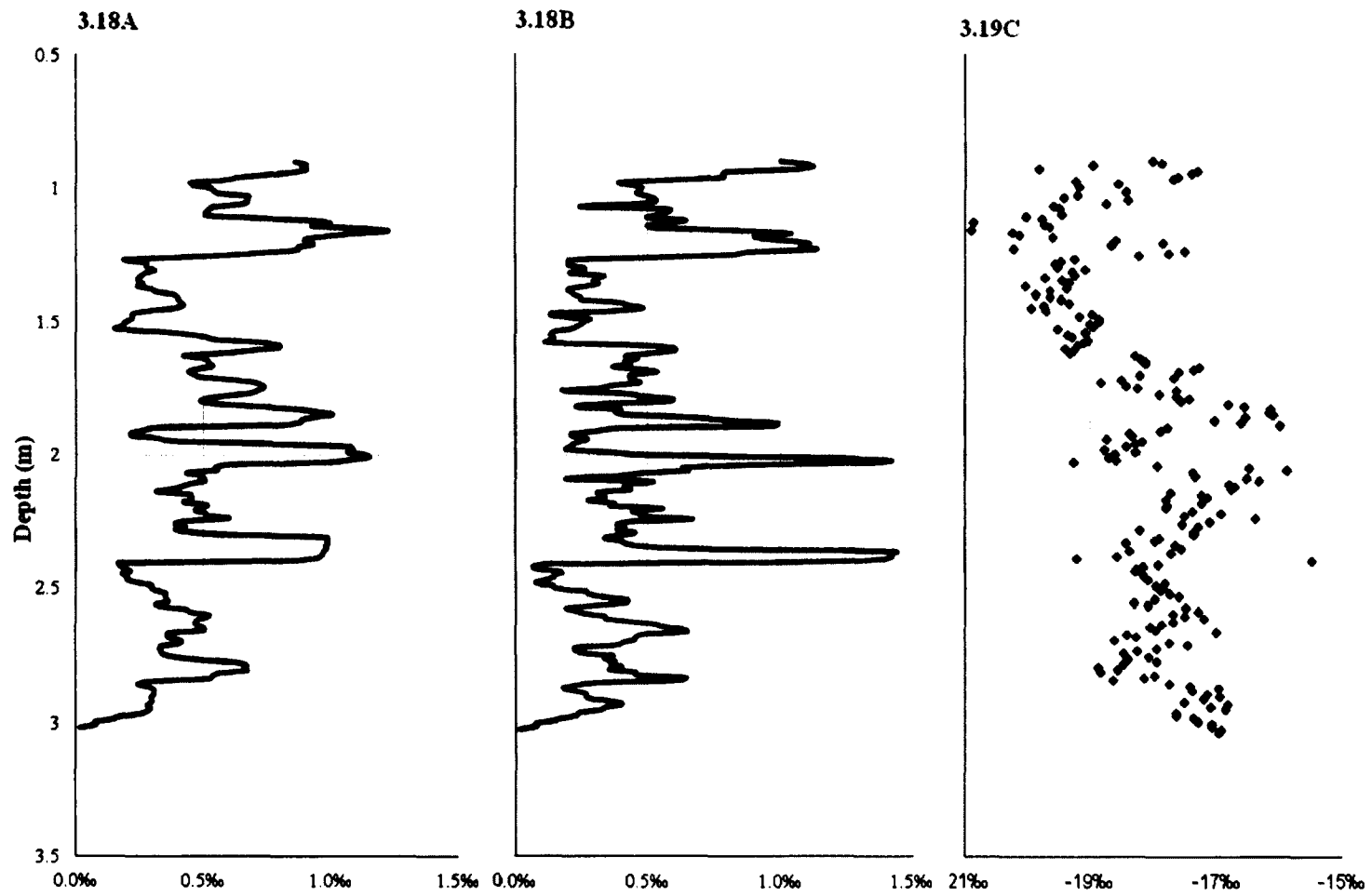
Figure 3.18 Standard deviation at 10 cm spacing (3.18A) and 5 cm spacing (3.18B) compared with $\delta^{18}O$ values in the shallow core (3.19C). Shaded bands show locations of double peaks in the core data.

permafrost meeting the new permafrost table after surface disturbance increased active layer depth. Because thawing of permafrost destroys the isotope signatures in the ice that has melted, the oldest permafrost in this core is below 2.4 m depth, the location of a double peak and probable location of an increased active layer depth in the past due to disturbance. The double peaks above 2.4 m depth are sequentially younger until at the top of the permafrost is the youngest ice of all. The isotope signatures between the double peaks, as indicated by the 5 cm standard deviations, form slanted profiles of data and represent mixing zones. This is confirming evidence of thawing and refreezing. The mixing zones have several different slopes. These zones would have been composed of varying combinations of rainwater, snowmelt and thawed permafrost ice in the groundwater, and would have refrozen at different times of year and at different rates.

This shallow zone of permafrost, about 3 m deep, is less than the 4 m depth of thaw modeled from fire in interior Alaska in a permafrost soil (Yoshikawa et al., 2003). Permafrost in the Alaskan discontinuous permafrost zone often experiences disturbance that increases the depth of the active layer, and the isotope signatures in the shallow core are representative of thawing and refreezing in that kind of "nonpermanent" permafrost.

At the shallow core site, the active layer meets the permafrost table at only 90 cm depth. The ground cover (moss, shrubs and black spruce trees) has made a great difference in permafrost persistence and recovery. During subsampling of the shallow core, charred plant parts were noted at depths of 108, 110, 111, 121, 134, 152 and 154 cm. These burned remnants could be the remains of as many as four separate fires. Percent water values below 1.75 m depth are more consistent than the values higher in

the core which could be evidence that the depth of thaw produced by the most intense fire in the area was approximately 1.75 m. Other fires of less intensity may have produced the other fluctuations in water content. It is likely that all the permafrost in the shallow core represents a single freezing era, mitigated by thawing due to fire, but refrozen quickly because of the local environment. Fire could easily have been the cause of some thawing and refreezing of the Hagelbarger core as well, even prior to the introduction of boreal forests to interior Alaska.

Fire is a common phenomenon in interior Alaska. Wildfire in the boreal forest has a return period of about 29 to 300 years (Yarie, 1981; Rupp et al., 2002; Yoshikawa et al., 2003). The effect of these fires on permafrost depends on the amount of insulating groundcover that is burned away, allowing the permafrost to thaw. When the surface organic layer is removed, the active layer over permafrost deepens. The stripping of vegetation for a fire line resulted in deepening from between 0.4 and 0.5 m to 2.1 m in 10 years (Viereck, 1982). Observations on burned sites in N.W.T. in Canada indicated that the active layer deepened for 10 to 20 years following fire (Mackay, 1995). Recent climatic conditions may be making it difficult for permafrost to recover after thawing by severe fire. A model created based on the Rosie Creek fire near Fairbanks, Alaska in 1983 showed that permafrost thawing was most rapid for the first 5 years (to a depth of 3.4 m) and continued, though slower, for the next 8 years (to a total depth of 4.15 m - an increase of only 0.8 m). Over the next 4 years the talik was practically stationary at 4.15 m. The simulation indicates that permafrost degradation due to fire continues for about 10 years under the current climatic conditions before the thaw stabilizes

(Yoshikawa et al., 2003). The layer of ash deposition at about 60 cm to 75 cm depth at the Hagelbarger site, as well as the 20- to 30-year-old age of the birch trees at the site in 1977, are two indicators of fairly recent fires that have occurred in this area, exacerbating the thawing trend in already warm permafrost.

The Hagelbarger data starts at 6.1 m depth because that is the top of the permafrost table in the core (Figure 3.4). The auger core starts at the ground surface and there are four values in the auger core above 6 m depth. The auger core location is only a few meters from the Hagelbarger core, but the top of the permafrost table at the auger site appears to be at 3 m depth (Figure 3.5), so the values above 3 m are modern ground water signatures. The $\delta^{18}O$ value for 3.05 m depth (below the permafrost table) is -17.919‰. The values above the permafrost table are; -20.185‰ at 1.83 m, -20.159‰ at 0.92 m, and -19.617‰ at 0.46 m (Figure 3.8B). The last three are all modern groundwater signatures, and are similar to the $\delta^{18}O$ signature of about -19.5‰ for well water in the Fairbanks area. The modern $\delta^{18}O$ water signature is lighter than the frozen groundwater which is older. It is unlikely that the isotope differences are due to climate change because groundwater isotopes are not reliable climate indicators. For example, groundwater isotopes represent signatures of combined rainwater and snowmelt. If there is proportionately less snowmelt than rainwater entering the ground during colder, drier periods, the isotope signature could be more enriched in spite of a colder climate (because rainwater is usually more enriched than snowmelt).

It is unlikely that permafrost below 6 m depth at the Hagelbarger site is syngenetic, considering that 6 m is the depth at various other loess sites in interior Alaska

(Halfway House, Birch Hill, Chena Hot Springs Road) in which organic material has

been radiocarbon dated to ages around 34,000-32,000 YBP (Muhs et al., 2003), a

relatively warm interstadial period (although not as warm as at present). It is more likely

that the permafrost below 6 m depth was formed (or reformed) later, during a colder

period. However, isotope evidence from the core points to several episodes of

permafrost formation, so there is no single date for permafrost at the site, but rather a

series of freeze-thaw cycles, probably occurring over thousands of years.

There is evidence that other permafrost which existed above 6 m depth at the

Hagelbarger site may have been syngenetic. The topography that resulted from

disturbance at the site makes clear that this area has been profoundly affected by cold

climate (Figure 3.2). Tops of ice wedges, possibly from the late Pleistocene or early

Holocene, are found at 1.8 m depth in this area (V.E. Romanovsky, personal comm.,

November 3, 2011). Currently the polygon mounds at the Hagelbarger site are over 4 m

apart and the trenches between the polygons are over 2 m deep and most of them seem to

have stabilized. The ice wedges that originally formed the polygons would have been

created when ground temperatures were colder than -6° C or less (Williams and Smith,

1989). The current high-centered mounds indicate that the polygon wedges are no longer

active, though at one time they formed a network at the site. The pond north of the

polygons has been formed in typical thaw-pond fashion and will no doubt disappear

when the underlying permafrost thaws and allows the pond to drain. The sunken

trenches, another wedge feature, continue to deepen each year. The deep trenches and

lack of surface soil disturbance by wedge growth suggest syngenetic permafrost (Mackay, 1990). The trench sizes also suggest that they formed over a long period.

The polygons and trenches which were exposed by melting of ice as a result of mechanical disturbance of vegetative ground cover are surface expressions of very cold climate in the past when the ice wedges were growing. While these shallower permafrost features may have been produced during the more recent cold period (about 11,000 yr BP), the deeper (> 6 m), older permafrost that has survived several thaw/freeze cycles is more likely to have been produced in the earlier cold period, between 14,000 and 40,000 yr BP.

Loess at Gold Hill at about 6 m depth was deposited over 35,000 yr BP (Muhs et al., 2003). The rate of deposition of loess in interior Alaska during the last glacial period was modest - a maximum of only 3-4 m at best, and in some places there was little or no accumulation. Estimates for Gold Hill loess deposits by ^{10}Be suggests 2 m of loess was deposited between 13,000 and 8,000 yr BP, and about 1 m of loess may have been deposited between ~32,210 and ~9,750 ^{14}C yr BP at Chena Hot Springs Road (Muhs et al., 2003). It seems likely that the loess at Hagelbarger has been deposited at about the same rate over the same time period.

For permafrost to form at depth and be maintained for a long period there must be a cold climate for an extended time. Shortly after deposition of the Hagelbarger loess at the current 6 m depth (assuming a close relationship with Gold Hill loess) the climate became relatively warm as indicated by the climate sequence from Beget (1996, 2001) and Muhs et al. (2003). Between about 45,000 to 18,000 yr BP climate fluctuated

erratically between extended cold and warm periods, and climate in the area was cooling

by about 30,000 yr BP. A long-term cold cycle at that time could have allowed formation

of permafrost to a depth beyond the current 25 m of the Hagelbarger core.

There was also a cold period between 11,000 and 10,500 yr BP. The formation of

permafrost to a depth of over 25 m may have been possible at that time, especially on the

north side of a hill, because the birch-shrub tundra then present could have insulated the

soil. Air temperature at that time was colder than at present which could have

"precooled" the soils, allowing permafrost to form at an increased rate. However,

because changes in the oxygen isotope signatures down the depth of the Hagelbarger core

indicate that there have been several episodes of thaw and refreezing of the pore ice

(Figure 3.8A) and the cold period only lasted about 500 years, it is not likely that several

freeze/thaw cycles could have been produced at the depths indicated by the isotope

signatures, even though the ground surface would probably have been 2 m to 4 m lower

than at the present time.

During the period from 45,000 to 18,000 yr BP there were long cold periods,

colder than any period since, except for 11,500 to 10,000 yr BP (Benn and Evans, 2003).

The advance and retention of permafrost would have been aided not only by the length

and severity of the colder climate, but by the changing plant cover in interior Alaska.

Between 35,000 and 30,000 yr BP forest tundra appeared and around 14,000 yr BP birch

shrub tundra became a prominent ecosystem in the interior. Around 9,000 yr BP birch

and white spruce forests appeared in interior Alaska (Lynch et al., 2003). These

vegetation types helped insulate the ground against warming in summer while allowing

cold to penetrate to the soil in winter. Permafrost would have been able to advance the full depth of the soil profile and on into the bedrock below. However, since climate fluctuations were large, there would have been times in the warmer periods when the ground thawed deeper than the active layer froze, even as loess deposition continued. The original permafrost may possibly have been syngenetic, but it is likely that all of the original permafrost has been replaced because of the alternating freeze-thaw cycles of this earlier time, especially before more insulating plant materials appeared in interior Alaska.

Permafrost at the Hagelbarger site extends from 6.1 m depth to 25 m depth. Since permafrost generally forms from the top down, the original permafrost table would have been at the depth of the bottom of the active layer. The talik that is now between the bottom of the active layer and the top of the permafrost table indicates that the original permafrost table has dropped below the active layer freezing depth as the permafrost has thawed. It is likely that the original permafrost extended into the bedrock beneath the loess at the Hagelbarger site, and that the material below 25 m depth has also thawed.

There are four distinct sections to the isotope data in the Hagelbarger core (Figure 3.19). At the top, the first section extends from 6.1 m to 9 m depth. There is a slanted profile of data with signatures from -17‰ at the top to -18.5‰ at about 9 m. This mixing zone suggests thawing followed by a change in groundwater (indicated by the different signature at the top of the mixing zone) and then refreezing. In this case a more enriched signature mixed with the more depleted signature of thawed permafrost deeper
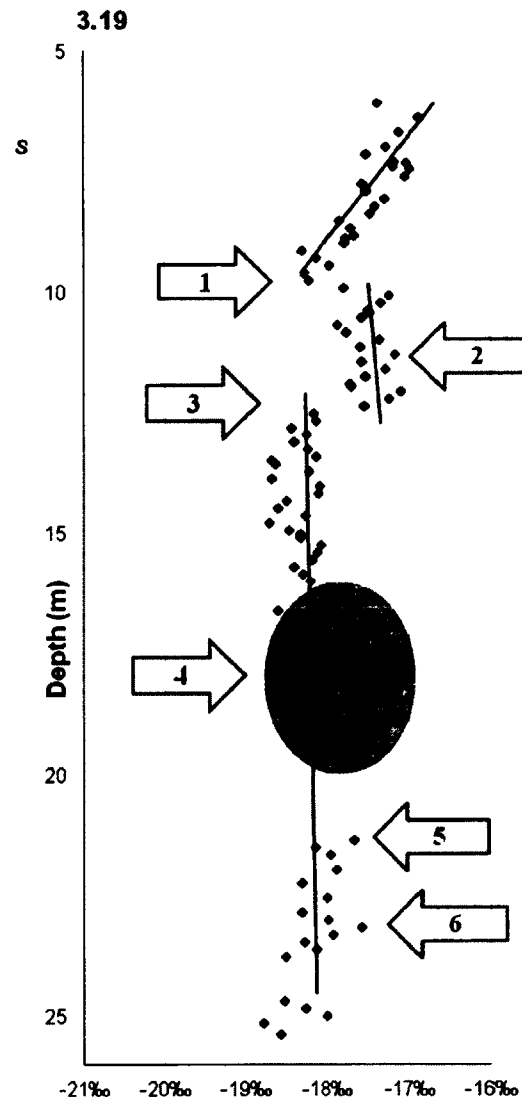
Figure 3.19 Annotated Hagelbarger core $\delta^{18}O$ data versus depth.

in the column. The bottom of the mixing zone does not meet the top of the next section, which starts at 10 m depth (arrow #1, Figure 3.19).

There is a hint of a mixing zone or part of a double peak at 10 m depth between the first and second sections that suggests more depleted pore ice was present and was nearly completely replaced by the material in the mixing zone. If permafrost formed around 30,000 yr BP, the ground surface would have been within a couple of meters of the current 6.1 m depth to the permafrost table. Double peaks and mixing zone isotope signatures would be normal in that situation as the then shallow permafrost responded to surface disturbances. The mixing zone may be a remnant of more reactive permafrost below a shallow active layer.

The second section goes from 9 m depth to about 12.5 m depth. Below the possible partial double peak at 10 m depth there is a column of data with signatures between -17‰ and -18‰ (arrow #2, Figure 3.19). There is an abrupt change between this section and the third section, with no apparent transition (arrow #3, Figure 3.19). The 15 cm sampling resolution may not have captured the data of a double peak at this depth, but the transition from one signature to another is quite definite.

The third section is a column of data with different signatures (-18‰ to -19‰) from 12.5 m depth to about 16 m depth, followed by what appears to be two oversized double peaks (arrow #4, Figure 3.20). Since the double peak signature is typically completed within a 5 cm to 10 cm span, this data represents large shifts in signatures forming mixing zone profiles. These profiles are similar to the pattern of signatures in

the shallow core (Figure 3.17) that form from repeated thawing and refreezing within a relatively short time period.

Lowest in the core is the fourth section, from below the possible mixing zones (about 19 m depth) to the bottom of the permafrost (25 m). This section is a column of data with a signature of about -17.5‰ to about -18.5‰. At about 21.5 m and 23 m depths there appear to be parts of two double peaks (arrows #5 and #6, Figure 3.19), but in general the values from 19 m to 25 m depth are consistent and if the possible mixing zones between 16 m and 19 m depth are excluded, the data between 12.5 m and 25 m depth are similar. The data below 25 m is below permafrost and not part of the permafrost column. The loss of data from between 19 m and 20 m is unfortunate, but there seems to be continuity in the signatures above and below the missing section.

The $\delta^{18}O$ isotope signatures show there have been significant changes to the permafrost at this site. Because of the numerous thaw/freeze cycles, the oldest permafrost is at the top of the bottommost continuous column (probably at 19 m), and the youngest is at the bottom of the transition zone at the top of the permafrost column (at about 9 m, probably the depth of the latest thaw after disturbance).

The three sections that are located between 9 m depth and 25 m depth represent three separate events down the column where permafrost was sustained below a thaw while new groundwater replaced the thawed ice in the soil. The top section, from 9 m to 6.1 m, is different. The thaw in this case was brief enough that the new groundwater did not replace the thawed permafrost, but mixed with it from the top down, and the ground refroze with the mixing zone *in situ*. It is possible that this was the second thaw event for

this section of the core as it appears that the bottom of the mixing zone does not connect with the top of the section below it. This suggests that the lower section of the mixing zone is composed of an older groundwater, almost totally replaced by the thaw of the top section.

The four different sections of the core appear to be stacked in sequential order, but it is entirely possible that there have been a number of thaw/freeze cycles down the core whose isotopic signatures have been erased by those now in place. It is difficult to suggest an explanation for the wide variations in signatures between 16 m and 19 m unless there had been a major series of thaw/freeze events that happened in fairly rapid succession. This means that at the time this happened, the top of the active layer must have been within, at most, 4 or 5 m of this section of the core, or at about the current 12 m depth. In that case, the pore ice below 12 m depth is older than 30,000 years, since the silt at about 6 m depth or less at several sites in the Fairbanks area (Halfway House, Birch Hill, and Chena Hot Springs) were dated to ages between 34,000 and 32,000 yr BP (Muhs et al., 2003), and there were chemical indications of pedogenesis at 7 m depth in the core that may be similar to a soil at 7 m depth at Gold Hill that was ^{14}C dated to have formed over 40,000 yr BP (Muhs et al., 2003).

Although rapidly alternating climate changes have not occurred in Alaska in the last few thousand years, increased fire activity, especially in spruce forests, has caused changes in permafrost, particularly in the discontinuous permafrost zones where minor changes in temperature can have a profound effect. The original permafrost at the Hagelbarger site has also thawed from the bottom upward so that the current depth of

permafrost is only about 25 m, and the talik below the active layer goes to 6 m depth, resulting in a column of 19 m of permafrost. Yet in spite of the current warm period the permafrost at Hagelbarger persists, and at the auger site the permafrost table is at a much shallower 3 m depth (Figure 3.5), while at the shallow core site the permafrost table is at less than 1 m depth. Ash layers in the soil show that fires have gone through this area often, and at the auger and shallow core sites the insulating moss and black spruce have returned to protect the permafrost, but not at the Hagelbarger site where the ground cover is generally birch trees and large shrubs. It is probably differences in microclimate, hydrology, and soil that has caused this difference in permafrost persistence and also may be the cause for the creation of permafrost ice wedges nearby. The Hagelbarger permafrost may have been able to survive the current warm trend, but the disturbance caused by thinning the shrubs and increased surface traffic around the house at the site is probably having a destabilizing effect. Temperature monitoring over the next few years may show changes in the depth to the permafrost table that reflects how destabilizing the local disturbance really is.

LITERATURE CITED

Beget, J.E. 1996. Tephrochronology and paleoclimatology of the last interglacial-glacial cycle recorded in Alaskan loess deposits. Quaternary International, vols 34-36, 121-126.

Beget, J.E. 2001. Continuous late Quaternary proxy climate records from loess in Beringia. Quat. Sci. Rev., 20, 499-507.

Beget, J.E. 2006. Characterizing pyroclastic-flow interactions with snow and water using environmental magnetism at Augustine volcano. *In*: The 2006 Eruption of Augustine Volcano, Alaska, J.A. Power, M.L. Coombs and J.T. Freymueller, (eds.) U.S. Geological Survey Professional Paper 1769, 269-275.

Beget, J.E., M. Edwards, D. Hopkins, M. Keskinen and G. Kukla. 1991. Old Crow tephra found at the palisades of the Yukon, Alaska. Quat. Res. 35, 291-297.

Benn, D.I. and D.J.A. Evans, 2003. *Glaciers and Glaciation*. London. Arnold. 734 pages.

Davis, N.T. 2000. *Permafrost: A Guide to Frozen Ground in Transition*. Univ. of Alaska Press. Fairbanks. 351 pages.

French, H.M. 1999. Past and present permafrost as an indicator of climate change. Polar Res. 18:2, 269-274.

Höfle, C. and C.L. Ping. 1996. Properties and soil development of late-Pleistocene paleosols from Seward Peninsula, northwest Alaska. Geoderma 71, 219-243.

Jorgenson, M.T., C.H. Racine, J.C. Walters and T.E. Osterkamp. 2001. Permafrost degradation and ecological changes associated with warming climate in central Alaska. Climatic Change 48, 551-579.

Lynch, J.A., J.S. Clark, N.H. Bigelow, M.E. Edwards and B.P. Finney. 2003. Geographic and temporal variations in fire history in boreal ecosystems of Alaska. J. Geophys. Res., 107, 8152, doi:10.1029/2001JD000332, 2002.

Mackay, J.R. 1990. Some observations on the growth and deformation of epigenetic, syngenetic and anti-syngenetic ice wedges. Permafrost and Periglacial Processes 1:1, 15-29.

Mackay, J.R. 1995. Active layer changes (1968 to 1993) following the forest tundra fire near Inuvik, N.W.T., Canada. Arc. and Alp. Res. 27:4, 323-336.

Michel, F.A. 1982. Isotope investigations of permafrost waters in northern Canada. Ph.D. dissertation, University of Waterloo, Waterloo, Ontario. 424 pages.

Michel, F.A. and P. Fritz. 1978. Environmental isotopes in permafrost related waters along the Mackenzie Valley corridor. Proceedings of the 3rd International Conference on Permafrost, National Research Council, Canada 1, 207-211.

Muhs, D.R., T.A. Ager, E.A. Bettis III, J. McGeehin, J.M. Been, J.E. Beget, M.J. Pavich, T.W. Stafford Jr. and D.S.P. Stevens. 2003. Stratigraphy and palaeoclimatic significance of late Quaternary loess–palaeosol sequences of the last interglacial-glacial cycle in central Alaska. Quat. Sci. Rev. 22, 1947-1986.

Muhs, D.R. and J.R. Budahn. 2006. Geochemical evidence for the origin of late Quaternary loess in central Alaska. Can. J. Earth Sci. 43, 323-337.

Pearson, R.W. and M. Hermans, (eds.) 2008. *Alaska in Maps: A Thematic Atlas.* CD-ROM. Fairbanks: University of Alaska Fairbanks.

Péwé, T.L. 1977. *Guidebook to the Quaternary Geology, Central and South-Central Alaska.* International Association of Quaternary Research, VIIth Congress. 141 pages.

Péwé, T.L. and R.D. Reger. 1989. *Quaternary Geology and Permafrost Along the Richardson and Glen Highways between Fairbanks and Anchorage, Alaska. Field Trip Guidebook T102.* 28th International Geological Congress. 54 pages.

Preece, S.J., J.A. Westgate, B.A. Stemper and T.L. Péwé. 1999. Tephrochronology of late Cenozoic loess at Fairbanks, central Alaska. GSA Bulletin, January 111:1, 71-90.

Pritchett, W.L and R.F. Fisher. 1987. Chemical properties of forest soils. In: *Properties and Management of Forest Soils,* 2nd ed. John Wiley and Sons. Toronto. 493 pages.

Romanovsky, V.E., T.S. Sazonova, V.T. Balobaev, N.I. Shender and D.O. Sergueev. 2007. Past and recent changes in air and permafrost temperatures in eastern Siberia. Global and Planetary Change 56, 399-413.

Rupp, T.S., A.M. Starfield, F.S. Chapin and P. Duffy. 2002. Modeling the impact of black spruce on the fire regime of Alaskan boreal forest. Climatic Change 55, 213-233.

Smith, S.L., V.E. Romanovsky, A.G. Lewkowicz, C.R. Burn, M. Allard, G.D. Clow, K. Yoshikawa and J. Throop. 2010. Thermal state of permafrost in North America: a contribution to the International Polar Year. Permafrost and Periglacial Processes 21, 117-135.

Toniolo, H., P. Kodial, L.D. Hinzman and K. Yoshikawa. 2009. Spatio-temporal evolution of a thermokarst in Interior Alaska. Cold Regions Science and Technology 56:1, 39-49.

Verosub, K.L., P. Fine, M.J. Singer and J. TenPas. 1993. Pedogenesis and paleoclimate: Interpretation of the magnetic susceptibility record of Chinese loess-paleosol sequences. Geology 21, 1011–1014.

Viereck, L.A. 1982. Effects of fire and firelines on active layer thickness and soil temperatures in interior Alaska. Proceedings of the 4th Canadian Permafrost Conference, Permafrost and Soils: 123-135.

Westgate, J.A. and B.A. Stemper. 1990. A 3 m.y. record of Pliocene-Pleistocene loess in interior Alaska. Geology. 18, 858-861.

Williams, P.J. and M.W. Smith. 1989. *The Frozen Earth, Fundamentals in Geocryology.* Cambridge University Press. Cambridge. 306 pages.

Yarie, J. 1981. Forest fire cycles and life tables: a case study from interior Alaska. Can. J. For. Res. 11:3, 554-562.

Yoshikawa, K., W.R. Bolton, V.E. Romanovsky, M. Fukuda and L.D. Hinzman. 2003. Impacts of wildfire on the permafrost in the boreal forests of Interior Alaska. J. Geophys. Res., 108, 1-14.

APPENDIX 3A

Table 3A-1. Hagelbarger Core % Gravimetric Water Content and Isotope Data.

Depth m	H_2O	$\delta^{18}O$ Relative to VSMOW	δD Relative to VSMOW	Depth m	H_2O	$\delta^{18}O$ Relative to VSMOW	δD Relative to VSMOW
6.10	21.42%	-17.3983‰	-142.1160‰	12.05	24.16%	-17.1061‰	-147.1497‰
6.40	25.38%	-16.8794‰	-142.5152‰	12.20	22.05%	-17.2507‰	-147.9010‰
6.71	25.47%	-17.1266‰	-138.9101‰	12.35	20.61%	-17.5546‰	-144.2441‰
7.01	27.70%	-17.3003‰	-140.5294‰	12.51	23.62%	-18.1804‰	-144.1121‰
7.16	26.79%	-17.5357‰	-141.3704‰	12.66	22.68%	-18.1485‰	-144.9502‰
7.32	25.27%	-17.1959‰	-136.4327‰	12.81	21.56%	-18.4441‰	-143.1833‰
7.35	24.04%	-17.0364‰	-145.4963‰	12.96	21.38%	-18.2653‰	-142.1208‰
7.38	23.13%	-17.2051‰	-139.7247‰	13.12	20.82%	-18.4145‰	-145.6889‰
7.41	24.96%	-17.2032‰	-130.1520‰	13.27	20.94%	-18.2503‰	-141.4995‰
7.47	24.56%	-16.9962‰	-135.2830‰	13.42	21.48%	-18.1417‰	-142.0618‰
7.63	24.23%	-17.0589‰	-136.5848‰	13.48	24.80%	-18.6895‰	-148.9166‰
7.78	24.93%	-17.582‰	-138.0560‰	13.57	23.64%	-18.6456‰	-149.0781‰
7.93	25.06%	-17.5439‰	-140.2659‰	13.73	25.94%	-18.2270‰	-147.1736‰
8.08	24.70%	-17.3166‰	-137.5684‰	13.88	24.80%	-18.6913‰	-149.8196‰
8.24	23.57%	-17.4295‰	-141.9789‰	14.03	22.80%	-18.0999‰	-147.7210‰
8.39	20.51%	-17.4879‰	-133.6381‰	14.18	24.41%	-18.1121‰	-149.1724‰
8.54	24.31%	-17.8595‰	-139.5753‰	14.34	20.47%	-18.5083‰	-149.9529‰
8.69	24.06%	-17.7261‰	-135.8273‰	14.49	21.47%	-18.6186‰	-151.1348‰
8.85	23.66%	-17.6721‰	-138.1516‰	14.64	20.87%	-18.2778‰	-149.0542‰
8.91	20.19%	-17.7741‰	-139.6214‰	14.79	21.99%	-18.7235‰	-150.8386‰
9.00	22.87%	-17.7991‰	-139.1035‰	14.95	22.61%	-18.4744‰	-151.1789‰
9.15	20.12%	-18.3252‰	-141.8045‰	15.01	23.96%	-18.3399‰	-149.4300‰
9.30	20.70%	-18.1422‰	-131.8590‰	15.10	22.33%	-18.3458‰	-149.0021‰
9.46	18.27%	-17.9733‰	-130.2969‰	15.25	21.22%	-18.0874‰	-148.9152‰
9.61	20.09%	-18.2907‰	-143.9566‰	15.40	19.99%	-18.1266‰	-143.6684‰
9.76	21.61%	-18.2290‰	-153.1449‰	15.56	21.28%	-18.1873‰	-145.7666‰
9.91	19.79%	-17.7897‰	-136.3712‰	15.71	23.64%	-18.4224‰	-152.6183‰
10.07	20.43%	-17.2559‰	-137.5249‰	15.86	22.30%	-18.3073‰	-149.3334‰
10.22	20.51%	-17.3574‰	-140.7877‰	16.01	22.91%	-18.2148‰	-146.5985‰
10.37	20.66%	-17.5065‰	-141.1954‰	16.17	25.83%	-17.8397‰	-148.9901‰
10.43	23.92%	-17.4905‰	-144.0976‰	16.32	22.35%	-17.9847‰	-146.8479‰
10.52	20.58%	-17.5862‰	-144.9905‰	16.47	23.64%	-18.1669‰	-148.7718‰
10.68	21.59%	-17.8652‰	-148.0730‰	16.53	23.84%	-18.1618‰	-149.7326‰
10.83	18.79%	-17.7590‰	-142.1568‰	16.62	20.95%	-18.6335‰	-146.9788‰
10.98	19.52%	-17.3718‰	-144.0927‰	16.78	27.79%	-18.2891‰	-150.9704‰
11.13	20.21%	-17.6032‰	-144.7857‰	16.93	21.16%	-17.6169‰	-146.6979‰
11.29	20.84%	-17.1757‰	-143.8196‰	17.08	23.57%	-18.0161‰	-149.8731‰
11.44	21.02%	-17.5888‰	-146.3641‰	17.23	19.79%	-17.2267‰	-141.6163‰
11.59	30.52%	-17.2991‰	-143.0245‰	17.39	23.35%	-17.4545‰	-146.6761‰
11.74	22.48%	-17.5414‰	-146.7414‰	17.69	20.17%	-17.7461‰	-142.2303‰
11.90	23.56%	-17.7215‰	-146.5113‰	18.00	19.32%	-18.0415‰	-145.9340‰
11.96	25.45%	-17.7049‰	-146.7234‰	18.15	20.80%	-18.1495‰	-143.5778‰

Table 3A-1. Continued.

Depth m	H₂O	δ¹⁸O Relative to VSMOW	δD Relative to VSMOW	Depth m	H₂O	δ¹⁸O Relative to VSMOW	δD Relative to VSMOW
18.30	20.55%	-18.1852‰	-141.1673‰	22.88	17.35%	-18.3304‰	-139.1148‰
18.45	20.90%	-17.8467‰	-141.1682‰	23.03	22.34%	-17.9891‰	-144.4464‰
18.61	22.13%	-17.7037‰	-147.4615‰	23.18	18.50%	-17.5829‰	-143.8467‰
18.76	20.66%	-17.5230‰	-142.9703‰	23.33	24.40%	-17.9349‰	-147.8436‰
18.91	20.15%	-17.8087‰	-143.7064‰	23.49	18.21%	-18.2970‰	-135.3681‰
19.22	21.19%	-17.8819‰	-149.6937‰	23.64	20.66%	-18.1492‰	-131.9122‰
21.50	15.85%	-18.1588‰	-136.3183‰	23.79	22.44%	-18.5235‰	-135.0759‰
21.66	20.96%	-17.9572‰	-140.6470‰	24.71	19.26%	-18.5341‰	-155.0709‰
21.96	20.35%	-17.8837‰	-143.0586‰	24.86	17.85%	-18.2801‰	-144.4320‰
22.27	17.56%	-18.3325‰	-142.2599‰	25.01	15.28%	-18.0063‰	-141.7709‰
22.57	18.67%	-18.0048‰	-146.1342‰				
				Average	22.06%	-17.88‰	-143.67‰
				StdDev	2.53	0.45	5.18
				High Value	30.52%	-16.88‰	-130.15‰
				Low Value	15.28%	-18.72‰	-155.07‰

Table 3A-2. Auger Core % Gravimetric Water Content and Isotope Data.

Depth m	H_2O	$\delta^{18}O$ Relative to VSMOW	δD Relative to VSMOW
0.46	20.99%	-19.6173‰	-160.6223‰
0.92	21.97%	-20.1587‰	-190.3986‰
1.83	17.20%	-20.1847‰	-176.0184‰
3.05	25.56%	-17.9192‰	-166.0461‰
6.10	23.28%	-18.2519‰	-168.0180‰
9.15	25.18%	-18.3316‰	-165.4880‰
12.20	21.67%	-18.1404‰	-163.9115‰
18.30	18.96‰	-17.9851‰	-152.8484‰
21.35	20.96%	-17.6220‰	-154.5168‰
Average	21.75%	-18.69‰	-166.43‰
Std Dev	0.03	1.01	11.38
High Value	25.56%	-17.62‰	-152.85‰
Low Value	17.20%	-20.18‰	-190.40‰

Table 3A-3. Shallow Core % Gravimetric Water Content and Isotope Data.

Depth m	H₂O	δ¹⁸O Relative to VSMOW	δ D Relative to VSMOW	Depth m	H₂O	δ¹⁸O Relative to VSMOW	δ D Relative to VSMOW
0.90	31.79%	-18.0214‰	-167.4110‰	1.31	44.10%	-19.0942‰	-160.0986‰
0.91	35.22%	-17.8693‰	-160.8177‰	1.32	47.87%	-19.2824‰	-162.6888‰
0.92	30.94%	-18.9687‰	-151.3896‰	1.33	39.93%	-19.2479‰	-162.1645‰
0.93	30.81%	-19.8376‰	-156.5725‰	1.34	40.86%	-19.7527‰	-156.7566‰
0.94	33.87%	-17.3172‰	-149.2099‰	1.35	36.64%	-19.4485‰	-160.2236‰
0.95	34.12%	-17.3971‰	-155.3860‰	1.36	38.17%	-19.3430‰	-159.0272‰
0.96	33.26%	-17.6184‰	-155.3978‰	1.37	31.54%	-20.0507‰	-146.6889‰
0.97	33.21%	-17.6871‰	-157.4835‰	1.38	32.91%	-19.3750‰	-160.6163‰
0.98	32.22%	-19.2426‰	-155.6145‰	1.39	33.11%	-19.6603‰	-161.6193‰
0.99	28.20%	-18.5685‰	-159.4759‰	1.40	32.21%	-19.8824‰	-157.8919‰
1.00	30.00%	-19.1798‰	-154.9346‰	1.41	31.35%	-19.6540‰	-154.1789‰
1.02	36.37%	-18.4284‰	-165.2894‰	1.42	41.72%	-19.4674‰	-152.8483‰
1.03	37.83%	-19.1965‰	-151.2454‰	1.43	47.84%	-19.3446‰	-155.4392‰
1.04	36.10%	-19.4199‰	-156.1331‰	1.44	37.32%	-19.7668‰	-150.2551‰
1.05	35.21%	-18.4026‰	-163.0839‰	1.45	43.64%	-19.9614‰	-156.1951‰
1.06	32.37%	-18.7366‰	-164.1976‰	1.46	49.72%	-19.7320‰	-150.6183‰
1.07	35.56%	-19.5843‰	-167.8747‰	1.47	49.96%	-18.9784‰	-160.8777‰
1.08	33.58%	-19.4832‰	-167.5368‰	1.48	36.92%	-19.1871‰	-155.6121‰
1.10	32.65%	-19.4523‰	-165.6139‰	1.49	40.65%	-18.8674‰	-155.7107‰
1.11	39.54%	-20.0401‰	-169.7867‰	1.50	33.22%	-18.8660‰	-165.1876‰
1.12	33.30%	-19.7734‰	-175.5778‰	1.51	40.90%	-19.0094‰	-162.9746‰
1.13	36.15%	-20.8690‰	-166.1911‰	1.52	41.14%	-18.9592‰	-157.7894‰
1.14	31.45%	-19.7428‰	-175.2279‰	1.53	28.40%	-19.5285‰	-154.6267‰
1.15	34.82%	-19.6581‰	-165.3841‰	1.54	28.92%	-19.0921‰	-157.8261‰
1.16	54.51%	-20.9030‰	-162.8066‰	1.55	35.52%	-19.3664‰	-162.2017‰
1.17	31.76%	-20.2621‰	-163.9719‰	1.56	30.95%	-19.2953‰	-159.5098‰
1.18	34.54%	-20.1500‰	-155.2455‰	1.57	31.67%	-19.0437‰	-161.7050‰
1.19	47.19%	-19.6046‰	-156.9673‰	1.58	29.62%	-19.1136‰	-148.5841‰
1.20	40.59%	-18.6054‰	-146.8865‰	1.59	30.31%	-19.1948‰	-155.0472‰
1.21	48.48%	-17.8532‰	-163.8477‰	1.60	30.83%	-19.3993‰	-151.1126‰
1.22	62.06%	-18.6788‰	-171.8572‰	1.61	28.79%	-19.2776‰	-156.4674‰
1.23	47.26%	-20.2306‰	-166.6474‰	1.62	25.56%	-19.3337‰	-140.6675‰
1.24	69.49%	-17.5150‰	-163.2162‰	1.63	33.28%	-18.2894‰	-163.3688‰
1.25	69.92%	-17.7564‰	-162.4456‰	1.64	36.08%	-18.2025‰	-158.4179‰
1.26	48.62%	-18.2281‰	-171.6655‰	1.65	38.64%	-18.1349‰	-167.5113‰
1.27	39.51%	-19.2588‰	-173.6275‰	1.66	39.75%	-18.1350‰	-156.8869‰
1.28	31.12%	-19.4731‰	-164.1468‰	1.67	44.72%	-17.2736‰	-170.4532‰
1.29	25.51%	-19.5700‰	-162.8276‰	1.68	46.93%	-17.3713‰	-167.4467‰
1.30	34.51%	-19.5181‰	-162.1550‰	1.69	42.34%	-17.5999‰	-157.7195‰

Table 3A-3. Continued.

Depth m	H$_2$O	δ^{18}O Relative to VSMOW	δ D Relative to VSMOW	Depth m	H$_2$O	δ^{18}O Relative to VSMOW	δ D Relative to VSMOW
1.70	33.86%	-18.2148‰	-170.6410‰	2.09	36.18%	-16.5295‰	-154.2558‰
1.71	37.93%	-17.6730‰	-162.8203‰	2.10	35.47%	-16.3361‰	-155.1161‰
1.72	34.94%	-18.5046‰	-170.2443‰	2.11	34.18%	-16.7944‰	-149.9628‰
1.73	36.69%	-18.8406‰	-158.9941‰	2.12	33.58%	-16.7072‰	-161.5406‰
1.74	34.66%	-18.4355‰	-169.6696‰	2.13	33.80%	-16.7608‰	-158.9539‰
1.75	34.18%	-18.2458‰	-163.4644‰	2.14	35.15%	-17.7186‰	-142.1897‰
1.76	34.28%	-17.6296‰	-167.4778‰	2.15	33.06%	-17.2377‰	-146.8593‰
1.77	35.25%	-17.9156‰	-160.0256‰	2.16	34.30%	-17.1374‰	-148.6275‰
1.78	35.98%	-17.6280‰	-151.9715‰	2.17	32.92%	-17.8078‰	-156.3044‰
1.79	32.52%	-17.4348‰	-160.1855‰	2.18	31.55%	-17.2412‰	-150.0217‰
1.80	32.28%	-17.5654‰	-159.6899‰	2.19	32.90%	-17.7910‰	-155.0268‰
1.81	33.88%	-16.8116‰	-159.2168‰	2.20	36.56%	-17.7988‰	-158.1681‰
1.82	33.04%	-16.5690‰	-161.3279‰	2.21	37.22%	-17.3735‰	-154.4926‰
1.83	36.00%	-16.1427‰	-171.7746‰	2.22	36.54%	-16.9305‰	-164.0249‰
1.84	36.98%	-16.1707‰	-152.5107‰	2.23	36.80%	-17.5145‰	-157.0021‰
1.85	37.17%	-16.1051‰	-154.2935‰	2.24	37.28%	-16.3807‰	-161.4113‰
1.86	35.36%	-16.5418‰	-145.2848‰	2.25	41.07%	-17.1078‰	-157.0144‰
1.87	35.21%	-17.0328‰	-142.2354‰	2.26	38.22%	-17.5407‰	-156.9757‰
1.88	35.29%	-16.6254‰	-145.6671‰	2.27	35.67%	-17.2846‰	-164.9454‰
1.89	33.78%	-15.9928‰	-138.9678‰	2.28	37.89%	-18.2181‰	-157.4664‰
1.90	40.40%	-17.7761‰	-153.1346‰	2.29	38.22%	-17.3699‰	-151.5593‰
1.91	42.88%	-17.8944‰	-147.7169‰	2.30	36.77%	-17.3660‰	-162.8344‰
1.92	42.87%	-18.3829‰	-145.5150‰	2.31	36.30%	-17.9175‰	-159.9405‰
1.93	42.32%	-18.3373‰	-147.5990‰	2.32	36.52%	-17.9863‰	-155.3807‰
1.94	41.77%	-18.7367‰	-142.8130‰	2.33	35.59%	-18.4279‰	-146.2998‰
1.95	38.16%	-18.1752‰	-150.0228‰	2.34	31.89%	-17.6615‰	-151.8249‰
1.96	37.78%	-18.2963‰	-147.3515‰	2.35	35.30%	-17.5704‰	-157.8137‰
1.97	38.59%	-18.4447‰	-148.2770‰	2.36	33.23%	-18.3800‰	-150.6729‰
1.98	41.28%	-18.7897‰	-147.4184‰	2.37	34.95%	-17.7250‰	-164.3539‰
1.99	39.44%	-18.2872‰	-151.1563‰	2.38	34.19%	-18.5891‰	-162.1781‰
2.00	38.54%	-18.6108‰	-145.0406‰	2.39	30.97%	-19.2254‰	-140.7278‰
2.01	44.46%	-18.7017‰	-149.3476‰	2.40	35.71%	-15.4958‰	-144.3053‰
2.02	37.67%	-18.5928‰	-153.5936‰	2.41	37.26%	-17.9347‰	-145.8292‰
2.03	37.85%	-19.2704‰	-143.1724‰	2.42	35.83%	-18.1692‰	-146.2187‰
2.04	38.22%	-17.9393‰	-149.4195‰	2.43	37.66%	-18.2710‰	-153.8770‰
2.05	37.65%	-16.4981‰	-136.1662‰	2.44	35.16%	-18.2865‰	-144.7006‰
2.06	34.07%	-15.8889‰	-145.9798‰	2.45	34.31%	-18.1717‰	-148.1452‰
2.07	36.74%	-17.3799‰	-152.9646‰	2.46	29.66%	-18.1406‰	-145.4620‰
2.08	37.09%	-17.3395‰	-157.2238‰	2.47	31.97%	-18.0995‰	-146.0594‰

Table 3A-3. Continued.

Depth m	H_2O	$\delta^{18}O$ Relative to VSMOW	δD Relative to VSMOW	Depth m	H_2O	$\delta^{18}O$ Relative to VSMOW	δD Relative to VSMOW
2.48	33.68%	-17.8203‰	-151.4947‰	2.87	32.01%	-16.9637‰	-149.7974‰
2.49	33.61%	-17.9566‰	-147.6792‰	2.88	31.24%	-17.3826‰	-151.3864‰
2.50	32.49%	-17.8580‰	-146.9521‰	2.89	31.06%	-17.1428‰	-151.0744‰
2.51	31.87%	-17.8905‰	-140.5024‰	2.90	29.14%	-16.9462‰	-150.0910‰
2.52	30.77%	-17.7537‰	-144.5502‰	2.91	29.51%	-17.1955‰	-153.6475‰
2.53	31.89%	-17.6000‰	-149.7029‰	2.92	30.66%	-17.5159‰	-152.3126‰
2.54	30.79%	-17.9888‰	-147.5307‰	2.93	32.26%	-16.8244‰	-161.7619‰
2.55	29.64%	-18.3005‰	-139.4825‰	2.94	32.88%	-17.0872‰	-148.8285‰
2.56	31.01%	-18.0931‰	-140.7378‰	2.95	31.92%	-16.8508‰	-165.4004‰
2.57	29.72%	-17.4980‰	-141.1845‰	2.96	39.70%	-17.6350‰	-138.6797‰
2.58	31.62%	-17.2981‰	-142.8430‰	2.97	31.88%	-17.6280‰	-164.4991‰
2.59	30.81%	-17.6860‰	-134.4027‰	2.98	31.52%	-17.3700‰	-156.1282‰
2.60	31.68%	-17.5016‰	-134.0147‰	2.99	32.43%	-17.2868‰	-143.2183‰
2.61	32.76%	-17.1948‰	-141.8638‰	3.00	33.15%	-17.0697‰	-159.0542‰
2.62	33.32%	-17.6847‰	-150.6178‰	3.01	34.12%	-17.0802‰	-163.6614‰
2.63	31.92%	-17.8773‰	-158.4460‰	3.02	30.51%	-16.9340‰	-173.8321‰
2.64	29.30%	-18.0523‰	-150.3248‰	3.03	32.26%	-16.9559‰	-159.7060‰
2.65	30.10%	-17.9573‰	-139.9843‰				
2.66	29.99%	-17.0082‰	-146.4394‰				
2.67	29.16%	-18.4213‰	-151.8362‰				
2.68	31.45%	-18.2696‰	-142.9377‰				
2.69	28.53%	-18.6181‰	-147.4210‰	Average	35.44%	-18.18‰	-154.08‰
2.70	28.44%	-17.7545‰	-146.3970‰	Std Dev	6.19	1.03	9.50
2.71	31.83%	-17.4482‰	-145.0546‰	High Value	69.92%	-15.50‰	-126.59‰
2.72	30.48%	-17.9443‰	-145.1300‰	LowValue	25.51%	-20.90‰	-175.58‰
2.73	28.05%	-18.2545‰	-141.3972‰				
2.74	28.02%	-18.4808‰	-126.5916‰				
2.75	27.26%	-18.0681‰	-135.6930‰				
2.76	29.55%	-18.4035‰	-132.3968‰				
2.77	30.40%	-17.9425‰	-141.3383‰				
2.78	29.51%	-18.4742‰	-141.8411‰				
2.79	31.75%	-18.8745‰	-131.7982‰				
2.80	32.41%	-18.5573‰	-132.8159‰				
2.81	30.92%	-18.8442‰	-145.1519‰				
2.82	31.68%	-17.9847‰	-145.7508‰				
2.83	30.86%	-18.1539‰	-148.5820‰				
2.84	31.69%	-18.6274‰	-137.0215‰				
2.85	31.45%	-17.7445‰	-139.9085‰				
2.86	30.81%	-17.4148‰	-145.7717‰				

Table 3A-4. Hagelbarger Core Chemical Results

Depth m	%N	%C	Ca mg/l	Fe mg/l	K mg/l	Mg mg/l	pH	Conductivity μS/cm	Bicarbonate meq/l	Magnetic Susceptibility
6.10	0.134	1.088	0.707	0.408	0.200	0.133	8.31	309	0.81	61
6.40	0.191	1.550	0.669	0.273	0.137	0.084	8.23	326	0.76	62
6.71	0.274	2.152	0.818	0.306	0.153	0.105	8.02	354	0.93	70
7.01	0.349	2.982	0.803	0.402	0.170	0.131	7.15	341	0.89	24
7.16	0.350	2.959	0.544	0.377	0.162	0.110	6.75	299	0.74	28
7.32	0.250	2.166	1.093	0.397	0.202	0.155	7.42	367	1.22	56
7.35	0.376	3.825	0.944	0.315	0.184	0.157	6.92	425	1.13	39
7.38	0.248	2.202	0.767	0.348	0.198	0.124	7.52	365	0.76	275
7.41	0.255	2.340	0.888	0.306	0.183	0.130	7.50	324	1.10	60
7.47	0.210	1.852	0.855	0.288	0.177	0.115	7.91	316	1.05	60
7.63	0.197	1.581	0.752	0.274	0.182	0.097	8.12	289	0.90	50
7.78	0.225	1.875	0.716	0.296	0.174	0.099	8.13	322	0.99	45
7.93	0.238	2.122	0.841	0.308	0.226	0.118	7.91	311	0.99	54
8.08	0.234	1.952	0.720	0.279	0.176	0.098	7.97	315	0.86	38
8.24	0.216	1.826	0.686	0.250	0.171	0.091	8.13	303	0.76	54
8.39	0.219	1.897	0.687	0.292	0.169	0.101	8.03	276	0.76	44
8.54	0.240	2.140	0.658	0.246	0.149	0.085	8.02	278	0.84	58
8.69	0.204	1.784	0.613	0.240	0.153	0.081	8.05	278	0.78	109
8.85	0.213	1.754	0.590	0.267	0.168	0.082	8.05	314	0.86	62
8.91	0.194	1.989	0.626	0.317	0.155	0.074	8.05	401	0.71	46
9.00	0.186	1.454	0.665	0.491	0.187	0.089	8.04	344	0.76	63
9.15	0.140	0.655	0.439	0.683	0.188	0.093	7.85	234	0.57	39
9.30	0.135	0.468	0.278	0.636	0.181	0.087	7.62	219	0.56	44
9.46	0.124	0.456	0.304	0.469	0.164	0.074	7.56	218	0.70	37
9.61	0.146	0.659	0.261	0.606	0.165	0.086	6.92	183	0.56	22
9.76	0.130	0.555	0.240	0.608	0.161	0.082	6.79	157	0.63	32
9.91	0.124	0.417	0.214	0.510	0.139	0.073	6.91	162	0.48	29
10.07	0.119	0.461	0.307	0.414	0.141	0.069	7.20	212	0.58	30
10.22	0.127	0.466	0.211	0.452	0.141	0.068	6.98	172	0.50	27
10.37	0.130	0.611	0.435	0.397	0.163	0.084	7.24	261	0.63	30
10.43	0.202	1.256	0.352	0.399	0.140	0.080	6.96	182	0.43	37
10.52	0.146	0.611	0.311	0.457	0.156	0.089	6.83	196	0.48	31
10.68	0.137	0.687	0.289	0.485	0.154	0.086	6.70	224	0.49	46
10.83	0.101	0.536	0.275	0.504	0.174	0.082	7.11	203	0.48	65
10.98	0.118	0.394	0.285	0.489	0.149	0.071	6.98	209	0.47	54
11.13	0.115	0.409	0.285	0.442	0.142	0.066	6.93	192	0.48	38
11.29	0.117	0.562	0.462	0.449	0.166	0.081	7.19	264	0.56	43
11.44	0.118	0.634	0.389	0.359	0.161	0.074	7.24	184	0.49	65
11.59	0.108	0.383	0.213	0.335	0.151	0.052	7.17	198	0.49	59
11.74	0.112	0.437	0.234	0.325	0.134	0.053	7.16	171	0.46	48
11.90	0.171	1.249	0.692	0.314	0.152	0.090	7.60	286	0.60	53

Table 3A-4. Continued.

Depth m	%N	%C	Ca mg/l	Fe mg/l	K mg/l	Mg mg/l	pH	Conductivity μS/cm	Bicarbonate meq/l	Magnetic Susceptibility
11.96	0.135	0.627	0.307	0.412	0.185	0.084	7.62	197	0.54	66
12.05	0.103	0.616	0.332	0.420	0.189	0.089	7.38	200	0.66	48
12.20	0.111	0.581	0.308	0.401	0.167	0.082	7.32	174	0.64	97
12.35	0.143	0.927	0.281	0.290	0.122	0.063	6.86	154	0.64	51
12.51	0.123	0.727	0.416	0.273	0.155	0.078	7.03	156	0.62	13
12.66	0.139	1.193	0.220	0.224	0.092	0.053	6.90	191	0.41	77
12.81	0.157	1.372	0.360	0.242	0.124	0.074	6.78	178	0.54	28
12.96	0.140	1.163	0.339	0.244	0.120	0.066	6.95	176	0.55	23
13.12	0.111	0.911	0.330	0.193	0.120	0.059	6.96	168	0.54	10
13.27	0.183	1.630	0.332	0.230	0.131	0.067	6.91	166	0.53	6
13.42	0.107	1.024	0.372	0.280	0.121	0.070	7.22	181	0.58	30
13.48	0.176	1.175	0.621	0.188	0.121	0.099	5.99	288	0.47	17
13.57	0.171	1.652	0.786	0.228	0.162	0.120	5.85	304	0.68	12
13.73	0.153	1.537	0.680	0.192	0.152	0.100	5.62	326	0.21	25
13.88	0.183	1.778	0.936	0.218	0.199	0.129	5.55	403	0.32	14
14.03	0.184	2.144	1.043	0.202	0.124	0.122	6.12	333	0.44	12
14.18	0.214	2.579	0.985	0.205	0.143	0.087	6.94	418	0.41	15
14.34	0.105	1.027	0.814	0.248	0.133	0.078	7.01	342	0.29	16
14.49	0.120	0.963	0.833	0.216	0.124	0.070	7.19	320	0.41	20
14.64	0.105	0.832	0.630	0.214	0.113	0.054	7.18	276	0.33	17
14.79	0.111	0.871	0.796	0.225	0.110	0.060	7.20	306	0.37	13
14.95	0.099	0.936	0.819	0.237	0.136	0.061	7.29	314	0.41	18
15.01	0.105	0.628	0.450	0.254	0.147	0.062	6.85	188	0.27	28
15.10	0.089	0.532	0.344	0.228	0.102	0.049	6.68	179	0.19	43
15.25	0.087	0.479	0.364	0.282	0.116	0.058	6.55	153	0.21	53
15.40	0.080	0.460	0.349	0.254	0.102	0.058	6.59	175	0.15	54
15.56	0.074	0.442	0.439	0.214	0.100	0.076	6.64	193	0.26	86
15.71	0.101	0.656	0.428	0.239	0.117	0.059	6.75	214	0.30	50
15.86	0.091	0.465	0.341	0.266	0.194	0.056	6.65	189	0.26	60
16.01	0.075	0.381	0.338	0.242	0.112	0.051	6.65	154	0.26	62
16.17	0.072	0.335	0.304	0.230	0.099	0.048	6.70	151	0.24	68
16.32	0.079	0.386	0.333	0.252	0.109	0.054	6.66	164	0.25	69
16.47	0.087	0.498	0.331	0.241	0.095	0.056	6.73	162	0.24	51
16.53	0.092	0.595	0.455	0.254	0.127	0.070	6.96	198	0.28	62
16.62	0.151	1.335	0.909	0.235	0.166	0.107	7.20	236	0.54	35
16.78	0.142	1.199	0.770	0.231	0.136	0.095	7.22	205	0.50	25
16.93	0.107	0.647	0.363	0.340	0.130	0.061	6.87	176	0.29	8
17.08	0.107	0.821	0.277	0.160	0.123	0.035	6.68	160	0.18	12
17.23	0.074	0.627	0.281	0.398	0.128	0.062	6.50	134	0.26	10
17.39	0.104	1.297	0.235	0.224	0.107	0.043	6.43	144	0.25	39

Table 3A-4. Continued.

Depth m	%N	%C	Ca mg/l	Fe mg/l	K mg/l	Mg mg/l	pH	Conductivity μS/cm	Bicarbonate meq/l	Magnetic Susceptibility
17.69	0.091	0.897	0.023	0.341	0.100	0.053	6.51	117	0.20	11
18.00	0.107	0.779	0.387	0.333	0.200	0.072	6.84	167	0.31	36
18.15	0.110	1.373	0.354	0.332	0.152	0.072	6.51	84	0.20	11
18.30	0.119	0.600	0.247	0.618	0.174	0.093	6.76	105	0.29	18
18.45	0.087	0.476	0.185	0.621	0.109	0.077	6.68	94	0.21	29
18.61	0.117	0.454	0.157	0.646	0.095	0.066	6.46	94	0.15	33
18.76	0.094	0.715	0.180	0.564	0.118	0.066	6.31	86	0.15	21
18.91	0.109	0.493	0.157	0.699	0.109	0.068	6.40	78	0.47	41
19.22	0.092	0.379	0.177	0.532	0.126	0.063	5.97	86	0.14	17
19.52	0.090	0.425	0.120	0.721	0.088	0.049	5.89	101	0.16	18
20.13	0.091	0.459	0.143	0.500	0.099	0.062	6.64	77	0.27	29
20.44	0.104	0.287	0.098	0.539	0.081	0.060	6.57	76	0.33	19
21.05	0.087	0.389	0.111	0.687	0.113	0.075	6.78	104	0.20	26
21.35	0.092	0.397	0.159	0.513	0.140	0.066	6.40	66	0.25	22
21.50	0.074	0.307	0.108	0.506	0.123	0.056	6.79	54	0.24	16
21.66	0.078	0.288	0.090	0.660	0.087	0.057	6.45	82	0.27	25
21.96	0.088	0.351	0.091	0.633	0.104	0.062	6.61	65	0.23	36
22.27	0.072	0.280	0.108	0.565	0.132	0.063	6.36	87	0.19	49
22.57	0.085	0.389	0.125	0.546	0.129	0.063	6.70	63	0.26	55
22.88	0.093	0.299	0.110	0.527	0.127	0.068	6.97	65	0.19	54
23.03	0.090	0.629	0.107	0.488	0.091	0.059	6.64	81	0.17	N/A
23.18	0.083	0.322	0.100	0.537	0.084	0.056	6.72	77	0.21	16
23.33	0.086	0.575	0.101	0.523	0.082	0.062	6.83	76	0.20	46
23.49	0.079	0.399	0.095	0.538	0.081	0.063	6.49	74	0.17	75
23.64	0.065	0.310	0.086	0.434	0.065	0.055	6.53	90	0.14	247
23.79	0.085	0.312	0.081	0.511	0.070	0.054	6.39	100	0.20	28
24.71	0.072	0.240	0.105	0.588	0.085	0.053	6.02	86	0.14	62
24.86	0.064	0.235	0.088	0.632	0.100	0.059	5.93	72	0.16	56
25.01	0.070	0.316	0.122	0.778	0.119	0.071	5.94	75	0.20	15
25.16	0.068	0.208	0.113	0.744	0.127	0.092	6.81	117	0.20	32
25.39	0.081	0.300	0.120	0.557	0.072	0.062	6.41	105	0.21	21
25.54	0.065	0.165	0.105	0.676	0.092	0.078	6.54	63	0.15	86
25.62	0.066	0.229	0.087	0.667	0.079	0.058	6.50	54	0.20	65
Average	0.134	0.94	0.41	0.39	0.14	0.08	6.95	197.82	0.45	43.71
Std Dev	0.063	0.72	0.27	0.16	0.03	0.02	0.60	97.49	0.26	36.12
High Value	0.376	3.83	1.09	0.78	0.23	0.16	8.31	425.00	1.22	275.00
Low Value	0.064	0.17	0.08	0.16	0.07	0.04	5.55	54.00	0.14	6.33

Table 3A-5. Auger Core Chemical Results.

Depth m	%N	%C	Ca mg/l	Fe mg/l	K mg/l	Mg mg/l	pH	Conductivity μS/cm	Bicarbonate meq/l
0.46	0.119	1.175	0.2123	0.4527	0.0727	0.1289	7.23	68	0.17
0.92	0.155	1.657	0.2386	0.4341	0.0712	0.1376	6.47	64	0.14
1.83	0.101	0.904	0.1745	0.4675	0.0739	0.1135	6.97	62	0.09
3.05	0.230	2.763	0.2639	0.2929	0.1691	0.1662	6.36	130	0.25
6.10	0.154	1.377	0.7046	0.2789	0.1918	0.1440	7.77	169	0.44
9.15	0.218	1.973	0.9044	0.2373	0.1968	0.1764	7.73	249	0.56
12.20	0.118	0.778	0.3309	0.3843	0.1913	0.0918	7.42	125	0.32
18.30	0.118	0.668	0.1833	0.4239	0.1320	0.0593	6.68	83	0.26
21.35	0.099	0.485	0.1584	0.4438	0.1587	0.0644	6.99	79	0.15
Average	0.15	1.31	0.35	0.38	0.14	0.12	7.07	114.36	0.26
Std Dev	0.05	0.73	0.27	0.09	0.05	0.04	0.51	62.36	0.15
High Value	0.23	2.76	0.90	0.47	0.20	0.18	7.77	249.00	0.56
Low Value	0.10	0.49	0.16	0.24	0.07	0.06	6.36	62.00	0.09

Table 3A-6. Shallow Core "Running" Standard Deviation Values Over 5 cm Intervals, Staggered at 1cm.

$\delta^{18}O$	Depth m	Std Dev	Std Dev	Std Dev	Std Dev	Std Dev
-18.02	0.90	0.998437				
-17.87	0.91		1.092655			
-18.97	0.92			1.121496		
-19.84	0.93				1.054269	
-17.32	0.94					0.791908
-17.40	0.95	0.778056				
-17.62	0.96		0.782306			
-17.69	0.97			0.63456		
-19.24	0.98				0.391533	
-18.57	0.99					0.433478
-19.18	1.00	0.475151				
-18.43	1.02		0.456823			
-19.20	1.03			0.489769		
-19.42	1.04				0.524153	
-18.40	1.05					0.528884
-18.74	1.06	0.467939				
-19.58	1.07		0.243537			
-19.48	1.08			0.580084		
-19.45	1.10				0.541121	
-20.04	1.11					0.497437
-19.77	1.12	0.637548				
-20.87	1.13		0.593816			
-19.74	1.14			0.49677		
-19.66	1.15				0.527511	
-20.90	1.16					0.860632
-20.26	1.17	1.038809				
-20.15	1.18		0.902737			
-19.60	1.19			0.92922		
-18.61	1.20				1.048486	
-17.85	1.21					1.109621
-18.68	1.22	1.074986				
-20.23	1.23		1.131376			
-17.52	1.24			0.881103		
-17.76	1.25				0.814897	
-18.23	1.26					0.561306
-19.26	1.27	0.200106				
-19.47	1.28		0.196698			
-19.57	1.29			0.197993		
-19.52	1.30				0.258181	
-19.09	1.31					0.250575

Table 3A-6. Continued.

$\delta^{18}O$	Depth m	Std Dev	Std Dev	Std Dev	Std Dev	Std Dev
-19.28	1.32	0.203625				
-19.25	1.33		0.329576			
-19.75	1.34			0.302445		
-19.45	1.35				0.292998	
-19.34	1.36					0.309756
-20.05	1.37	0.256213				
-19.38	1.38		0.196344			
-19.66	1.39			0.205608		
-19.88	1.40				0.218315	
-19.65	1.41					0.243217
-19.47	1.42	0.246906				
-19.34	1.43		0.393088			
-19.77	1.44			0.419735		
-19.96	1.45				0.478839	
-19.73	1.46					0.363053
-18.98	1.47	0.131737				
-19.19	1.48		0.132135			
-18.87	1.49			0.276576		
-18.87	1.50				0.257906	
-19.01	1.51					0.245541
-18.96	1.52	0.225081				
-19.53	1.53		0.199687			
-19.09	1.54			0.140292		
-19.37	1.55				0.13101	
-19.30	1.56					0.141676
-19.04	1.57	0.13919				
-19.11	1.58		0.112647			
-19.19	1.59			0.458746		
-19.40	1.60				0.599857	
-19.28	1.61					0.603514
-19.33	1.62	0.515197				
-18.29	1.63		0.414906			
-18.20	1.64			0.459488		
-18.13	1.65				0.411765	
-18.14	1.66					0.433686
-17.27	1.67	0.366958				
-17.37	1.68		0.469583			
-17.60	1.69			0.53283		
-18.21	1.70				0.432198	
-17.67	1.71					0.430284

Table 3A-6. Continued.

$\delta^{18}O$	Depth m	Std Dev	Std Dev	Std Dev	Std Dev	Std Dev
-18.50	1.72	0.447205				
-18.84	1.73		0.467243			
-18.44	1.74			0.363506		
-18.25	1.75				0.316156	
-17.63	1.76					0.175882
-17.92	1.77	0.408457				
-17.63	1.78		0.4798			
-17.43	1.79			0.595722		
-17.57	1.80				0.582601	
-16.81	1.81					0.314504
-16.57	1.82	0.229186				
-16.14	1.83		0.39569			
-16.17	1.84			0.376037		
-16.11	1.85				0.420231	
-16.54	1.86					0.662476
-17.03	1.87	0.796471				
-16.63	1.88		0.988765			
-15.99	1.89			0.978251		
-17.78	1.90				0.390572	
-17.89	1.91					0.307781
-18.38	1.92	0.210864				
-18.34	1.93		0.212465			
-18.74	1.94			0.268952		
-18.18	1.95				0.238677	
-18.30	1.96					0.215071
-18.44	1.97	0.201806				
-18.79	1.98		0.18992			
-18.29	1.99			0.358795		
-18.61	2.00				0.472712	
-18.70	2.01					1.062565
-18.59	2.02	1.416499				
-19.27	2.03		1.312096			
-17.94	2.04			0.81054		
-16.50	2.05				0.631516	
-15.89	2.06					0.650089
-17.38	2.07	0.470893				

Table 3A-6. Continued.

$\delta^{18}O$	Depth m	Std Dev	Std Dev	Std Dev	Std Dev	Std Dev
-17.34	2.08		0.37778			
-16.53	2.09			0.191361		
-16.34	2.10				0.512128	
-16.79	2.11					0.432591
-16.71	2.12	0.40976				
-16.76	2.13		0.432688			
-17.72	2.14			0.30994		
-17.24	2.15				0.328042	
-17.14	2.16					0.336118
-17.81	2.17	0.273493				
-17.24	2.18		0.372367			
-17.79	2.19			0.358058		
-17.80	2.20				0.554855	
-17.37	2.21					0.443099
-16.93	2.22	0.477514				
-17.51	2.23		0.473287			
-16.38	2.24			0.667632		
-17.11	2.25				0.42848	
-17.54	2.26					0.381773
-17.28	2.27	0.413872				
-18.22	2.28		0.384909			
-17.37	2.29			0.451442		
-17.37	2.30				0.395128	
-17.92	2.31					0.335835
-17.99	2.32	0.395818				
-18.43	2.33		0.415692			
-17.66	2.34			0.465056		
-17.57	2.35				0.672545	
-18.38	2.36					1.437994
-17.73	2.37	1.413097				
-18.59	2.38		1.421612			
-19.23	2.39			1.388844		
-15.50	2.40				1.202108	
-17.93	2.41					0.140611
-18.17	2.42	0.066138				
-18.27	2.43		0.081799			
-18.29	2.44			0.173013		
-18.17	2.45				0.146802	

Table 3A-6. Continued.

$\delta^{18}O$	Depth m	Std Dev	Std Dev	Std Dev	Std Dev	Std Dev
-18.14	2.46					0.1422
-18.10	2.47	0.109647				
-17.82	2.48		0.075918			
-17.96	2.49			0.139221		
-17.86	2.50				0.14806	
-17.89	2.51					0.264365
-17.75	2.52	0.276509				
-17.60	2.53		0.338046			
-17.99	2.54			0.420948		
-18.30	2.55				0.415157	
-18.09	2.56					0.300247
-17.50	2.57	0.19225				
-17.30	2.58		0.223041			
-17.69	2.59			0.257253		
-17.50	2.60				0.332869	
-17.19	2.61					0.340228
-17.68	2.62	0.418121				
-17.88	2.63		0.521372			
-18.05	2.64			0.552592		
-17.96	2.65				0.632978	
-17.01	2.66					0.647135
-18.42	2.67	0.485956				
-18.27	2.68		0.453417			
-18.62	2.69			0.451275		
-17.75	2.70				0.406517	
-17.45	2.71					0.387455
-17.94	2.72	0.22441				
-18.25	2.73		0.224984			
-18.48	2.74			0.25095		
-18.07	2.75				0.367042	
-18.40	2.76					0.336161
-17.94	2.77	0.376182				
-18.47	2.78		0.359573			
-18.87	2.79			0.40183		
-18.56	2.80				0.353976	
-18.84	2.81					0.455099
-17.98	2.82	0.45392				
-18.15	2.83		0.643984			
-18.63	2.84			0.624366		

Table 3A-6. Continued.

$\delta^{18}O$	Depth m	Std Dev	Std Dev	Std Dev	Std Dev	Std Dev
-17.74	2.85				0.296221	
-17.41	2.86					0.222773
-16.96	2.87	0.180018				
-17.38	2.88		0.220309			
-17.14	2.89			0.264773		
-16.95	2.90				0.265004	
-17.20	2.91					0.28292
-17.52	2.92	0.375251				
-16.82	2.93		0.402498			
-17.09	2.94			0.343062		
-16.85	2.95				0.320944	
-17.64	2.96					0.239791
-17.63	2.97	0.230844				
-17.37	2.98		0.176828			
-17.29	2.99			0.1401		
-17.07	3.00				0.075708	
-17.08	3.01					0.078851
-16.93	3.02	0.015486				
-16.96	3.03					

Table 3A-7. Shallow Core "Running" Standard Deviation Values Over 10 cm Intervals, Staggered at 1cm.

$\delta^{18}O$	Depth m	Std Dev	Std Dev	Std Dev	Std Dev	Std Dev	Std Dev	Std Dev	Std Dev	Std Dev	Std Dev
-18.02	0.90	0.858561									
-17.87	0.91		0.900972								
-18.97	0.92			0.883726							
-19.84	0.93				0.902057						
-17.32	0.94					0.837917					
-17.40	0.95						0.746596				
-17.62	0.96							0.635878			
-17.69	0.97								0.583953		
-19.24	0.98									0.448988	
-18.57	0.99										0.464933
-19.18	1.00	0.526145									
-18.43	1.02		0.557142								
-19.20	1.03			0.677881							
-19.42	1.04				0.673077						
-18.40	1.05					0.672159					
-18.74	1.06						0.652673				
-19.58	1.07							0.538492			
-19.48	1.08								0.52214		
-19.45	1.10									0.509177	
-20.04	1.11										0.665306
-19.77	1.12	0.939347									
-20.87	1.13		0.99729								
-19.74	1.14			0.927337							
-19.66	1.15				1.12701						
-20.90	1.16					1.224719					
-20.26	1.17						1.084867				

Table 3A-7, Continued.

δ¹⁸O	Depth m	Std Dev	Std Dev	Std Dev	Std Dev	Std Dev	Std Dev	Std Dev	Std Dev	Std Dev	Std Dev
-20.15	1.18							0.98556			
-19.60	1.19								0.90127		
-18.61	1.20									0.897557	
-17.85	1.21										0.930746
-18.68	1.22	0.870014									
-20.23	1.23		0.871409								
-17.52	1.24			0.765237							
-17.76	1.25				0.632762						
-18.23	1.26					0.417915					
-19.26	1.27						0.191077				
-19.47	1.28							0.273078			
-19.57	1.29								0.275031		
-19.52	1.30									0.280177	
-19.09	1.31										0.308343
-19.28	1.32	0.272444									
-19.25	1.33		0.256588								
-19.75	1.34			0.243845							
-19.45	1.35				0.244878						
-19.34	1.36					0.262845					
-20.05	1.37						0.240068				
-19.38	1.38							0.29417			
-19.66	1.39								0.314197		
-19.88	1.40									0.38016	
-19.65	1.41										0.397338
-19.47	1.42	0.400673									
-19.34	1.43		0.411703								
-19.77	1.44			0.419575							

Table 3A-7, Continued.

$\delta^{18}O$	Depth m	Std Dev	Std Dev	Std Dev	Std Dev	Std Dev	Std Dev	Std Dev	Std Dev	Std Dev	Std Dev
-19.96	1.45				0.386549						
-19.73	1.46					0.294191					
-18.98	1.47						0.223559				
-19.19	1.48							0.220052			
-18.87	1.49								0.218842		
-18.87	1.50									0.201638	
-19.01	1.51										0.189232
-18.96	1.52	0.177844									
-19.53	1.53		0.152848								
-19.09	1.54			0.322809							
-19.37	1.55				0.439238						
-19.30	1.56					0.508377					
-19.04	1.57						0.546347				
-19.11	1.58							0.721704			
-19.19	1.59								0.799553		
-19.40	1.60									0.796024	
-19.28	1.61										0.696456
-19.33	1.62	0.593558									
-18.29	1.63		0.423707								
-18.20	1.64			0.502713							
-18.13	1.65				0.518548						
-18.14	1.66					0.522489					
-17.27	1.67						0.535424				
-17.37	1.68							0.476735			
-17.60	1.69								0.442205		
-18.21	1.70									0.46419	
-17.67	1.71										0.483925
-18.50	1.72	0.60708									

Table 3A-7, Continued.

$\delta^{18}O$	Depth m	Std Dev	Std Dev								
-18.84	1.73		0.695441								
-18.44	1.74			0.729539							
-18.25	1.75				0.736904						
-17.63	1.76					0.713564					
-17.92	1.77						0.688944				
-17.63	1.78							0.592518			
-17.43	1.79								0.516877		
-17.57	1.80									0.489503	
-16.81	1.81										0.539748
-16.57	1.82	0.681962									
-16.14	1.83		0.864468								
-16.17	1.84			0.935926							
-16.11	1.85				1.006235						
-16.54	1.86					0.933699					
-17.03	1.87						0.886969				
-16.63	1.88							0.876859			
-15.99	1.89								0.800338		
-17.78	1.90									0.318503	
-17.89	1.91										0.267776
-18.38	1.92	0.21674									
-18.34	1.93		0.216859								
-18.74	1.94			0.317696							
-18.18	1.95				0.372314						
-18.30	1.96					0.738216					
-18.44	1.97						1.072174				
-18.79	1.98							1.087167			

Table 3A-7, Continued.

δ^{18}O	Depth m	Std Dev	Std Dev	Std Dev	Std Dev	Std Dev	Std Dev	Std Dev	Std Dev	Std Dev	Std Dev
-18.29	1.99								1.066029		
-18.61	2.00									1.12913	
-18.70	2.01										1.148638
-18.59	2.02	1.073133									
-19.27	2.03		0.973338								
-17.94	2.04			0.590869							
-16.50	2.05				0.546783						
-15.89	2.06					0.552111					
-17.38	2.07						0.434403				
-17.34	2.08							0.49366			
-16.53	2.09								0.48791		
-16.34	2.10									0.507651	
-16.79	2.11										0.453936
-16.71	2.12	0.417845									
-16.76	2.13		0.383818								
-17.72	2.14			0.316952							
-17.24	2.15				0.448458						
-17.14	2.16					0.453008					
-17.81	2.17						0.454052				
-17.24	2.18							0.424444			
-17.79	2.19								0.513437		
-17.80	2.20									0.494168	
-17.37	2.21										0.468991
-16.93	2.22	0.507335									
-17.51	2.23		0.517087								
-16.38	2.24			0.600103							

Table 3A-7, Continued.

$\delta^{18}O$	Depth m	Std Dev	Std Dev	Std Dev	Std Dev	Std Dev	Std Dev	Std Dev	Std Dev	Std Dev	Std Dev
-17.11	2.25				0.434197						
-17.54	2.26					0.387659					
-17.28	2.27						0.429669				
-18.22	2.28							0.389598			
-17.37	2.29								0.441461		
-17.37	2.30									0.566447	
-17.92	2.31										0.984584
-17.99	2.32	0.984637									
-18.43	2.33		0.988119								
-17.66	2.34			0.980336							
-17.57	2.35				0.983204						
-18.38	2.36					0.97476					
-17.73	2.37						0.967984				
-18.59	2.38							0.963358			
-19.23	2.39								0.945024		
-15.50	2.40									0.835275	
-17.93	2.41										0.167254
-18.17	2.42	0.171773									
-18.27	2.43		0.193073								
-18.29	2.44			0.213533							
-18.17	2.45				0.180858						
-18.14	2.46					0.203334					
-18.10	2.47						0.19865				
-17.82	2.48							0.23195			
-17.96	2.49								0.295851		
-17.86	2.50									0.294721	
-17.89	2.51										0.307742

Table 3A-7, Continued.

$\delta^{18}O$	Depth m	Std Dev	Std Dev	Std Dev	Std Dev	Std Dev	Std Dev	Std Dev	Std Dev	Std Dev	Std Dev
-17.75	2.52	0.35084									
-17.60	2.53		0.350158								
-17.99	2.54			0.35368							
-18.30	2.55				0.359715						
-18.09	2.56					0.311122					
-17.50	2.57						0.340507				
-17.30	2.58							0.430377			
-17.69	2.59								0.446894		
-17.50	2.60									0.519776	
-17.19	2.61										0.506462
-17.68	2.62	0.47342									
-17.88	2.63		0.466816								
-18.05	2.64			0.476759							
-17.96	2.65				0.503218						
-17.01	2.66					0.503009					
-18.42	2.67						0.363157				
-18.27	2.68							0.357316			
-18.62	2.69								0.372472		
-17.75	2.70									0.415469	
-17.45	2.71										0.404867
-17.94	2.72	0.334185									
-18.25	2.73		0.328468								
-18.48	2.74			0.334511							
-18.07	2.75				0.342613						
-18.40	2.76					0.388872					
-17.94	2.77					0.489453					

Table 3A-7, Continued.

$\delta^{18}O$	Depth m	Std Dev	Std Dev	Std Dev	Std Dev	Std Dev	Std Dev	Std Dev	Std Dev	Std Dev	Std Dev
-18.47	2.78							0.636255			
-18.87	2.79								0.66986		
-18.56	2.80									0.658131	
-18.84	2.81										0.671403
-17.98	2.82	0.557581									
-18.15	2.83		0.536817								
-18.63	2.84			0.523753							
-17.74	2.85				0.28836						
-17.41	2.86					0.243321					
-16.96	2.87						0.279058				
-17.38	2.88							0.306349			
-17.14	2.89								0.305635		
-16.95	2.90									0.305007	
-17.20	2.91										0.294375
-17.52	2.92	0.298812									
-16.82	2.93		0.294618								
-17.09	2.94			0.279708							
-16.85	2.95				0.294203						
-17.64	2.96					0.281412					
-17.63	2.97						0.251819				
-17.37	2.98							0.176562			
-17.29	2.99								0.1401		
-17.07	3.00									0.075708	
-17.08	3.01										0.078851
-16.93	3.02	0.015486									
-16.96	3.03										

Chapter 4

Summary and Conclusions

SUMMARY

Samples from cores taken from the Copper River Basin and a site north of Fairbanks, Alaska were analyzed for water isotopes and basic soil chemistry to determine the environmental history of the pore ice of permafrost at the sites. An isotope ratio mass spectrometer was used to analyze the $\delta^{18}O$ and δD values. Water content was determined as well, and subsamples of the cores were analyzed for nitrogen and carbon content. Water extracts of the core samples were analyzed for cations (Ca, Mg, K and Fe), pH, conductivity, and bicarbonate. Magnetic susceptibility was determined on samples from the Fairbanks site.

At the Copper River Basin site, two cores taken from very similar sites but 400 m apart have two very different oxygen isotope profiles. One (core H1) has the generally slanted profile of a mixing zone signature that had been frozen in place not long after ancient Lake Atna drained, around 10,000 yr BP (Rubin and Alexander, 1960, Williams, 1989, Ferrians, 1989).

The other (core H2) has a profile showing the development of a thaw lake not long after permafrost had reached a depth of about 10 m, followed by the drainage of that thaw lake and the subsequent refreezing of the entire soil column. Both cores also show a lowering of the active layer due to disturbance, possibly fire, at some time after the thaw lake had drained and the drained lake bottom had frozen.

Chemical analyses of soils from the sample cores taken from this site show very little correlation between parameters except for magnesium with iron and magnesium with calcium, likely a mineralogical linking of mafic and carbonate minerals. The lack of correlations among the other chemical data is not surprising since the lake bed material was deposited largely through the erosional actions of glaciers in the area over several thousands of years, and the mineralogical character of the lake bed is not homogenous (Bennett et al., 2002; Williams and Galloway, 1986).

Statistical comparisons of the chemistries of the two cores showed differences between calcium, bicarbonate, conductivity, water content, and oxygen and deuterium isotopes in the two cores. These are parameters that would be different for different types of water rather than different types of soil and so confirm that the pore ice from the two cores is, for at least part of core H2, from different sources, as would be expected for waters from a glacial fed lake (core H1) versus water from a thaw lake (core H2).

The soil cores from the Fairbanks site are all composed of silt that was deposited as loess. A shallow core taken from a site where the permafrost table is about 1 m below the ground surface was analyzed as continuously as was possible for the sampling method used, from the top of the permafrost table down to 3.1 m depth. Oxygen isotope signatures for the core show a minimum of 5 separate thaw/refreeze events in the soil. Since thawing destroys older permafrost signatures, the 5 events are sequential from the bottom to the top of the core. Particles of charcoal and ash at several depths in the core as well as in other areas of the site suggest that the cause of these thawing events was fire. Comparing sampling of the data from the shallow core at spacing of 15 cm intervals

versus the original 1 cm intervals shows that some of the fractionation peaks would be missed at the 15 cm resolution, but that the profile of the signatures is in general the same as that of the full resolution data profile. Spacing greater than 15 cm should be used with caution, since it is almost certain some events will be missed in the data.

Widely spaced data from an augered core at the Hagelbarger site is not as useful for identifying specific events in the permafrost data, but these data points did confirm the data from a more intensively sampled core (Hagelbarger core) in a general way. The augered core data include samples from the active layer which were not available from the Hagelbarger core, and that allows a comparison of the deeper, older permafrost with the modern signatures at the top of the augered core. Depth to the permafrost table for the augered core was 3 m (Romanovsky, personal communication, 2011).

The Hagelbarger core starts at the permafrost table, 6.1 m deep (Romanovsky, personal communication, 2011) and continues to a depth of over 25 m though the permafrost did not go below 25 m. Oxygen isotope signatures of the core show a complicated series of freeze/thaw events that place the ages of data from the core sections with the oldest at the bottom of the core and the youngest near the top. There are four identifiably different sections to the core. The bottom-most three sections are in sequential order from bottom to top, each section with a different signature that indicates each section is the result of a thawing event that replaced the permafrost with groundwater of a different signature before the core refroze. The top section has the profile of a mixing zone, though the bottom of that profile does not meet the section below it, which suggests that the top section had been thawed more than once. Since this

section is at a depth of 6 m below the ground surface, and it is a mixing zone, there is a possibility that this section's pore ice was formed at a time when the ground surface was much closer to the permafrost table than it is today.

The highly variable data from the third section of the core indicating several freeze/thaw cycles similar to the shallow core data also suggests that at one time that section was nearer to the surface of the ground, but in this case it would have had to be before the loess deposits at 6 m depth had been made. This would make the pore ice in the third section older than 30,000 years.

Chemical analyses of the Hagelbarger core samples show strong correlations among the parameters. The only non-correlating parameters are iron and magnetic susceptibility. Increases in values of those chemicals associated with pedogenesis at three particular depths correspond with pedogenesis depths from other sites in the Fairbanks area (Beget et al., 1991; Muhs et al., 2003. The ages of pedogenesis events at depths similar to those in Hagelbarger core by other researchers suggests that the loess deposit at around 6 m depth has a radiocarbon age of about 32,000 – 34,000 YBP (Muhs et al., 2003).

The Hagelbarger site has also developed a number of thermokarst landforms (a thaw pond, polygons, and sunken trenches) where the ground surface was disturbed in the vicinity of the cores about 30 years ago. These landforms probably developed syngenetically during a cold period in Alaska when ground temperatures were colder than -6°C or less (Williams and Smith, 1989). The thermokarst developed after the ground

surface was scraped down to mineral soil and the subsurface ice-rich permafrost

subsequently thawed.

CONCLUSIONS

The water isotope differences between the two cores from the Copper River Basin

show very different histories since Lake Atna drained about 10,000 years ago. There is

strong evidence that core H1 water isotopes reflect Lake Atna water that mixed with

meteoric water from the surface, but that after permafrost had formed it was thawed for

several meters depth by a disturbance, probably fire. Core H2 shows evidence of the

same disturbance, but those signatures are superimposed on the signatures of a thaw lake,

and the thaw lake signature is superimposed on the signature of the drained thaw lake

water mixing with Lake Atna water. Although the core H1 results are not unexpected

for an ancient frozen lake bed, the core H2 results uncovered the existence of a

previously unknown thaw lake in the area. The differences between these two cores are

an unexpected but welcome demonstration of how effective water isotopes are in

uncovering permafrost history.

Isotope differences in the two cores and augered material from north of Fairbanks

show that the area at the site has been subject to surface disturbances and permafrost

thawing and refreezing intermittently for tens of thousands of years. Comparisons of

several different sampling intervals show that water oxygen isotopes should be sampled

with high resolution to discover as much of the information contained in the isotope

signature profile as possible.

Adding chemical analyses to the isotope data helps to describe the permafrost environment more specifically, such as confirming the differences between the permafrost of core H1 and core H2 at the Lake Atna site by showing the statistical differences between their water chemistries. At the Hagelbarger site, soil chemistry helps set the age of the 16 m depth freeze/thaw mixing zone signatures at older than 32,000 - 34,000 years.

The persistence of permafrost, the different forms that it takes and the great variation in the permafrost table depth within this small area highlights the localized conditions that support permafrost in the discontinuous zone in Alaska. Climate alone does not determine the location or extent of permafrost, nor its persistence. Permafrost both depends on and has direct influence on surface vegetation and wildfires.

This study shows that permafrost formation (and thaw) is a dynamic, sometimes bidirectional process. Use of water isotope data profiles in analysis of the cores taken from the Copper River Basin and the Hagelbarger site brings to light events in the history of these sites that cannot be determined by studying soil or water chemistry and surface vegetation ecology or by interpreting satellite imaging. The information is contained in the water itself.

The stated hypothesis for this research is that permafrost pore ice isotope signatures in frozen groundwater can provide information on the local environment at the permafrost site that is not available from other sources. The discovery of an unknown early thaw lake at the Lake Atna site and the minimum age of the permafrost ice below

15 m depth at the Hagelbarger site are evidence of the possibilities in water isotope

research on permafrost. I believe my hypothesis has been shown to be valid.

.

LITERATURE CITED

Beget, J.E., M. Edwards, D. Hopkins, M. Keskinen and G. Kukla. 1991. Old Crow tephra found at the palisades of the Yukon, Alaska. Quat. Res. 35, 291-297.

Bennett, M.R., D. Huddart and G.S.P. Thomas. 2002. Facies architecture within a regional glaciolacustrine basin: Copper River, Alaska. Quat. Sci. Rev. 21, 237-2279.

Ferrians, O.J. 1989. Glacial Lake Atna, Copper River Basin, Alaska. *In*: Carter, L.D., T.D. Hamilton, and J.P. Galloway, (eds), Late Cenozoic History of the Interior Basins of Alaska and the Yukon. United States Geological Survey, Circular 1026, 85-88.

Muhs, D.R., T.A. Ager, E.A. Bettis III, J. McGeehin, J.M. Been, J.E. Beget, M.J. Pavich, T.W. Stafford Jr. and D.S.P. Stevens. 2003. Stratigraphy and palaeoclimatic significance of late Quaternary loess–palaeosol sequences of the last interglacial-glacial cycle in central Alaska. Quat. Sci. Rev. 22, 1947-1986.

Rubin, M. and C. Alexander. 1960. U.S. Geological Survey radiocarbon dates 5: Am. Jour. Sci. Radiocarbon Supp. 2, 129-185.

Williams, J.R. 1989. A working glacial chronology for the Western Copper River Basin, Alaska. *In*: Carter, L.D., T.D. Hamilton and J.P. Galloway (eds). Late Cenozoic History of the Interior Basins of Alaska and the Yukon. United States Geological Survey, Circular 1026, 81-84.

Williams, J.R. and J.P. Galloway. 1986. Map of western Copper River Basin, Alaska, showing lake sediments and shorelines, glacial moraines, and location of stratigraphic sections and radiocarbon-dated samples. United Stats Geological Survey Open-File Report 86:390, 30 pages.

Willliams, P.J. and M.W. Smith. 1989. *The Frozen Earth, Fundamentals of Geocryology*. Cambridge University Press. Cambridge. 306 pages.